REVIEW ARTICLE

Nonlinear physics of electrical wave propagation in the heart: a review

Sergio Alonso[1,2], **Markus Bär**[1], **and Blas Echebarria**[2]

[1] Physikalisch-Technische Bundesanstalt, Abbestr. 2-12 10587, Berlin, Germany
[2] Department of Physics, Universitat Politècnica de Catalunya, Av. Dr. Marañón 44, E-08028 Barcelona, Spain

E-mail: s.alonso@upc.edu, Markus.Baer@ptb.de, blas.echebarria@upc.edu

Abstract. The beating of the heart is a synchronized contraction of muscle cells (myocytes) that are triggered by a periodic sequence of electrical waves (action potentials) originating in the sino-atrial node and propagating over the atria and the ventricles. Cardiac arrhythmias like atrial and ventricular fibrillation (AF,VF) or ventricular tachycardia (VT) are caused by disruptions and instabilities of these electrical excitations, that lead to the emergence of rotating waves (VT) and turbulent wave patterns (AF,VF). Numerous simulation and experimental studies during the last 20 years have addressed these topics. In this review we focus on the nonlinear dynamics of wave propagation in the heart with an emphasis on the theory of pulses, spirals and scroll waves and their instabilities in excitable media and their application to cardiac modeling. After an introduction into electrophysiological models for action potential propagation, the modeling and analysis of spatiotemporal alternans, spiral and scroll meandering, spiral breakup and scroll wave instabilities like negative line tension and sproing are reviewed in depth and discussed with emphasis on their impact in cardiac arrhythmias.

Contents

1. Introduction

Cardiovascular disease (CVD) is the leading cause of death in the developed world and accounts for about a third of all deaths [1, 2]. CVD may occur due to problems in the veins or arteries (arteriosclerosis) giving rise to heart attacks or strokes, in the disruption of the proper contraction of the ventricles resulting in heart failure and impaired blood supply. A loss of rhythm and synchronization of cardiac electrical impulses orchestrating the pumping of blood is associated with a number of arrhythmias (i.e., abnormal or irregular heart rhythm) including atrial (AF) and ventricular (VF) fibrillation and ventricular tachycardia (VT) [3].

The main motivation for modeling in cardiology is nicely summarized in a short introduction written by J. Jalife for a series of articles on recent advances in computational cardiology in the leading journal *Circulation research* [4]: "*Of all the cardiac arrhythmias seen in clinical practice, atrial fibrillation (AF) and ventricular tachycardia/fibrillation (VT/VF) are among the leading causes of morbidity and mortality in the developed world. AF is the most common sustained arrhythmia and is associated with an increased risk of stroke, heart failure, dementia, and death. In developed nations overall prevalence of AF is 0.9% and the number of people affected is projected to more than double over the next 2 decades. VT/VF is the most important immediate cause of sudden cardiac death (SCD). Incidence of SCD is estimated to be 4 to 5 million cases per year worldwide. Thus arrhythmias and SCD are among the most significant manifestations ofcardiovascular diseases worldwide, but their underlying mechanisms remain elusive.*" Over the years, many researchers have developed, tested and sometimes validated hypotheses regarding the nonlinear dynamics of sudden changes in cardiac dynamics associated with arrhythmias. We will review crucial instabilities and disruptions of the normal heartbeat like alternans, rotor dynamics and electrical turbulence and the related theoretical approaches.

Nowadays, the incorporation of available experimental data - obtained from electrophysiological studies of cardiac muscle cells, electrocardiogram (ECG) recordings, optical imaging of the voltage and calcium content in cardiac tissue, or magnetic resonance imaging (MRI) of the anatomy and the mechanical motion of the heart permits the developments of detailed and realistic models of the heart. The adequate representation of the normal function of the heart and of various forms of CVD presents big challenges for mathematical modeling and simulations. The heart acts as an electromechanical pump, and its complete mathematical description would have to take into account electric wave propagation, muscle contraction and blood fluid dynamics making cardiac modeling a formidable multiphysics problem [5]. A second equally formidable task is the integration of largely different spatial and temporal scales in cardiac modeling. It is of great relevance to predict the impact of mutations as well as the influence of pharmacological substances on the organ function of the heart in simulation studies. Attempts in this direction require not only models at different levels - from molecules and cells to tissue and organs - but also multiscale approaches that

allow to estimate the impact of processes at small scales on the dynamics at larger scales [6, 7]. Consequently, continuum models at tissue and organ level are typically derived by mathematical homogenization procedures that average over a microscopic scale [8]. A prominent example of this approach in cardiac modeling is the derivation of the macroscopic spatially homogeneous, continuum bidomain equations for electrical propagation from a homogenization procedure that averages over the discrete and potentially heterogeneous microscopic cellular scale [9, 10]. Most studies that focus on the electrical propagation and the related dynamic diseases like tachycardias and fibrillation in the atria and ventricles employ the monodomain equations that can be derived as an approximation of the bidomain model [11]. The monodomain equation describes electrical wave propagation in the heart by coupled reaction-diffusion type equations that are prototype models in nonlinear dynamics of spatially extended systems [12]. The theory of nonlinear dynamics has introduced important concepts like the distinction between periodic and chaotic dynamics as well as classification of bifurcations that describe parameter-dependent qualitative changes in the dynamics in a unified language [13]. Early on, it was realized, e.g., by Glass and Mackey, that physiological rhythms such as the heartbeat offer a rich variety of nonlinear dynamical behavior and the concept of dynamical diseases was introduced [14]. In an equally pioneering spirit, Winfree pointed out the link between cardiac arrhythmias and generic dynamics of excitable media [15].

The present review will focus mostly on electrical wave propagation in the heart. It will thus not provide a complete mathematical framework for cardiac dynamics and mostly neglect phenomena that involve mechanical aspects (e.g., the contraction and motion of the heart) or fluid dynamics (e.g., with cardiac valves or arteries that involve fluid dynamics). The aim of this review is twofold: on the one hand, we will discuss phenomena familiar to cardiac modelers and cardiologists from the viewpoint of the theory of nonlinear dynamics in excitable media; on the other hand, we would like to provide a presentation of the basics of cardiac electrical wave propagation in a form that is familiar to researchers working on nonlinear dynamics. This, we hope, will help to overcome potential barriers of understanding, resulting from the different terminologies used by physicians and biologists on the one side and computational and mathematical modelers on the other side. Due to this broad scope, we have sacrificed a natural historical prospective on the development of the different concepts to provide a more tractable version. Our goal is to stimulate thereby the communication of the rapidly growing community of cardiac modelers with scientists from the areas of nonlinear physics and applied mathematics. These disciplines have developed suitable tools of theoretical and numerical analysis that may support the impressive efforts in modeling and simulation of the heart. In particular, we will put our focus on the understanding of arrhythmias and fibrillation. Hopefully this will attract the attention from people generally interested in modeling of nonlinear systems into mathematically challenging problems that pertain to important issues of cardiac modeling.

With respect to electrical propagation, the basic local dynamics at the cellular

level describe the temporal evolution of the transmembrane voltage (i.e. potential difference accross the cell membrane) and of the important ionic channels (i.e. membrane proteins allowing the flow of ions across the cell membrane). The resulting equations are based on experimental data from physiological measurements at the cellular level and are extended to the tissue level by assuming a resistive intercellular coupling. This combination of local cellular dynamics and the spatial coupling between cells yields a set of nonlinear reaction-diffusion equations, that exhibit solitary pulses and pulse trains as solutions, characteristic of excitable systems, and describe the propagation of action potentials in the tissue. A finite superthreshold perturbation can bring these systems far from their stable quiescent state for a given amount of time known as action potential duration, that typically depends on the time elapsed from the previous excitation.

Many cardiac malfunctions are associated with disturbances of normal propagation, sometimes involving the formation of re-entries often called rotors (i.e., sustained rotational electrical activity in cardiac tissue), which are believed to underlie ventricular tachycardias (VT) characterized by a rapid heartbeat [16, 17]. Note, that the term "rotor" similar to the term "pinwheel" was originally introduced by Winfree [18] to denote the center of the spiral wave. In physics literature this region is usually called the "core" [19], while in contemporary medical literature the term "rotor" is often used as a synonym to "spiral wave" , see e. g. [20]. They also constitute one building block of ventricular fibrillation (VF), a particularly dangerous malfunction of the heart, in which synchronous excitation and contraction of different parts of the ventricles is lost, potentially causing sudden death if left untreated for more than a few minutes. Re-entries underlying VT are usually rotors or spiral waves, and are sketched as spiraling excitationsrotating around an unexcited core (i.e., neighborhood of the internal end of such wavefront). A common explanation for the transition from VT to VF is related to breakup of an initially created rotor near [21] or far-away [22] its core, resulting in the continuous creation and destruction of spirals or to breakup of scroll waves (i.e., rotating waves in resp. two or three-dimensional media with a spiral-like shape around an unexcited filament). Thus, a major challenge is to classify and understand the mechanisms that cause, first, the creation of rotors, and second, their subsequent destabilization.

Although most biologically relevant mechanisms of rotor initiation are driven by tissue inhomogeneities, this review will deal mostly with homogeneous, continuous models that describe the tissue and organ scale of cardiac propagation. This is done typically by comparing phenomena observed in simple cardiac models with even simpler, generic models for propagation in excitable media. As a result, we neglect a number of important issues in the cardiac modeling that have been covered in depth in preceding, excellent reviews and books. More details on electrophysiological cell models that form the basis of models for cardiac propagation by giving the local excitable dynamics are summarized, e.g., in the book by Pullan et al. [23] and in an article by Fenton and Cherry [24]. A more detailed account on the basic mechanism of cardiac propagation than the one provided by us below was given by Kleber and Rudy [25].

We neglect also many recent efforts towards an improved and extended modeling of the intracellular calcium dynamics as an active process that typically requires a stochastic modeling approach. For more information on these topics see, e.g., the excellent reviews by Falcke [26] for a general discussion of intercellular calcium handling and by Qu and colleagues [27] for a description of recent progress on stochastic calcium dynamics in cardiac cells. Recently, many efforts have been undertaken to employ information on cardiac anatomy and geometry from MRI imaging, histology and other experimental techniques in order to built realistic models of three dimensional propagation. We do not cover these topics here and refer to the articles by Plank, Bishop, Clayton, Smaill, Lamata and colleagues [28–32].

Moreover, a number of shorter review articles are also available which offer valuable information on the central topics of nonlinear dynamics and cardiac arrhythmias discussed in this article. A short survey on cardiac arrhythmias can be found in the article by Fenton et al. [33]. The phenomenologies of alternans [34, 35] and fibrillation [36] as well as a dynamics-based classification of ventricular arrhythmias [37] were given by Weiss and colleagues. The current understanding and experimental knowledge on the role of spirals (or rotors) is summarized in a short review by Pandit and Jalife [20]. A shorter concise review of the physics of cardiac arrhythmogenesis was presented by Karma [38].

This review is organized as follows: In the next section, we consider basic facts regarding the electrophysiology of the heart at different scales. Mathematical details of the models needed for the rest of the review are described in Section 3. Aspects of wave propagation in excitable media in general and cardiac tissue in particular are introduced in Section 4, that discusses also the influence of heterogeneities and geometry effects. Different types of dynamics are studied in Sections 5-7, namely alternans in one dimension, meandering and breakup in two dimensions and instability of scroll waves in three dimensions. Methodic approaches to analyze these instabilities are discussed in Section 8. Finally, Section 9 provides a summary of the main results and a short discussion and outlook for future investigations.

2. Electrophysiology of the cardiac electrical activation

2.1. The heart

Situated at the chest cavity, between the right and left lungs, and supported by a membranous structure, the heart is a muscle that pumps blood throughout the body. The pumping is generated by a coordinated contraction, triggered by an electrical impulse that propagates along cardiac tissue. The heart is separated in two halves and has four main chambers. The lower chambers are the ventricles, while the smaller upper chambers are called atria. The cardiac muscle, or myocardium, constitutes the bulk of the heart. In Figure 1 the main parts of the heart are identified.

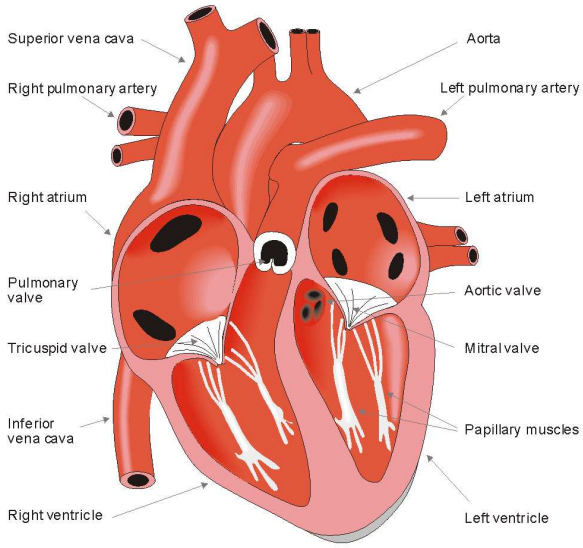

Figure 1. Explanatory sketch of the different parts of heart, including the four electrically active chambers: two atria and two ventricles; and the main elements of the heart's blood circulation system, including most relevant arteries and veins. Reprinted from the free open access book [39].

The heart is composed of cardiac muscle with intervening connective tissue, blood vessels and nerves. Cardiac tissue is divided into three layers called endocardium, myocardium and epicardium. The endocardium and epicardium are the internal and external layers, respectively. In the middle lies the myocardium, thicker than the former. Between the endocardium and myocardium is the subendocardial layer, where the impulse-conducting system (Purkinje fibers) is located.

2.2. The cardiac myocytes

Cardiac cells are called myocytes, having a length of $80 - 100\mu$m and a diameter of $10 - 20\mu$m. Each of these cells is separated from the extracellular space by a phospholipid bilayer membrane. This membrane presents selective permitivity, allowing

some ions (Na^+, K^+, Ca^{2+}, etc) to flow between the extracellular and intracellular media through a set of specific ion channels. The resulting charge imbalance produces a transmembrane potential difference, whose evolution is governed by the balance between the electrical and chemical gradients across the membrane of the cell. The potential at which chemical and electrical forces are in equilibrium is called the reversal or Nernst potential, and is specific to each ion. The potential at which the cell is at rest is known as the resting potential, and in cardiac cells its value is typically around -85 mV. If a sufficiently large stimulus is given to the cell, the transmembrane potential rises above a threshold potential and an active response occurs, known as an action potential. The amplitude of a cardiac action potential is of the order of 130 mV.

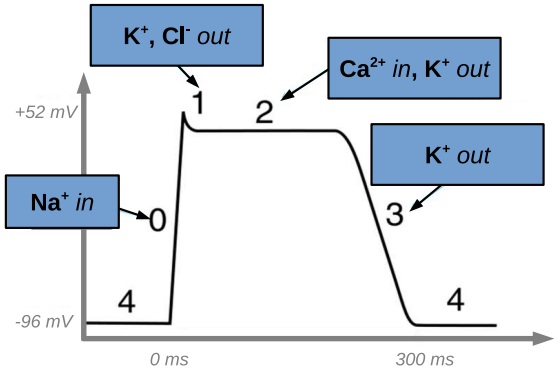

Figure 2. Sketch of a typical action potential in a ventricular myocyte. Phases and ion currents responsible for the action potential: sharp increase due to sodium influx (0), rapid decrease due to potassium outflux (1), balance currents and plateu phase (2), end of calcium influx (3) and return to the resting potential (4).

In Figure 2, a typical time evolution of the transmembrane potential is shown, resulting in an action potential with different phases. *Phase 0* is characterized by a sharp stroke due to rapid influx of sodium ions. During *phase 1* there is a rapid decrease in the membrane potential due to a fast outward potassium current. This is then balanced by the inward Ca^{2+} currents giving rise to the characteristic plateau of *phase 2*. Finally, in *phase 3* the calcium currents cease and the membrane returns to its resting potential, or *phase 4*, due to a slow outward potassium current. In summary, during *phase 0* there is a depolarization (i.e., change in membrane potential from negative to positive values) of the cell membrane while *phase 3* corresponds to repolarization (i.e., change in membrane potential that returns it to a negative value) of the membrane.

Myocytes are connected to each other by means of intercalated discs, which are responsible of the mechanical and electrical coupling among cells. The latter is produced through gap junctions (i.e., pipe-like channels that permit the flow of ions from one cell to another). This results in the propagation of the action potential in tissue, giving rise to an excitation wave, with a propagation speed characteristic of the type of cardiac

tissue. Gap junctions are located at the longitudinal ends of the myocytes, that are bundled in cardiac fibers along which the propagation speed is faster. Thus, cardiac action potential propagation is both discrete and anisotropic.

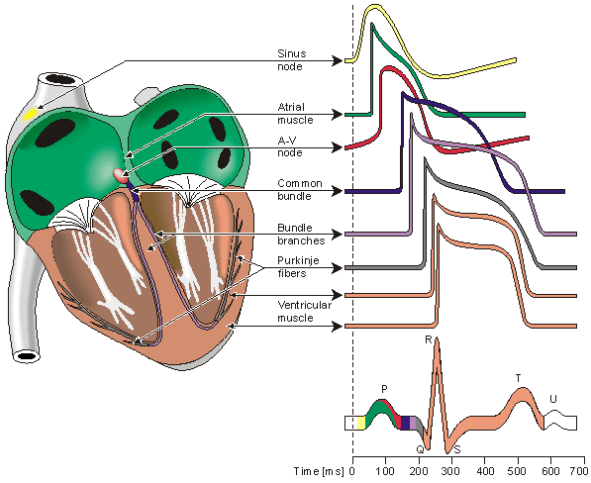

Figure 3. Conduction system of the heart and its relation to the electrocardiogram. The P waves are related to the atrial signal, the QRS complex to the depolarization of the ventricles, and T waves to the repolarization of the ventricles. Reprinted from the free open access book [39].

2.3. Electrical activity propagation

Cardiac electrical activity is initiated at the sinoatrial node (i.e., the natural pacemaker of the heart) where action potentials are produced periodically. Then, the electrical impulse is propagated along the atrium and, through the atrio-ventricular node, to the His bundle. It finally arrives at the ventricular myocardium through the Purkinje fibers (Figure 3), depolarizing first the endocardium and proceeding transmurally to the epicardium.

The electrical activity of the heart is visible in the electrocardiogram (ECG). In this, a series of electrodes is set on a person's thorax, that record the small voltage changes at that point (of the order of the microvolt). The voltage difference between a pair of electrodes is known as a lead. For a typical 12 lead ECG, 10 electrodes are needed, that are placed on the right and left arms (RA and LA), right and left legs (LR and LL), and on the chest (precordial electrodes V_{1-6}). From the recordings of these electrodes, the different leads are defined. With the ECG both the rhythm and the morphology of the cardiac excitation is recorded. The several phases of propagation along the heart leave different traces in the ECG (Figure 3). Thus, anomalies in propagation result in distinctive variations of these waves in the different leads.

The propagation of the electrical impulse gives rise to a series of events that result in the contraction of the heart (Figure 4). The depolarization of the cell membrane induces an inward flux of extracellular calcium ions through L-type calcium channels.

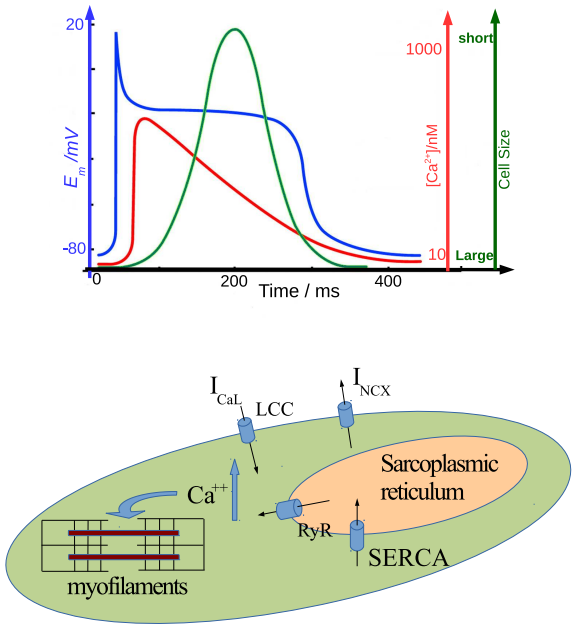

Figure 4. Excitation-contraction coupling. Top: Dynamics of the membrane action potential (blue), the concentration of calcium (red) and contraction of the myocyte (green). Bottom: During depolarization, calcium enters the cell through the L-type calcium channels (LCC), opening the calcium gated ryanodine receptors (RyR) and releasing the calcium content of the sarcoplasmic reticulum. This induces the shortening of the myofilaments and the contraction of the cell.

This elevates the Ca concentration in the cytosol, allowing the release of calcium from the sarcoplasmic reticulum (SR) (i.e., cell organelle that sequesters intracelullar calcium) increasing further the calcium concentration in the cytosol in a process known as calcium induced calcium release (CICR) (Figure 4). Then calcium binds to the thin-filament protein troponin C (TnC), allowing myosin (i.e., type of molecular motor) heads to bind to actin filaments and pull them by a process called a power stroke. Besides, the presence of stretch-activated channels at the cell membrane results in a feedback from contraction to action potential propagation. In this way, the coupling between excitation and contraction represents a complex process, that involves the dynamics of transmembrane potential, ion currents, intracellular calcium concentration, stretching-induced currents, and fibers strain and stress.

2.4. Cardiac arrhytmias

The contraction of the heart is thus generated by a single wave of electrical excitation, see Fig. 5(a), that signals the cells to contract in a smooth and highly coordinated way for pumping blood to the body. Tachycardia corresponds to a rotor that accelerates the rate of contraction, and typically is associated to a spiral wave, see Fig. 5(b). Fibrillation occurs when the normal electrical activity is masked by higher frequency circulation waves which create small, out-of-phase localized contractions. Even if these contractions

can be created by small foci of cardiac stimulus, the most prevalent hypothesis is that one or more spiral waves break into multiple waves leading to fibrillation. It can be transient or degenerate into fibrillation if the spiral wave breaks, see Fig 5(c). The mechanisms leading to arrhytmias and fibrillation are diverse and have been studied both experimentally and computationally, for a review see [40].

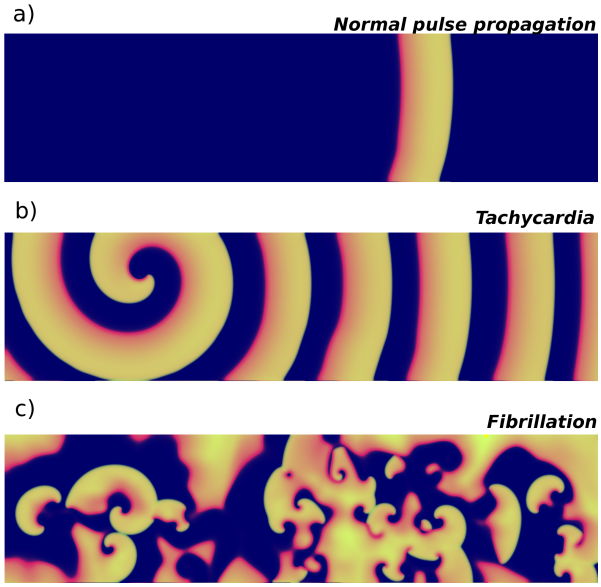

Figure 5. Two dimensional sketch of the regular action potential propagation through the tissue (a), a periodic rapid re-entrant wave related with tachycardia (b), and irregular dynamics related to fibrillation (c).

Ion	Extracellular (mM)	Intracellular (mM)	Nernst Potential (mV)
Na^+	145	15	60
K^+	4.5	160	-95
Ca^{2+}	1.8	0.0001	130
Cl^-	100	5	-80

Table 1. Typical concentration of ions in the intracellular and extracellular media and associated Nernst potentials.

3. Mathematical description of the action potential propagation

3.1. Action potential

3.1.1. Nernst potential. In a cell, a phospholipid bilayer separates the intra and extracellular media, resulting in a difference in the concentration of the different ions across the cell membrane. The membrane is full with proteins that act as ion channels and ion pumps, that allow the passive or active transport of ions across the membrane. All together, the cell membrane is equivalent to a set of (voltage dependent) resistors, batteries, and a capacitor.

Due to the concentration difference between the intra and extracellular media, there exists a potential difference, known as the Nernst potential, specific to each kind of ion. If the potential in the intra and extracellular media is V_{i0} and V_{e0}, respectively, then, according to Boltzmann statistics, the probability of finding an ion in each medium is:

$$p_i \propto \mathrm{e}^{-eV_{i0}/k_BT}; \;\; p_e \propto \mathrm{e}^{-eV_{e0}/k_BT}, \tag{1}$$

where e is the elementary charge and k_B is the Boltzmann constant.

The ratio in the concentrations is equal to the ratio of probabilities, so

$$\frac{c_i}{c_e} = \frac{\mathrm{e}^{-eV_{i0}/k_BT}}{\mathrm{e}^{-eV_{e0}/k_BT}}, \tag{2}$$

resulting in the equilibrium potential difference, or Nernst potential

$$V_{Nernst} = V_{i0} - V_{e0} = \frac{RT}{F} \ln \frac{c_i}{c_e}, \tag{3}$$

where $F = eN_A$ and $R = k_BN_A$ are the Faraday and gas constants, respectively.

3.1.2. Ion currents. The total potential drop across the membrane for a given ion is obtained from the concentration difference between the interior and the exterior of the cell, i.e. the Nernst potential, see Eq. (3), plus the potential drop due to the current across the corresponding ion channel, assuming that the channel is ohmic. For a schematic version of the two components see Fig. 6. Then, the transmembrane potential can be written as

$$V = r_X I_X + V^X_{Nernst}, \tag{4}$$

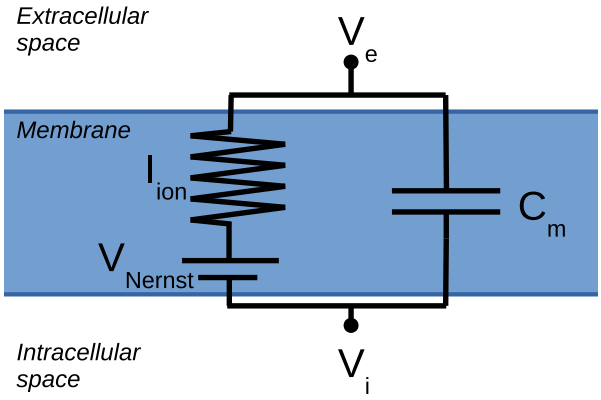

Figure 6. Electric circuit model of the membrane action potential of a myocyte including the capacitance, resistivity and the rest potential of the membrane.

where r is the channel resistance, the transmembrane potential V is the difference between the potentials in the intra- and extracellular media $V = V_i - V_e$ and I_X is the transmembrane current, where the subindex X corresponds to the ion considered. Then, for each ion there is a current across the cell membrane that is proportional to the difference between the transmembrane potential and its equilibrium Nernst potential

$$I_X = g_X(V - V^X_{Nernst}), \tag{5}$$

where $g_X = 1/r_X$ is the membrane conductance for that ion. Such linear dependence on the potential can be derived from more realistic calculations and, for specific ions it agrees with experimental current voltage I-V curves, see an example in Figure 7. For some ion currents other approaches based on the Goldman-Hodgkin-Katz current equation are more adequate [11].

The conductances g_X are in general not constants, but depend on membrane voltage. The permeability of the channels is regulated by the state of gates which permit the pass of ions through the channel. The gates represent the state of proteins which open and close the corresponding channel in response to, for instance, a change in transmembrane voltage. The dynamics of the gates is described by Hodgkin-Huxley type equations [41] for w, i.e. the opening probability of the gate:

$$\frac{dw}{dt} = \frac{w_\infty(V) - w}{\tau_w(V)}, \tag{6}$$

where the functions $w_\infty(V)$ and $\tau_w(V)$ can be obtained experimentally measuring the current-voltage relations. Thus, $g_X = g_X(V, w, ...)$, together with the opening and closing dynamics of the gates describe the dynamic value of the conductances.

The total current carried by all ions is just $I_{ion} = \sum_X I_X$. In steady state the total current is zero $I_{ion} = 0$, so the resulting resting potential V_r can be expressed in terms of the Nernst potential and the conductances of the different ions:

$$V_r = \frac{\sum_X g_X V^X_{Nernst}}{\sum_X g_X}. \tag{7}$$

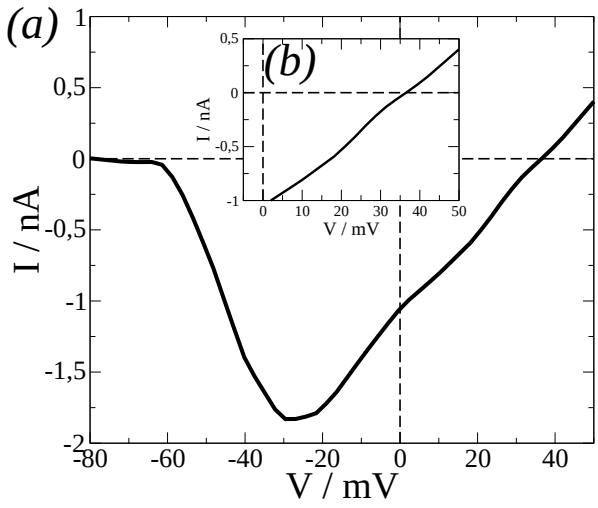

Figure 7. I-V relationship for the Na current. In the inset the linear regime around the Nernst potential is shown.

In addition to the ion current, there is a capacitive current related to the accumulation of charge at the membrane $I_m = dQ/dt = C_m dV/dt$. Since global charge is conserved, the sum of all the currents must be zero, resulting in:

$$C_m \frac{dV}{dt} = -\sum_X I_X, \tag{8}$$

which determines the action potential, that is specific for each type of cell (ventricular, atrial, etc), and for each species.

3.2. Connection among cells

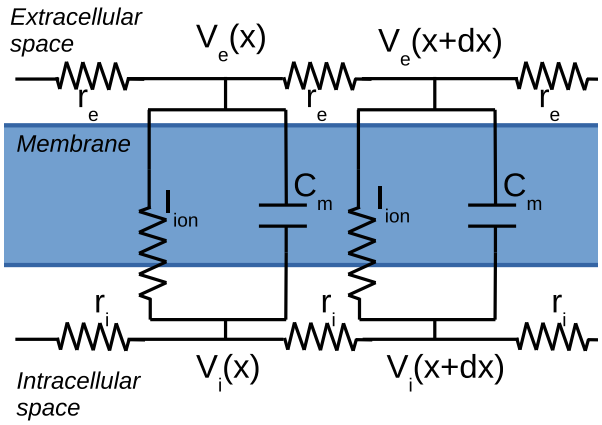

Figure 8. Electric circuit model of the membrane action potential including the capacitance, resistances in intracellular and extracellular media.

3.2.1. Intracellular action potential propagation. The standard way of introducing intercellular coupling is through the cable equation, originally developed to treat action

potential propagation along nerve cells. In this formulation, the potential is considered to vary along the longitudinal direction of the cell, while it is constant in the transversal (or radial) directions. Due to the variation of transmembrane potential along the cable, intra- and extracellular axial currents per unit length appear, given by [11]:

$$\begin{aligned} I_i(x) &= g_i[V_i(x+dx) - V_i(x)]/dx, \\ I_e(x) &= g_e[V_e(x+dx) - V_e(x)]/dx; \end{aligned} \tag{9}$$

where we have assumed that Ohm's law is satisfied and g_i, g_e are the conductances per unit length of the intra- and extracellular media.

Also, from Kirchhoff's law, the sum of the currents entering and leaving a given point must sum up to zero, so:

$$I_i(x) - I_i(x+dx) = I_t dx = I_e(x+dx) - I_e(x). \tag{10}$$

Besides, the transmembrane current is the sum of the ionic and capacitive currents:

$$I_t = p\left(C_m \frac{dV}{dt} + I_{ion}\right), \tag{11}$$

where p is the perimeter of the cell. In the continuous limit $dx \to 0$, the previous equations become

$$I_i(x) = g_i \frac{\partial V_i}{\partial x}, \quad I_e(x) = g_e \frac{\partial V_e}{\partial x}, \tag{12}$$

and

$$I_t = -\frac{\partial I_i}{\partial x} = \frac{\partial I_e}{\partial x}, \tag{13}$$

Substituting in Eq. (11) one obtains the one dimensional bidomain model

$$p\left(C_m \frac{\partial V}{\partial t} + I_{ion}\right) = \frac{\partial}{\partial x}\left(g_i \frac{\partial V_i}{\partial x}\right) = -\frac{\partial}{\partial x}\left(g_e \frac{\partial V_e}{\partial x}\right), \tag{14}$$

or, using $V_i = V + V_e$:

$$p\left(C_m \frac{\partial V}{\partial t} + I_{ion}\right) = \frac{\partial}{\partial x}\left(g_i \frac{\partial V}{\partial x}\right) + \frac{\partial}{\partial x}\left(g_i \frac{\partial V_e}{\partial x}\right). \tag{15}$$

Besides, from Eq. (13), it is satisfied that:

$$\frac{\partial}{\partial x}\left(g_i \frac{\partial V_i}{\partial x} + g_e \frac{\partial V_e}{\partial x}\right) = \frac{\partial}{\partial x}\left[g_i \frac{\partial V}{\partial x} + (g_i + g_e)\frac{\partial V_e}{\partial x}\right] = 0, \tag{16}$$

Eqs. (15) and (16) constitute the bidomain formulation of the cable equation. In one dimension with homogeneous conductances it is always possible to reduce it to a monodomain model, just noticing that, from Eq. (13), the divergence of the total axial current is zero

$$\frac{\partial}{\partial x}(I_i + I_e) = \frac{\partial}{\partial x}\left(g_i \frac{\partial V_i}{\partial x} + g_e \frac{\partial V_e}{\partial x}\right) = 0, \tag{17}$$

whose solution is:

$$g_e \frac{\partial V_e}{\partial x} = -g_i \frac{\partial V_i}{\partial x} + C, \quad \text{or} \quad \frac{\partial V_e}{\partial x} = -\frac{g_i}{g_i + g_e}\frac{\partial V}{\partial x} + \frac{C}{g_i + g_e}, \tag{18}$$

from which we obtain the monodomain cable equation:

$$p\left(C_m\frac{\partial V}{\partial t}+I_{ion}\right)=\frac{\partial}{\partial x}\left(\frac{g_i g_e}{g_i+g_e}\frac{\partial V}{\partial x}\right), \tag{19}$$

where we can define an effective conductante $g_{eff}=g_i g_e/(g_i+g_e)$, which is the harmonic mean of the conductances

$$\frac{1}{g_{eff}}=\frac{1}{g_i}+\frac{1}{g_e}, \tag{20}$$

which ensures a null conductance if any of the conductances is zero [11].

3.2.2. Intercellular action potential propagation. So far, the equations derived above are valid for propagation in a single cardiomyocyte. For the modeling of tissue one has to consider cardiac cells coupled through gap junctions, and different approaches can be employed.

Continuum model. In the continuum model one has to solve the cable equation in each cardiomyocyte and impose boundary conditions at the gap junctional space, such that

$$g_i\frac{\partial V_i}{\partial x}(x=x_j^-)=g_i\frac{\partial V_i}{\partial x}(x=x_j^+)=g_j V_j, \tag{21}$$

where g_j is the gap junction conductance, x_j^+ and x_j^- represent the positions of the right and left sides of the junction, and $V_j=V_i(x=x_j^+)-V_i(x=x_j^-)$ is the intracellular voltage drop across the gap junction. A simpler formulation is to consider the continuum cable equation (19), but for an effective conductance g_{eff} that is an average of the conductances at the intracellular medium and gap junctional spaces in a similar way than the harmonic mean employed in Eq. (20) and obtained from a homogenization approach [42]. In any of these cases, the difference between a continuum and a discrete description only appears when studying the effects of propagation failure [43], typical for low conductivities and determined by the interplay between the properties of the action potential of the myocytes and structural properties of the tissue.

Isopotential model. An alternative approach is to assume an isopotential model, in which the whole cell is at the same potential and the potential drops occur only at the gap junction resistances. Then, one should consider the discretized version of the continuum equations, with a spatial step equal to the size of the cell $dx\simeq 100\mu$m, and $g_i\equiv g_j$, the gap junction conductance. Such a model is convenient when considering the effects of the time and voltage dependence of the gap junction conductances. In general terms $g_j=g_j(V_j,t)$, where V_j is the transjunctional potential, so $V_j=V_i^{n+1}-V_i^n$ is the difference in intracellular potential of the two cells joined by the gap junction. The gap junction itself behaves as a gate, so

$$\frac{dg_j}{dt}=\frac{g_{ss}(V_j)-g_j}{\tau_j(V_j)} \tag{22}$$

with the steady state conductance and time constant depending on the intercellular potential, such that

$$g_{ss} = g_{min} + \frac{g_{max} - g_{min}}{1 + \exp\left[A(V_j - V_{1/2})\right]}, \qquad \tau_j(V_j) = \tau_{j0} e^{-V_j/V_\tau}. \tag{23}$$

Typical values are $V_{1/2} \sim 40 - 60$ mV, $V_\tau \sim 15$ mV, and $\tau_{j0} \sim 100$s [44]. For typical wave speeds of 50-70 cm/s and durations of the upstroke of $\sim 3 - 5$ ms the width of the front of the depolarization pulse is $\sim 0.15 - 0.45$cm, corresponding to 15-45 cells. Given the upstroke voltage difference of ~ 100mV, then the voltage difference between cells is, at most, $\sim 6 - 7$mV. Thus, under normal conditions, the dynamics of the gap junction conductances does not seem to play a role, and one can assume it to be constant. However, in some cardiac diseases there is a reduction or redistribution of the protein molecules forming gap junction channels, from intercalated disks to lateral cell borders [45]. The resulting gap junction and connexin expression remodeling [46, 47] reduces conduction velocity and enhances anisotropy in diseased myocardium [48].

3.2.3. 3D formulation. A generalization of the cable equation to three dimensional tissue can be made, assuming that cardiac tissue is composed of two media, so at each point of space we can define intracellular and extracellular potentials. Then, assuming Ohm's law, we can write the currents as $J_e = \sigma_e \nabla V_e$, $J_i = \sigma_i \nabla V_i$, where $\sigma_i(\mathbf{x})$ and $\sigma_e(\mathbf{x})$ are the conductances of the intra- and extracellular media, that in this case are assumed to be of tensorial character, so they define directions where propagation is faster (or slower) and depend on the distribution of cardiac fibers in tissue. Here, implicitly we are assuming that these conductances are average values over gap junctions, inhomogeneities, etc. Again, applying Kirchhoff's law, we obtain the bidomain model for three-dimensional tissue, which are the equivalent of Eqs. (14) and (17):

$$\chi \left(C_m \frac{\partial V}{\partial t} + I_{ion} \right) = \nabla \cdot (\sigma_i \nabla V_i) = -\nabla \cdot (\sigma_e \nabla V_e), \tag{24}$$

$$\nabla \cdot (\sigma_i \nabla V_i + \sigma_e \nabla V_e) = 0; \tag{25}$$

where now χ is the ratio of surface to cell volume. In the case when $\sigma_i = \lambda \sigma_e$, so the anisotropy ratios are the same in the intracellular and extracellular media (which is not the case in cardiac tissue), the above description can be reduced to a monodomain equation for the transmembrane potential. In effect, in this case

$$\nabla \cdot (\sigma_e \nabla V_e) = -\frac{\lambda}{1 + \lambda} \nabla \cdot (\sigma_e \nabla V), \tag{26}$$

so we obtain the monodomain equation:

$$\chi \left(C_m \frac{\partial V}{\partial t} + I_{ion} \right) = \frac{\lambda}{1 + \lambda} \nabla \cdot (\sigma_e \nabla V). \tag{27}$$

Then, the propagation of the transmembrane potential is described by the equation:

$$\frac{\partial V}{\partial t} = -\frac{I_{ion}}{C_m} + \nabla \cdot (D \nabla V), \tag{28}$$

where typical values of the membrane capacitance are $C_m \sim 1 - 10\mu\text{F/cm}^2$, varying for different types of cells or different species [49]. The diffusion coefficient $D \sim 0.001$ cm^2/ms is derived from the resistivity between cells, and the cell capacitance and surface to volume ratio [11]. Resistivity and surface to volume ratio, usually obtained from an approximation of a cardiac cell by a cylinder, may also change from cell to cell.

For the rest of the review we will consider the monodomain description of cardiac tissue propagation Eq. (28). Although this is not a correct description for two and three-dimensional tissue [50], since the intracellular medium is more anisotropic than the extracellular medium, it is usually a sufficient description of action potential propagation in most situations. A relevant exception is the case of defibrillation, where a bidomain description is required [51, 52]. The injection of current into resting cardiac tissue produces the formation of virtual electrodes, that are thought to be behind the mechanism by which an external electric shock is able to annihilate reentrant waves. Such virtual electrodes are virtual cathodes and anodes resulting from unequal anisotropy ratios of the intracellular and extracellular spaces of the cardiac [51–53] or from the borders of non-conducting heterogeneities [54, 55].

3.3. Ionic models

Ion currents across the ion channels at the cell membrane are governed by highly nonlinear processes. There are different types of active cells in the heart and the explicit form of the total current I_{ion} depends on the type of cell and species [33].

- *Ventricular myocytes.* The action potential dynamics of ventricular myocytes has been amply studied. There is a large list of ventricle cell models [33], which are developed for different type of species, from mice or rabbits to dogs and humans. The ventricles are the largest chambers of the heart and where electrical discoordination becomes more dangerous [56]. Furthermore the thickness of the ventricular walls makes it necessary to consider the three-dimensional structure of the tissue.
- *Atrial myocytes.* The models for atrial cells are characterized by a short action potential due to the reduced calcium current with respect to ventricular myocytes. There are several models for the action potential of atrial cells, for a comparison between two of the latest models in human tissue see [57].
- *Cells forming the sinoatrial node.* The regular activity of the heart is initiated by this specialized population of cardiac cells. Their membrane potential oscillates periodically [58], generating electrical oscillatory signals. A detailed comparison of all the numerical models of automaticity has been recently presented [59].
- *Purkinje fibers.* The first models of cardiac cells were derived for this type of cells [60]. The network of the Purkinje fibers produces a fast conduction pathway to transmit electrical excitation from the atria into the ventricles [61]. The action potentials of the myocytes at the Purkinje fibers present characteristic features:

the velocity of propagation is faster than in other types of cardiac cells, and the action potential duration is longer [61]. These cells can also present automaticity and produce oscillations. For a review of several models of the Purkinje fibers cells see [62].

For concreteness, in this review we focus in models of ventricular cardiac tissue. A full description of all the possible ion currents, together with the dynamics of the ion channel gates, is complex and produces models with a large number of equations. In contrast, generic models try to reproduce the main properties of such ion currents with a reduced number of parameters. In this section, we classify the models employed for the study of wave instabilities in cardiac tissue in three classes. First, we consider realistic ionic models that describe in detail several ion currents across the cell membrane. Second, we study simple cardiac models that fit the main characteristic experimental features of the action potential into simpler formulations. Finally, we consider generic models of excitable media.

3.3.1. Detailed electrophysiological models. Electrophysiological detailed models [30] are based on direct experimental observations from voltage and patch clamp studies. Typically, these models include many Hodgkin-Huxley type equations [41] to describe individual ion currents (I_X) forming the total current $I_{ion}(V, w, p_i) = \sum_X I_X$ across the cell membrane [63]. Modern ionic models also describe the changes of concentrations of all major ions inside cardiac cells, and generally consist of anywhere between 10 and 60 equations [64, 65]. The quantitative descriptions of ion currents in cardiac tissue are continually being revised, and there is not general agreement on the best model for all circumstances [66]. Detailed models are adequate to numerically explore the effects of different drugs in the propagation properties of the action potential [67]. The nonlinear terms are typically stiff so adaptive methods are usually required to obtain fast integration speeds [68, 69].

Below, we present some detailed electrophysiological models that have been amply used in studies of cardiac wave propagation.

- *Beeler-Reuter model.* One of the first models of action potential in ventricular myocytes is the Beeler-Reuter model [70]. It was the first ionic model used to simulate spatio-temporal propagation in two dimensions [71]. It reproduces important experimental phenomena by the use of four individual ion currents in terms of Hodgkin-Huxley type equations. The total current for this model is $I_{ion} = I_{Na} + I_{Ca} + I_{x1} + I_{K1}$, where the corresponding ion currents are:

$$\begin{aligned} I_{Na} &= (G_{Na} m^3 hj + G_{NaC})(V - E_{Na}), \\ I_{Ca} &= G_s df(V - E_{si}), \\ I_{x1} &= x_1 0.8 \frac{e^{0.04(V+77)} - 1}{e^{0.04(V+35)}}, \\ I_{K1} &= 0.35 \left(4 \frac{e^{0.04(V+85)} - 1}{e^{0.08(V+53)} + e^{0.04(V+53)}} + 0.2 \frac{V + 23}{1 - e^{-0.04(V+23)}} \right), \end{aligned} \tag{29}$$

where I_{Na} is the fast inward Na^+ current, adapted from the sodium activation parameter determined for squid axon by Hodgkin and Huxley [41]; I_{Ca} is the slow inward Ca^{2+} current, which follows the same functional form; I_{x1} is the time-activated outward current and I_{K_1} is the time-independent K^+ outward current. The dependence on the membrane voltage of the latter two currents is chosen to match current-voltage relations seen in myocardium, and they produce a reasonable plateau and repolarization and it was originally introduced for purkinje fibers modeling in [72]. The values E_{Na}, E_{si} are reversal potentials and m, h, j, d, f and x_1 are gating variables, whose dynamics can be modeled as

$$\frac{dw_i}{dt} = (w_{i\infty} - w_i)/\tau_{w_i}, \tag{30}$$

where w_i represents any of the gating variables, and $w_{i\infty}$ and τ_{w_i}, which depend on V, are the steady state value and the relaxation time constant for the corresponding variable, see Eq. (6). The shape of the action potential can be seen in Fig.9(a) with standard values of the parameters of the model.

This model was posteriorly modified giving rise to several versions of the model. A calcium speedup was introduced in [71] to suppress spiral wave breakup present in the original equations giving rise to the modified Beeler-Reuter model.

- *Luo-Rudy model.* Multitude of results regarding ventricular tissue have been illustrated with the Luo-Rudy phase 1 (LR1) model [64]. It describes the biophysical mechanism of generation of action potential in cardiac guinea pig cells by a relatively small number of state variables and was widely used to study wave propagation in 2D and 3D cardiac tissue [73, 74]. This model speeds up the opening and closing rate coefficients for the sodium current from Beeler-Reuter model, see Eqs. (29), and adds three new currents following the classical Hodgkin and Huxley description. The representation of the total current is $I_{ion} = I_{Na} + I_{si} + I_K + I_{K1} + I_{Kp} + I_b$, where the corresponding currents are:

$$\begin{aligned} I_{Na} &= G_{Na} m^3 hj(V - E_{Na}), \\ I_{si} &= G_{si} df(V - E_{si}), \\ I_K &= G_K x x_1 (V - E_K), \\ I_{K_1} &= G_{K_1} K_{1\infty}(V - E_{K_1}), \\ I_{Kp} &= G_{Kp} K_p (V - E_{Kp}), \\ I_b &= G_b (V - E_b); \end{aligned} \tag{31}$$

where I_{Na} is the fast Na^+ current, I_{si} is the slow inward Ca^{2+} current, I_K is the slow outward K^+ current, I_{K_1} is the time-independent K^+ current, I_{Kp} is the plateau K^+ current, and I_b is a background current with constant conductance. The values E_{Na}, E_{si}, E_K, E_{K_1}, E_{Kp} and E_b are the reversal potentials and m, h, j, d, f and x are again gating variables, whose dynamics can be modeled by Eq. (30).

The sodium conductance G_{Na} controls the speed of the waves [75] and in a general sense the excitability of the tissue, and G_{si} is responsible for the front-tail interaction between the pulses.

An extension of this model is the Luo-Rudy phase 2 (LR2) model that includes a more detailed description of intracellular Ca^{2+} [76].

- *TenTusscher-Noble-Noble-Panfilov model.* This model was developed for human ventricular tissue [65]. It is based on experimental data on most of the major ion currents and includes a basic intracellular calcium dynamics. The model reproduces the experimentally observed data on action potential duration restitution. The representation of the total current is $I_{ion} = I_{Na} + I_{K1} + I_{to} + I_{Kr} + I_{Ks} + I_{CaL} + I_{NaCa} + I_{NaK} + I_{pCa} + I_{pK} + I_{bCa} + I_{bNa}$, where currents through ion channels (for example I_{Na}) and ion exchangers (for example I_{NaCa}) are considered. The ion currents depend on gating variables and a total of 17 equations are integrated to account for the total transmembrane current. The main characteristics of wave propagation obtained with this model were compared with more complex versions of human ventricular models [66].

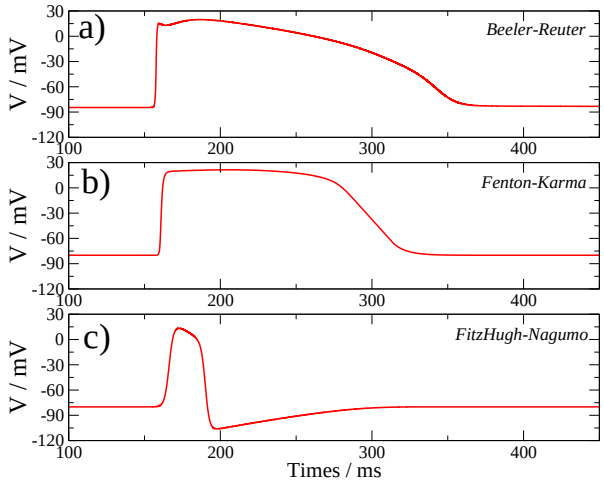

Figure 9. Comparison of the temporal evolution of the action potential for three representative models of the three classes of ionic models: (a) Beeler-Reuter model as electrophysiological model, (b) Fenton-Karma model as a simple cardiac model and (c) the FitzHugh-Nagumo model as generic reaction-diffusion model.

3.3.2. Cardiac models with simplified ion currents. Simple models of cardiac tissue typically consist of a reduced number of equations, between two and four, aimed to reproduce general qualitative properties of the cardiac action potential. Some of these models are obtained as reduction of ionic models [77], but normally they are adaptable models where $I_{ion}(V, w, p_i)$ is a phenomenological expression of V and w with several tuning parameters. Such models can reproduce quantitatively the overall characteristics of cardiac tissue that are relevant for propagation, such as restitution of action potential duration [78, 79] and restitution of conduction velocity [78].

- *Fenton-Karma model.* Perhaps the best known example of a simple cardiac model is the Fenton-Karma model [78], an extension of a previous simpler model [80]. It

consists of the usual cable equation:

$$\frac{\partial v}{\partial t} = -\frac{I_{fi} + I_{so} + I_{si}}{C_m} + \nabla \cdot (D \nabla v), \tag{32}$$

for a renormalized variable v. From this the transmembrane potential can be approximated by $V = (100v - 80)mV$. The three phenomenological currents read:

$$\begin{aligned} I_{fi} &= -up(v - V_c)(1 - v)/\tau_d, \\ I_{so} &= v(1 - p)/\tau_o + p/\tau_r, \\ I_{si} &= -w\left\{1 + \tanh[k(v - V_c^{si})]\right\}/(2\tau_{si}), \end{aligned} \tag{33}$$

mimicking fast inward sodium (I_{fi}), slow outward potassium (I_{so}) and slow inward calcium (I_{si}) currents. The variables u and w are gating variables which are used to regulate inactivation of the fast inward and slow inward currents. Their evolution depends on the transmembrane potential:

$$\begin{aligned} \frac{du}{dt} &= (1 - p)(1 - u)/\tau_u^-(v) - pu/\tau_u^+, \\ \frac{dw}{dt} &= (1 - p)(1 - w)/\tau_w^- - pw/\tau_w^+; \end{aligned} \tag{34}$$

where

$$p = \begin{cases} 1 & \text{if} \quad v \geq V_c, \\ 0 & \text{if} \quad v < V_c, \end{cases} \tag{35}$$

and

$$\tau_u^-(v) = (1 - q)\tau_{u1}^- + q\tau_{u2}^- \quad \text{with} \quad q = \begin{cases} 1 & \text{if} \quad v \geq V_v, \\ 0 & \text{if} \quad v < V_v. \end{cases} \tag{36}$$

The gate variables u and w are related respectively to the product of the gates h and j of the sodium current, as well as to the gate f controlling the inactivation and reactivation of the calcium current, in the more elaborated models of section (3.3.1). Expressions (33) are not based on physical models of realistic ion currents, however the flexibility of the functions Eqs. (34) permits the tunning of the parameters to reproduce different propagation properties of experiments or other more realistic models. Figure 9(b) shows an example of the action potential with this model.
The Fenton-Karma model with different parameter values has been employed to study diverse types of instabilities in cardiac tissue [40]. More realistic action potential shapes have been obtained with the extension of this model by an additional equation [81, 82].

- *Aliev-Panfilov model.* This is another frequently used model with simplified kinetics [79]. It does not describe ion currents but the model is formed by nonlinear functions which may be tuned to reproduce pulse shape and the restitution properties of the canine myocardium with good precision. The model consists of just two equations

$$\begin{aligned} \frac{\partial v}{\partial t} &= -p_0 v(v - p_3)(v - 1) - vw + \nabla \cdot (D \nabla v), \\ \frac{\partial w}{\partial t} &= \left(\epsilon_0 + \frac{p_1 w}{v + p_2}\right)(w - p_0 v(v - p_3 - 1)) \end{aligned} \tag{37}$$

where v is a renormalized transmembrane potential, related to the physiological one by $V = 100v - 80\ mV$. The parameters ϵ_0, p_1 and p_2 specify the scale between v and the control variable w. The parameters p_0 and p_3 determine the shape of the cubic function which controls the action potential dynamics. This model can also be considered an extension of the FitzHugh-Nagumo model, discussed in the next section.

Besides these two models, there is a collection of reduced models created with the same spirit as the ones here described. Other two-variable cardiac models were employed for the incipient simulations of cardiac arrhythmias [83] and the first descriptions of spiral breakup [84].

3.3.3. Generic reaction-diffusion models. Generic excitable media can be described by a system of two coupled reaction-diffusion equations:

$$\begin{aligned} \frac{\partial v}{\partial t} &= \nabla \cdot (D \nabla v) + I(v, w, p_i), \\ \frac{\partial w}{\partial t} &= R(v, w, p_i); \end{aligned} \tag{38}$$

where v corresponds to a scaled transmembrane potential V.

These generic models of excitable media are not derived from physiological data and some properties of the waves often differ from waves of transmembrane potential in physiologically realistic models. Since they do not aim at quantitative agreement, it is usual to consider the functions $I(v, w, p_i)$ and $R(v, w, p_i)$ as simple as possible [85, 86]. A simple model should contain at least a stable equilibrium state, a threshold for wave triggering and a refractory period [87].

The main advantage of these models is their simplicity, together with their ability to reproduce general qualitative properties of cardiac excitation, such as generation and propagation of a pulse, refractory properties, dispersion relations, etc. They are specially appropriate to study features of cardiac wave propagation that are generic to a whole range of excitable media. Besides, due to their simplicity, they allow the implementation of effective numerical solvers and in some cases (or in some limits) they are amenable to analytic treatment. For historical and practical reasons, here we consider three examples of generic models:

- *FitzHugh-Nagumo model.* This historical model was derived in the 60s [85, 88]. It reproduces the plateau observed in cardiac cells which was absent in the Hodgkin-Huxley model of the nerve impulse [63]. The specific form of the reaction terms is:

$$\begin{aligned} I(v, w, p_i) &= \frac{1}{\epsilon} \left(v - \frac{v^3}{3} - w \right), \\ R(v, w, p_i) &= v + p_1 - p_2 w; \end{aligned} \tag{39}$$

  where the parameters p_1 and p_2 specify the inhibitor kinetics. The small parameter ϵ is the ratio of the temporal scales between v and w. The evolution of the model

is shown in Fig. 9(c) in comparison with more realistic description of the action potential. The action potential is shorter than the other type of models because of the inhibitory tail produced by the second variable w.

- *Barkley model.* A very popular simple model for excitable media, given by [89]:

$$\begin{aligned} I(v,w,p_i) &= \frac{1}{\epsilon} v(1-v)\left(v - \frac{w+p_2}{p_1}\right), \\ R(v,w,p_i) &= v - w; \end{aligned} \tag{40}$$

  where ϵ is the ratio of the temporal scales between v and w. The parameters p_1 and p_2 specify the activator kinetics, with p_2 effectively controlling the excitation threshold of the system.
  This model has been widely used for large and systematic numerical studies due to the particularly fast numerical implementation in two [90] and three [89] dimensions.

- *Bär-Eiswirth model.* The Bär-Eiswirth model is an extension of the Barkley model, introduced to study spiral breakup [91]:

$$\begin{aligned} I(v,w,p_i) &= \frac{1}{\epsilon} v(1-v)\left(v - \frac{w+p_2}{p_1}\right), \\ R(v,w,p_i) &= f(v) - w; \end{aligned} \tag{41}$$

  with a different reaction function of the inhibitor:

$$f(v) = \begin{cases} 0 & if \quad v < 1/3 \\ 1 - 6.75v(v-1)^2 & if \quad 1/3 \leq v \leq 1 \\ 1 & if \quad v > 1 \end{cases} \tag{42}$$

  This function leads to inhibitor production only above a threshold value of v, giving rise to a rich variety of patterns.

There are several other examples of generic models which are used to study wave dynamics in excitable media. For example the *Puschino* model, extensively used in incipient numerical simulations of excitable media [92], and its modification [93].

The boundary between generic and simple cardiac models is obviously diffuse and some FitzHugh-Nagumo-like models have been modified to obtain more physiological descriptions of the cardiac tissue by the introduction of additional temporal scales in the model [94].

3.4. Excitation-contraction coupling

In section 2.3 we considered wave propagation in a static medium. The heart, however, contracts, and this effect goes beyond a mere change in the geometry, since it induces a modification of the electrical properties of tissue [95, 96]. This has been shown to have important implications for the creation of a proarrhythmic substrate [97].

3.4.1. Excitation-induced contraction Cardiac depolarization prompts the opening of the L-type calcium channels at the cell membrane, resulting in an influx of calcium ions into the cell. This, in turn, opens the Ryanodine Receptors (RyR) at the sarcoplasmic reticulum (SR), a bag inside the cell where the concentration of calcium is about 1000 larger than at the cytosol, in a process known as calcium induced calcium release (CICR). When the concentration at the cytosol rises, the crossbridge cycle starts through the coupling of Ca^{2+} to the protein complex troponim C (TnC), finally resulting in the generation of force by the muscle fiber. Although complex, the process of generation of force at the cellular level is quite well understood [98]. Unfortunately, it is not easy to translate this knowledge at the cellular level to a macroscopic description. The passive viscoelastic properties of cardiac tissue are not well known, due to its high anisotropy, history dependency, and the combination of contractile and passive material (collagen, connective tissue).

The deformation of the tissue is usually modeled using continuum models of finite elasticity [99, 100] (although discrete models have been also considered [101]). In the former, the conservation of linear momentum gives a condition for local stresses, that in equilibrium results in:

$$\nabla \cdot \sigma + \mathbf{f} = \mathbf{0} \tag{43}$$

where σ is the stress tensor and f are the body forces. To obtain the deformation, stress has to be related to strain and rate of strain, through constitutive equations [99, 100]. During cardiac contraction, the total stress acting at a given point is considered as the sum of active T_a and passive stresses. The expression for the active tension is based in the cross-bridge mechanism, in which the myosin molecules form cross-bridges that interact with the thin filaments in the sarcomeres to generate force. Experiments show that attachment and detachment of cross-bridges depends not only on the current state of the muscle, but also on the history of length changes. Thus, a detailed mathematical model for the development of active tension should take into account the concentrations of intracellular calcium and of calcium bound to Troponin C, the proportion of actin sites available for cross-bridge binding, the length-tension dependence and a force-velocity relation [98]. To circumvent the complex cross-bridge mechanism responsible for the development of active tension, simplified models have been proposed, that couple tension directly to the transmembrane potential $T_a = T_a(V)$ [102].

3.4.2. Stretch activated channels. Besides the contraction of the tissue due to its excitation, there exists electro-mechanical coupling by which mechanical deformation affects the electrical properties of tissue through the opening of stretch activated channels (SACs). This effect is responsible, for instance, of the *commotio cordis*, an often fatal arrhythmia generated by a sudden blow in the chest [103], or of acute cardiac death in ischaemia [95]. The observation that the occurrence of atrial fibrillation is higher upon pressure overload is probably also related to this effect. The ion current I_{SAC} corresponding to the stretch activated channels is added to the cable equation

giving rise to

$$\frac{\partial V}{\partial t} = \nabla \cdot (D\nabla V) + \frac{I_{ion}}{C_m} + \frac{I_{SAC}}{C_m}. \tag{44}$$

In simple formulations [104, 105] I_{SAC} was assumed to be linearly proportional to deformation and to the deviation of the transmembrane potential from its Nernst equilibrium value E_{SAC}, so

$$I_{SAC} = G_{SAC}(\sqrt{C} - 1)(V - E_{SAC}). \tag{45}$$

In fact, it has been observed that the conductance of this current is not a constant, but varies with time, having an activation time of 20 ms to peak current, and then a decay to half the peak current value in about 50 ms [106, 107].

3.5. Anisotropy.

One of the main characteristics of cardiac myocytes is their elongated shape, that induces their alignment in the tissue. A myocyte can be seen as a cylinder 100 μm long and 10-20 μm wide. The fibers of the cell are oriented parallel to their long axis, and contract in such direction.

The gap junctions mainly accumulate at both ends of the cylinder. In tissue, this asymmetrical distribution of gap junctions produces a faster propagation of the action potential along the direction parallel to the myocytes axis than perpendicularly to it, with a 2:1 velocity ratio. More detailed models consider also the laminar order of the cells in the tissue, introducing an additional anisotropy in the velocity of the waves, giving rise to three different velocities with ratio 4:2:1. Such velocities correspond, respectively, to the fiber axis, parallel to the laminar arrangement of myocytes, and normal to the arrangement of myocytes [108].

The effect of anisotropy can be incorporated into a model of wave propagation in cardiac tissue by the modification of the diffusion coefficient in the cable equation (28). In the monodomain approach the diffusion tensor is usually determined by two diffusion coefficient values: one in the direction of fast propagation ($D_\parallel$) and a second value for the two perpendicular directions ($D_\perp$). To obtain a ratio 1:2 in the velocities a relation $D_\perp \sim D_\parallel/4$ is used. Typical values of the velocities employed in the monodomain approach are $c_\parallel \sim 50$ cm/s and $c_\perp \sim 20$ cm/s for the longitudinal and the transversal direction of the fibers.

However, extra and intracellular anisotropy ratios are different. It implies that a strict reduction to a monodomain description is not possible. The values in the longitudinal direction of the extra and intracellular conductivities are similar, but intracellular transversal conductivities is one or two orders of magnitude smaller than the extracellular conductivity [109, 110].

3.5.1. Modeling three-dimensional anisotropy. The direction of anisotropy in the tissue varies in the transmural direction such that the fiber direction rotates, giving rise to

rotational anisotropy [78, 111]. This effect produces a continuous rotation of the fiber axis of $\Delta\theta \simeq 120^\circ$ between the endocardium and the epicardium. This total angle is roughly constant independently of the local thickness of the ventricle. In order to model such change in the propagation properties the diffusion tensor is accordingly modify:

$$D = \frac{\sigma}{S_o C_m} = \begin{pmatrix} D_{11} & D_{12} & 0 \\ D_{21} & D_{22} & 0 \\ 0 & 0 & D_{33} \end{pmatrix}$$

where σ in the conductivity tensor and S_0 is the cell surface to cell volume ratio. The elements are defined then

$$D_{11} = D_{\parallel} \cos^2 \theta(z) + D_{\perp,1} \sin^2 \theta(z), \tag{46}$$

$$D_{22} = D_{\parallel} \sin^2 \theta(z) + D_{\perp,1} \cos^2 \theta(z), \tag{47}$$

$$D_{12} = D_{21} = (D_{\parallel} - D_{\perp,1}) \cos \theta(z) \sin \theta(z), \tag{48}$$

where the function $\theta(z)$ corresponds to the transmural distribution of the anisotropy. This function can be obtained from experimental data, see for example [112], and included into detailed whole heart models [113].

The variation on the fiber axis can be constant or it may accumulate in the regions with transitions between different zones of the tissue [114].

4. Wave propagation in models of cardiac tissue

4.1. Homogeneous isotropic tissue

The complete modeling of the heart requires the combination of approaches from different areas of physics [115]. The fluid dynamics in the blood vessels and the cavities of the heart depends on the stresses generated by the heart walls, which are described by continuum mechanics. Their motion is in turn the result of the electro-mechanical coupling [102]. Therefore, the electrophysiology of the tissue determines the contraction of the heart, its pumping properties and the resulting blood flow.

The electrophysiological dynamics of the atria and ventricles are connected through the electrical propagation across the atrio-ventricular node and on the Purkinje fibers. Since this affects only the initial condition for wave propagation in the ventricles, it is possible to study both regions independently. For the ventricles, there have been efforts to create detailed electrophysiological models incorporating realistic geometries [116]. The first geometric models of the ventricles were obtained by averaging of histological sectioning. Examples of such studies are the San Diego rabbit model [117] and the Auckland swine model [118]. Similarly, detailed models of human atria are also available [119]. More recently, individual geometries of the hearts are obtained by magnetic resonance imaging like e. g. in the Oxford rabbit model [29].

The distribution of cells within the ventricles is not homogeneous. Epicardial and endocardial cells have different electrophysiological properties and, therefore, the local action potential dynamics is different depending on the location of the cell inside the ventricle. More controversial is the presence of midmyocardial M-cells in between the endocardium and the epicardium, cells with a prolonged action potential in comparison with cells in normal epicardium or endocardium [120].

The cable equation (28), together with the highly nonlinear dynamics of the action potential, describes the electrical excitation that propagates through the heart. A complete knowledge of all the factors that affect the propagation of the electrical signal is not possible, therefore simplifications and approximations are commonly used. Although cardiac tissue is three-dimensional, many properties of propagation can be studied in lower dimensions. For example, the characterization of the conduction velocity depending on different electrophysiological properties or the dispersion relation during periodic pacing can be analyzed in one dimensional systems, the characteristic frequency of rotors can be obtained in two-dimensional domains. On the other hand, while the ventricular wall is thick and anisotropic, the atria are much thinner and a two-dimensional approximation is not unreasonable. In effect, fibrillation in atria is clearly different from ventricular fibrillation [56]. While many modelers assume that atrial fibrillation is produced in a thin tissue by a pure two-dimensional mechanism, fibrillation in the ventricles requires inclusion of the third dimension in the models [121, 122]. Nevertheless, more and more detailed structural information is included in current three-dimensional models of the atria see e.g. [123] and ventricles, see e.g. [31]. Other elements of the heart like the Purkinje fibers can be conveniently approximated as one-dimensional

fibers to study the propagation of the electrical signal. Finally, the sinoatrial node is highly localized and descriptions based on pure ordinary differential equations are useful to study the characteristics of the oscillation.

Under normal pacing, cardiac tissue receives a periodic, localized stimulation, and the excitation propagates in the form of traveling waves. Besides, there exist self-maintained excitations in the form of rotors, corresponding to spiral (in two-dimensions) or scroll waves (in three-dimensions).

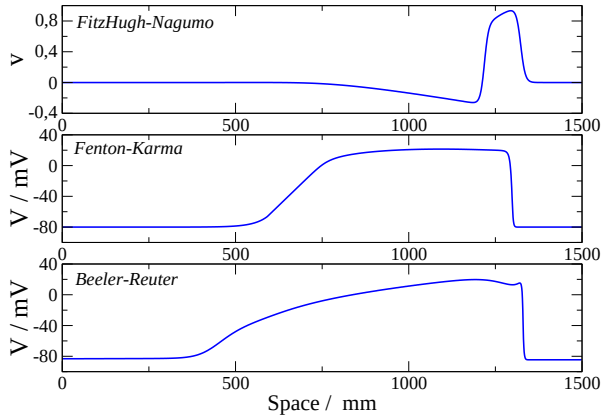

Figure 10. Different examples of one-dimensional traveling wave. Action potential wave moving to the right with the FitzHugh-Nagumo, Fenton-Karma and Beeler-Reuter models.

4.1.1. Traveling waves. Myocytes are connected through gap junctions, see Section 3.2. The electrical signal propagates fast along the cell body, but the velocity is reduced at the gap junctions. If the connectivity between cells is too small propagation failure may occur because adjacent cells are not excited anymore and propagation therefore stalls. If the connectivity is large enough the propagation velocity can be averaged, so an action potential excitation propagagates along a one-dimensional strand of myocytes with roughly constant velocity. Models of one-dimensional cardiac tissue in the continuum limit then support traveling waves with constant shape and velocity. The shape of the action potential depends on the specific model employed, see Fig. 10 for examples of traveling waves in three models of cardiac tissue.

The parameters which control the propagation properties of the tissue are the conductivity and the fast and slow ion currents.

- *Conductivity:* The change on the conductivity and the corresponding diffusion parameter D, see cable equation (28), modifies the velocity of propagation of the wave without changing the characteristic times of the ion currents, which remain unaffected, see Fig. 11(a-b). The structure of the cable equation implies a square root dependence of the velocity on the parameter D ($c \propto \sqrt{D}$). Regions of decreased conductivity correspond to the border of severe ischaemic regions [124] or to zones

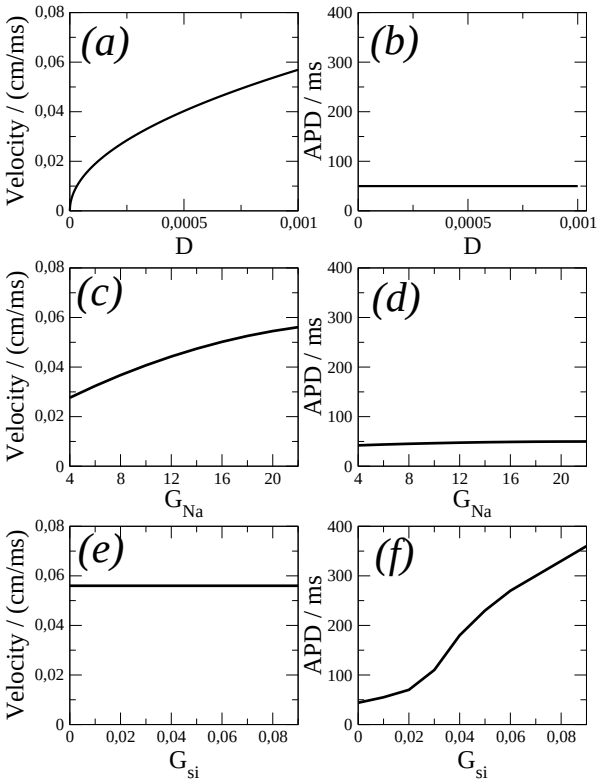

Figure 11. Effects on wave velocity and APD in the Luo-Rudy model of the changes on the conductivity of different ion currents. Dependence of the velocity (a) and APD (b) on the diffusion constant D, keeping $G_{si} = 0.01$ and $G_{Na} = 23$ mS/cm^2 constant. Dependence of the velocity (c) and APD (d) on the sodium current conductance, keeping $G_{si} = 0.01$ mS/cm^2 and $D = 0.001$ cm^2/ms constant. Dependence of the velocity (e) and APD (f) on the slow inward current conductance, keeping $G_{Na} = 23$ mS/cm^2 and $D = 0.001$ cm^2/ms constant. The effect of a decrease of G_{Si} is a shortening of the action potential duration (APD), while the velocity of the traveling wave is almost independent of the value of G_{Si}. On the contrary, a decrease of G_{Na} substantially reduces wave velocity, while the APD remains almost constant [75].

with a large fraction of fibrosis, a very common process in cardiac remodeling, effectively decreases the conductivity [125]. In general, remodeling processes in cardiac disease affects conductivity and elevates the risk of severe arrhythmia [47]

- *Fast depolarizing ion currents:* Fast gating of ion channels inside the myocyte and the corresponding currents, typically associated to sodium in the physiological models of cardiac tissue, can also control the conduction velocity [126], see Fig. 11(c-d). These processes are associated to the ratio between two characteristic temporal scales in generic models which can also control the velocity of the action potential waves [40].
- *Slow repolarizing ion currents:* Slow processes control the repolarization of the cell and therefore the action potential duration. These processes are associated to calcium or potassium currents and the action potential decrease is decoupled from

the decrease of the velocity in physiological models, see Fig. 11(e-f). In simpler models such decoupling is not achieve. An inhomogeneous reduction of action potential is associated to ischaemia [126] and other pro-arrhythmic mechanisms [127] as, for instance, the Brugada Syndrome [128, 129]. Such dispersion of refractoriness may result in localized block and the induction of reentry [130, 131].

When two waves propagating in different directions collide, they annihilate each other. Relevant for cardiac tissue is also the study of interactions between consecutive waves traveling in the same direction. When one end of the tissue is forced periodically to produce waves, a periodic sequence of excitations often called a wave train propagates through the system. At low pacing frequencies, there is practically no interaction between consecutive waves and the velocity of the wavetrain is the same as the one for a solitary traveling wave. On the other hand, at fast pacing, a wave may not be able to propagate because it enters the refractory tail (i.e. the region behind the wave where tissue has not yet fully recovered) of the preceding wave and propagation is blocked. In between these two extreme situations, waves are able to propagate under the influence of the refractory tail of the previous wave by reducing their propagation velocity and their action potential duration. Both quantities depend on the local time elapsed between consecutive pulses (i.e. the diastolic interval, DI), see Fig. 12 for a particular example. The information on this dependence gives the action potential duration (APD) and conduction velocity restitution (CV) curves. When this dependence becomes very strong, an initially periodic wavetrain may become unstable and evolve into alternans, a state in which the speed of the waves changes as they propagate along tissue, see Section 5.

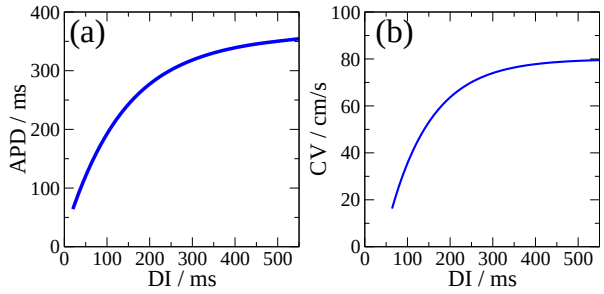

Figure 12. Restitution curves or dependence of the (a) action potential duration (APD) and (b) conduction velocity (CV) on the diastolic interval (DI).

In two- and three-dimensional media the diversity in wave propagation increases. Planar, circular, elliptical or even more complex waves can be generated depending on the initial condition. Planar waves propagate at the same velocity as in the equivalent one-dimensional system. When the wavefront is curved, however, the velocity of the waves decreases with respect to the corresponding planar wave. In effect, the velocity of an excitation pulse in cardiac tissue depends on the local curvature (κ) through the

eikonal relation:

$$c = c_0 - D\kappa, \tag{49}$$

where c_0 is the velocity of the planar wave, and D is the diffusion coefficient [132]. This expression fails for curved periodic traveling waves. Under such conditions a pre-factor multiplying D in Eq.(49) is needed, see [133] for more details.

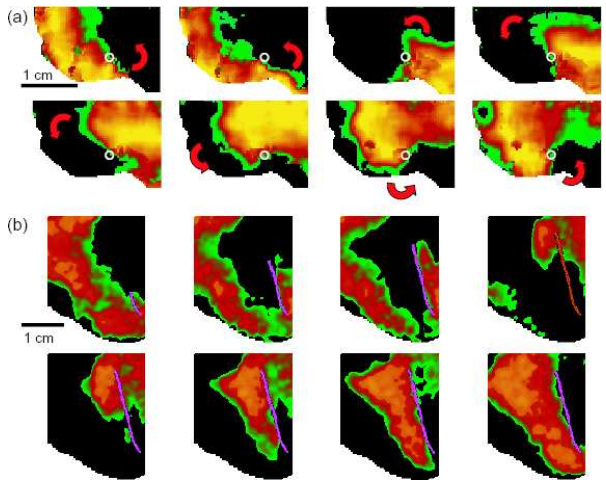

Figure 13. Reentrant wave dynamics in experimental preparations. (a) Spiral wave in canine atrium where the tip follows a circular trajectory and (b) spiral wave in canine ventricle where the tip follows a linear trajectory. Reproduced with permission from [134]. All rights reserved

4.1.2. Spiral waves. Besides pulses, models for two-dimensional tissue often admit rotating spiral waves, which are related to functional re-entry in cardiac tissue [135], see Sec. 6.2. There are several experimental observations of spiral wave rotation in cardiac tissue [16, 134, 135], see for example Fig. 13. If reentry in the form of spirals occurs in the atria or the ventricles, spirals may be implicated with arrhythmias like atrial flutter or ventricular tachycardia. The latter can be further classified into monomorphic or polymorphic VT depending on whether there is only a single main frequency or additional beats (amplitude modulations). The latter phenomenon is believed to appear either due to the meandering motion of a single spiral or due to the existence of several spiral waves in the tissue.

A way to create a spiral wave is to start with a broken pulse (a finger), so the excitation front propagates around its free-end giving rise to the formation of a rotating spiral wave. Depending on parameters, it is also possible that the newly generated free-end does not grow but retracts. Such condition corresponds to a sub-excitable medium. Another way to generate a spiral wave in cardiac tissue is the introduction of an excitation in the wake of a two-dimensional traveling wave. The new excitation cannot propagate in the direction of the refractory tail of the first wave. Hence, it slides along the refractory tail until the tissue becomes again excitable and then rotates,

creating the spiral, see the whole process in Fig. 14. Depending on the shape of the secondary excitation, one or two spiral waves can be formed. The generation of the spiral wave after the second excitation only occurs during a particular window of time, known as the vulnerability window [136]. If the second perturbation comes too early, a new wave cannot be generated because that part of the tissue is still in the refractory state. If it comes too late, the perturbation generates a circular wave and no reentry is formed.

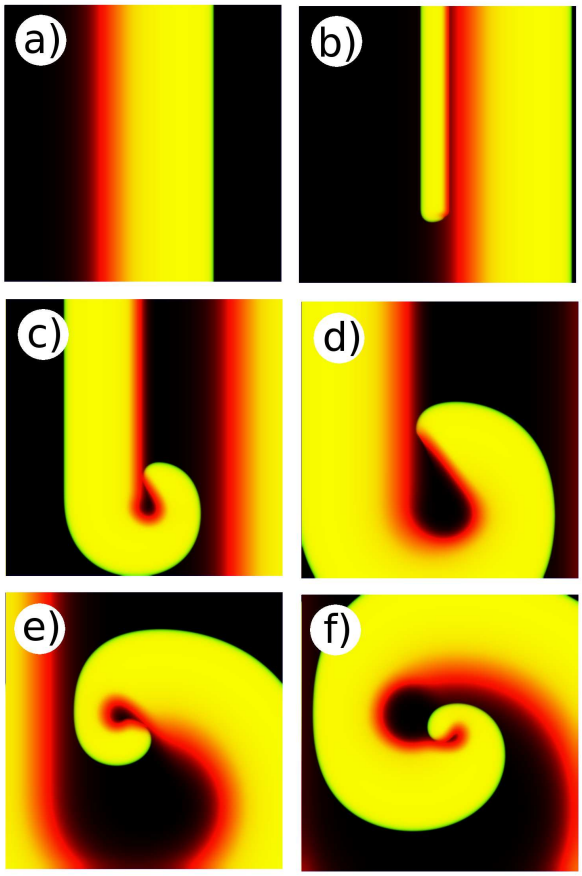

Figure 14. Generation of a spiral waves in a model of cardiac tissue by a S1-S2 protocol: An initial perturbation produces a travelling wave (a), second perturbation, shorty after the passing of the travelling wave (b), generation of a free end (c), evolution into a rotating spiral wave (d-f). Time between consecutive snapshots 90 ms.

The whole spiral wave rotates around its free-end, or tip. The motion of the tip determines most properties of the spiral motion, as it has been demonstrated by the calculation of the response function, which is different than zero only close to the spiral tip [137, 138]. The dynamics of the tip can change from a circular motion producing rigidly rotating spiral waves to more complex dynamics, giving rise to meandering spiral waves, see Sec. 6.1. If the interaction between pulses of the spiral is too strong the spiral can break and a final chaotic dynamic state of pieces of rotating spirals fills out the whole system, see Sec. 6.2. Such a state has been proposed to be the responsible of cardiac

fibrillation.

4.1.3. Scroll waves. A scroll wave is the three-dimensional equivalent to a two-dimensional spiral wave. It can be considered as a stack of spiral waves. The connection of the tips of these spirals defines a filament, around which the scroll wave rotates. The dynamics of the whole wave is often dictated by the motion of the filament.

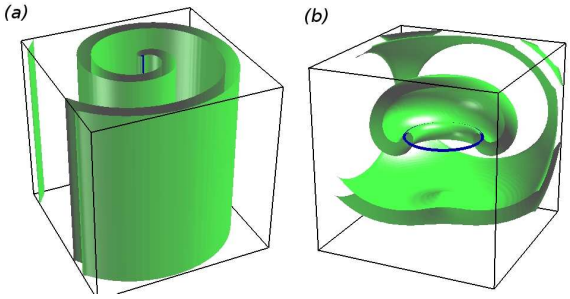

Figure 15. Examples of a scroll wave rotating around the straight filament (a), and of a scroll ring rotating around a circular filament (b). In the latter case, half of the waves are not displayed to permit the visualization the filament. Adapted from [75] with permission of Springer.

There are different types of scroll waves, whose presence in the medium and stability depends on the initial and boundary conditions. A simple solution in a homogeneous isotropic medium is a straight scroll wave rotating around the filament (Fig. 15a). As in the case of two-dimensional spiral waves, the rotation can be rigid or the waves may perform a meandering motion. Straight rigidly rotating scroll waves move with the same frequency as in the two-dimensional equivalent. However, the meandering in three-dimensional systems appears in a broader region of parameters [139], accompanied with an helical deformation of the initially straight filament, see Sec. 7.1.

The stability of a straight filament is determined by the dependence of filament tension with curvature. In isotropic media, scroll waves are usually found to be stable. However, depending on the initial condition, anisotropy or heterogeneities, the filaments of the scroll waves can be bent. An extreme case of a curved scroll wave is a scroll ring, where the filament is closed into a ring, see an example in Fig. 15(b). Scroll rings have been extensively studied because their constant radius permits a convenient measurement of the dependence of the filament dynamics on the local curvature. Depending on the sign of the filament tension, two main dynamics have been observed in rings with large radius: either they collapse when filament tension is positive, which is the usual case, or they expand if the tension is negative. In Sec. 7.3 we show that the latter case is associated to scroll wave turbulence [93, 140]. On the other hand, small drifting scroll rings can survive without neither collapsing nor expanding, or several scroll rings can be knotted, resulting in a stable configuration [141].

Sometimes the positions of the tips of the spirals are not aligned along the filament, but present a shift in the phase of rotation. This effect is due to a twist on the filament.

As with local curvature, scroll waves typically reduce the twist. There are, however, cases where twist persists, like three-dimensional meandering where some amount of twist is stable, or initially twisted scroll waves with periodic boundary conditions where the twist cannot be released, see Sec. 7.2. Twist may also be induced in heterogeneous systems, see Section 4.2.

Complex and chaotic wave dynamics can be the result of:

- *scroll wave turbulence:* originated by the destabilization of the filament due to an instability or to anisotropy.
- *scroll breakup:* originated by the interaction among the waves forming the scroll. While the previous mechanism does not have any equivalent in two-dimensional systems, the mechanism of scroll breakup is basically the same as the equivalent mechanism in two dimensions, but it has been described to occur in a larger parameter region of the phase diagram [122].

4.2. Heterogeneous tissue

The description of cardiac tissue as continuous and homogeneous facilitates the modeling of such a complex problem. However, tissues in living organisms are nonuniform, and the heart muscle is not an exception. Cardiac tissue is highly heterogeneous, with multiple sources of inhomogeneity. For example, the whole cardiac vein system has to provide energy to the heart and therefore frequently crosses the muscle, interacting with the propagation of electric waves. Furthermore, the properties of the tissue are far from being homogeneous, presenting physiological gradients and local variations. Finally, there are different types of cells in the myocardium with different electrical properties which may produce small-scale heterogeneities.

Particular modeling of the different types of heterogeneities is possible, and some situations have been extensively studied. However, generic results from qualitative descriptions, like parametric changes, gradients or non-conducting inclusions, have helped to interpret some properties of cardiac tissue.

Next we review different types of organization of the inhomogeneities in cardiac tissue and the most relevant effects in action potential propagation.

4.2.1. Large non-excitable local heterogeneities. Blood vessels supply oxygen and energy to the myocardium. They form a complex network of pipes with different sizes [54], introducing large inclusions in the tissue. They are typically modeled as inert obstacles which do not propagate the electric wave, see an example in Fig. 16(a). Scars produced by an infarct could be modeled similarly as inclusions. A traveling wave propagates around the inclusion, however a spiral or scroll wave can pin around the heterogeneity, typically an artery, and produce an abnormal periodic excitation of the heart [16]. Paradoxically, the inclusions themselves can generate new waves when an electric field is applied [142], producing the unpinning of spirals under repetitive perturbations [143], and, furthermore, eliminating ventricular fibrillation [54, 55]. Such

a method is known as far-field pacing and it is more efficiently than periodically forcing the tissue from outside, or anti-tachycardia pacing, to unpin spirals [144].

On the other hand, elongated obstacles can produce propagation along them. Such single large heterogeneity may produce a reentry under adequate conditions [20, 145] or under high frequency stimulation [146]. The combination of several obstacles may block in one direction and propagate in the other one, giving rise to the possibility of anatomical reentry depending on the geometrical properties of the obstacles. Curvature of the waves reduces the speed of propagation, see Eq. (49), thus, highly curved fronts, obtained at the exit from small channels, may stall [147, 148].

Equivalent to the pinning of the tip of spiral waves, filament of scroll waves can anchor in three-dimensional systems to small heterogeneities [149].

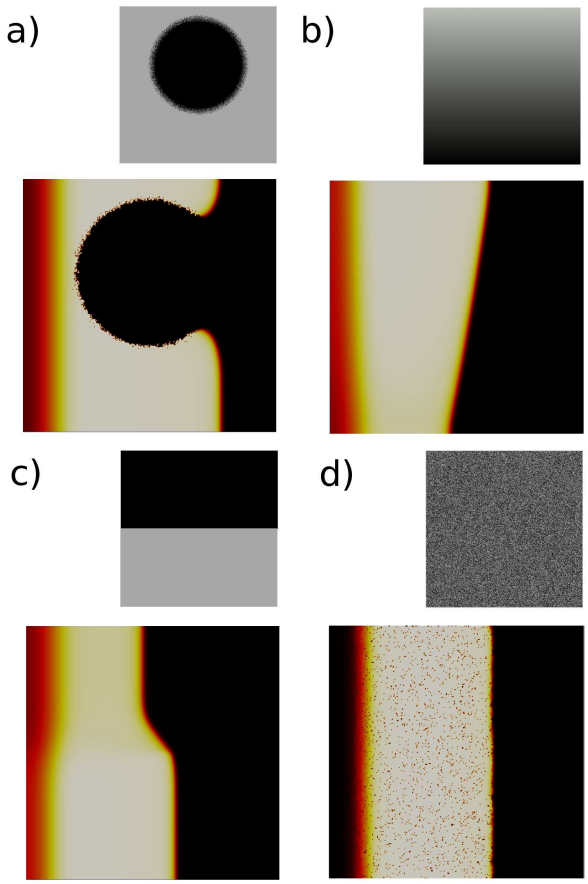

Figure 16. Four examples of different types of heterogeneities (small black and white panel) and the effects on wave propagation in tissue (large color figure) with the Fenton-Karma model: Large non-excitable circle (a), linear gradient on the excitability (b) step gradient on the excitability (c), and small non-conducting regions randomly distributed. System size in the four cases is 4×4 cm^2.

4.2.2. Gradients of electrophysiological properties. The myocardium is not homogeneous and different types of gradients are present and affect wave propagation. For

example, the transmural distribution of cell types is not homogeneous so the cell properties at the epicardium are different to the properties of the myocytes forming the endocardium of the heart [150]. A third type of cells, the M-cells are located between the two previous types. Proximity to ischemic regions may also alter the local properties of the myocardium and introduce different types of gradients in the tissue.

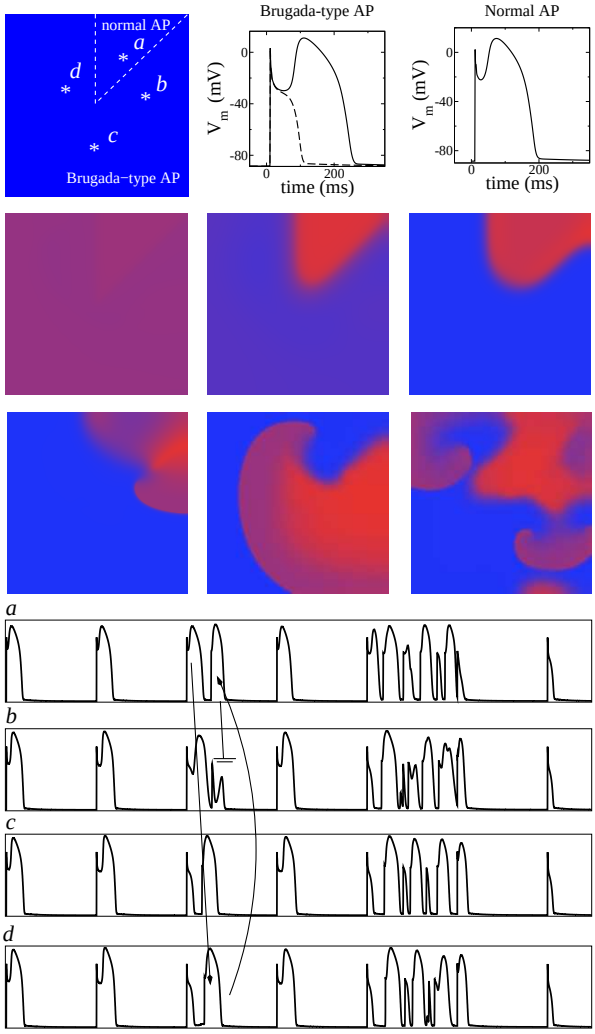

Figure 17. Creation of a spiral wave in a sheet of epicardial tissue, with regions of normal and Brugada-type action potentials (upper panels). All epicardial tissue is stimulated simultaneously with a period of 1000 ms. In the six middle panels we show the distribution of the transmembrane potential V at time intervals of 50 ms, except for the last illustration, which shows a typical snapshot some time after the first spiral has broken up. In the lower panels we show the time evolution of the transmembrane potential V at four different sites of tissue. The arrows correspond to the beat shown in the upper panels, indicating the reexcitation at the points b, c and d, and the appearance of reentry with the reexcitation of point a, that finally results in block at the point b. A couple of beats later, reentry occurs again, resulting in six extra beats. Adapted from [130], with permission from Elsevier.

The variations in the action potential duration (APD) corresponding to regional

differences of electrophysiological properties result in dispersion of repolarization. This has been linked to an increased risk of cardiac death [151] and, in particular, to a higher risk of arrhythmogenicity in short QT, long QT and Brugada syndromes [152–155]. In Brugada syndrome, for instance, dispersion of repolarization is thought to be caused by an abbreviation of the APD of the right ventricular epicardium due to loss of the action potential dome [156]. Then, a region of depolarized tissue (during calcium current entrance, or phase-2 of the AP) can re-excite adjacent regions that exhibit shorter action potential duration (APD) [130], producing an extrasystole which can eventually initate phase-2 reentry (see Figure 17). This same mechanism has also been proposed to explain reentry associated to dispersion of repolarization around ischemic regions [157]. Thus, reexcitation due to phase-2 reentry needs two conditions to be met: first, that a heterogeneous loss of dome is produced in tissue and, second, that the spike-and-dome regions are able to reexcitate the loss-dome areas. The latter has been shown to occur due to the propagation of a slow pulse sustained by the inward calcium current, that is then able to reexcitate adjacent tissue [131].

Linear Gradients. A continuous change on the properties of propagation will cause an acceleration (deceleration) of the pulse moving in the direction (opposite direction) of the excitability gradient. It may also modify the vulnerability window and even induce conduction block [136].

In a two-dimensional slab of tissue a gradient of excitability induces variations in wave velocity, see Fig. 16(b), and produces the drift of a spiral wave pushed by the change of the rotation frequency during each period of rotation due to the gradient. The direction of the drift depends on the model parameters [158]. A gradient in the gap junction conductances produces similar behavior [159].

A straight scroll wave with the filament parallel to a gradient of excitability produces the formation of constant twist along the filament [160]. Furthermore, if the scroll wave is not oriented in the direction of the gradient it turns and tries to align in the same direction. On the other hand, scroll rings are also affected by gradients and the normal vector of the filament plane also orientate with the gradient [161].

Step Gradients. Sudden changes on the excitability or in other properties of the myocytes may substantially affect the dynamics of the waves. A traveling wave propagating from a region of higher excitability to a region of lower excitability will change velocity adapting to the local properties of the the tissue. However, in the opposite direction it may block and do not propagate.

Step gradients produce two different velocities, see Fig. 16(c). Spiral waves located at the border of two regions with different properties of propagation may be affected if the core of the spiral rotates crossing this border. The difference of rotating frequencies produces a directed drift along the boundary between the two regions [162].

A scroll wave oriented perpendicularly to the border between two regions with different propagation properties will deform. The filament in the region with faster

rotation frequency will maintain its original shape. In the other region, the filament twists because of the difference in frequency. Thus, to keep the filament connected and compensate this phase difference twist develops [160].

4.2.3. Localized heterogeneity. The accumulation of different types of cells or the presence of light infarct areas or scars may result in a localized change in excitability of a determinate region of the tissue. Apart from the effects of the borders discussed in the previous section, the shape, size and degree of excitability of the heterogeneity may be determinant for the propagation properties of the waves. A two-dimensional pulse crossing a region with different excitability will change locally its velocity and curvature. If the difference in excitability in this region in comparison with the rest of the medium is large enough reentry can be produced [163].

One of the most accepted mechanism of reentry formation is the interaction of two consecutive waves with a large heterogeneity formed by cells with a refractory period larger than the rest [163–167]. The second pulse stops in the heterogeneity because of the refractory state produced by the previous wave. It can, however, propagate outside of the heterogeneity producing a free end which re-enters into the heterogeneity when the refractory period ends.

4.2.4. Small-scale heterogeneities. Small-scale heterogeneities are inevitable and omnipresent in cardiac tissues. This is due to the variability of individual cells, the presence of different cell types as well as the potential inclusion of fibrotic cells inside otherwise healthy tissue. Another factor is the discrete nature of the tissue that is composed of myocytes separated by extracellular space filled with interstitial fluids. As discussed in Section 3.2, homogenization procedures [8] are employed to derive the bidomain equations of cardiac dynamics based on periodic arrangements of cells and related periodic variation of medium properties [9, 10]. Often, the bidomain equations are further reduced to the monodomain equations [11], resulting in a set of coupled nonlinear reaction-diffusion equations that is the main model type discussed in this review. A homogenization of reaction-diffusion equations with small-scale heterogeneities was carried out recently [168, 169] to obtain effective diffusivities resp. conductivities and effective local excitation kinetics assuming a random structure. The procedure was validated with simulations in discrete models with randomly assigned coupling between cells and/or local kinetics with small fraction of non-excitable elements and/or blocked connections. Homogenization fails badly if such obstacles to perturbation reach fractions close to percolation. Then, large cluster occur and the assumption of homogenization regarding a large differences in scales between variation of local kinetics and spatial coupling on the one hand and the typical interface width of excitation on the other hand breaks down [168]. As a result, heterogeneities may induce disruption and subsequent reentry, as has been observed in very schematic models [170], in simplified ionic models [171], and in more complex models [172]. Homogenization has also been used to predict effective wave speeds in periodic media [42, 173]. As long

as the excitation front width is larger than the characteristic size of the heterogeneities the wave speed is approximately constant. Interestingly, intermediate periods of the heterogeneity length scale may yield conduction block of waves, whereas propagation is possible at small and large length scales [173].

In contrast to such approximations of spatial homogeneity and/or smooth changes of parameters in cardiac modeling, cardiac tissue may be modeled not as a continuous medium but as a discrete interconnected collection of cells, some of which, e. g. the fibroblasts, are non-excitable, see and example in Fig. 16(d).

Approximately two thirds of the volume of cardiac tissue is formed by myocytes, the rest of the volume is basically composed by fibroblasts. Since the size of myocytes is around five times larger than the size of the fibroblasts, the fibroblasts are the largest cell population by number [174]. One of the main function of fibroblasts is the production of the proteins forming the extracellular matrix (ECM) which give support to the whole tissue. An excess production of such proteins leads to fibrosis, which increases the risk of malfunction in the heart. It has been shown in *in vitro* experiments that fibroblasts form gap junctions with myocytes [175] and, therefore, may be electrically active in the tissue.

The effects of a large fraction of fibroblast in the myocardium and its implications in the formation of arrhythmias have been recently studied [176]. Although commonly a heterogeneous description of the tissue was considered in such studies, homogenization techniques were also employed to create a tridomain model [177], which is an extension of the bidomain model with an additional third phase representing the fibroblasts. Nevertheless, fibroblasts are usually included in the modeling of tissue as non-excitable elements in a discrete version of the cable equation. Because of the smaller size of the fibroblasts with respect to the myocytes, they are sometimes included in the discrete lattice as an additional connection to each myocyte [178, 179], or with a smaller size in models at the sub-cellular scale [180, 181].

The effect of fibrosis, details of tissue structure obtained from histology and other heterogeneities on the cellular level have also been included in a number of discrete models for cardiac tissue in two and three dimensions [171, 172, 182–189]. The disconnection among myocytes has been also employed as a model to explain reentry around the pulmonary vein in the atria [190], which is one of the major causes of atrial fibrillation [191], and in the formation of ectopic pacemakers [171].

In general the inclusion of randomly distributed non-excitable cells or the uncoupling of myocites produces a reduction of wave velocity and an increase of spiral period [192, 193]. It can stabilize spiral waves and preclude their breakup, typically occurring at rapid rotation frequencies [194]. In all the different models that incorporate non-excitable tissue, a decrease in the velocity of wave propagation is observed, that can induce the formation of reentries [171, 190, 194] due to the source-sink mismatch mechanism [25, 195], see a realization of such reentry formation in Fig. 18.

On the other hand, a heterogeneous description of the medium is also particularly convenient for the modeling of cell cultures. In this case cells grow in vitro, establishing

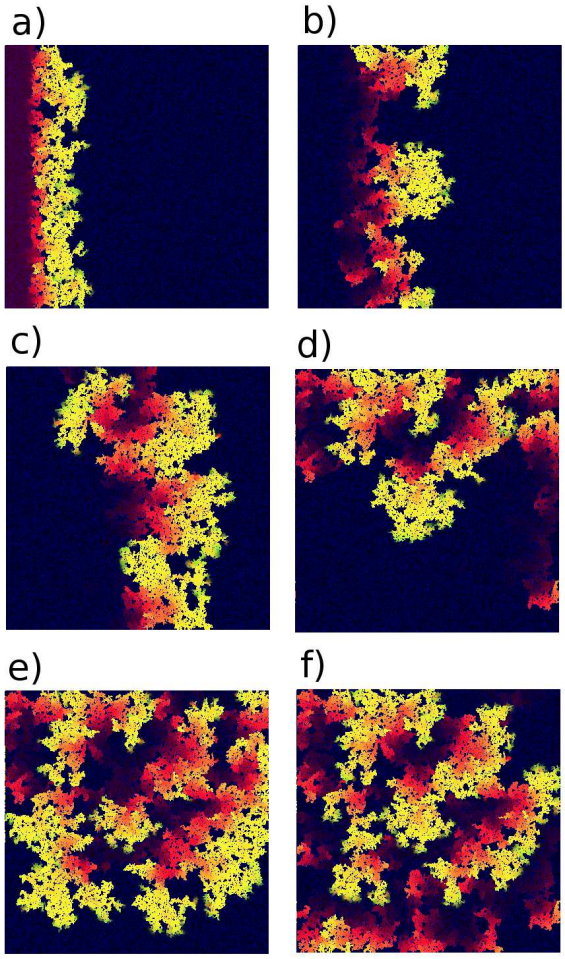

Figure 18. Example of anatomical re-entry obtained with the Fenton-Karma model with randomly distributed non-conducting bonds. System size 4×4 cm^2. Snapshots correspond to times: 82 ms (a), 200 ms (b), 300 ms (c), 500 ms (d), 650 ms (e), and 770 ms (f). For more details see [171].

connections among them. Because of the lack of a solid tissue they form irregular networks of connected cells. This facilitates the spontaneous generation of spiral waves [196] where the role of the heterogeneities in the connectivities is crucial [197].

4.2.5. Geometry effects. For the most of this review we discuss propagating structures independent from specific geometric constraints, distance to boundaries or obstacles to propagation. In many realistic situations, the geometry of the medium or the shape and location of boundaries may have an important influence on electrical propagation in excitable media and specifically in cardiac tissue. Many relevant effects stem from the fact that geometric constraint cause curvature of the excitation waves. According to Eq. (49), convex shape (positive curvature) slows down or even blocks wave propagation, whereas a concave shape (negative curvature) leads to faster wave motion. A situation of

interest is propagation within narrow pathways, where unidirectional block and reentry were found in simulations [198, 199]. Reflection of fronts and block of excitation pulses have been observed experimentally in the Belousov-Zhabotinsky reaction [200] and in catalytic surface reactions [201, 202]. Analogous phenomena have been reported in parallel for cardiac tissue, see e. g. [148, 203]. Theoretical analysis of wave propagation in channels or pathways with varying diameter has bee carried out based on, e. g., conformal mapping [204] and perturbation theory [205].

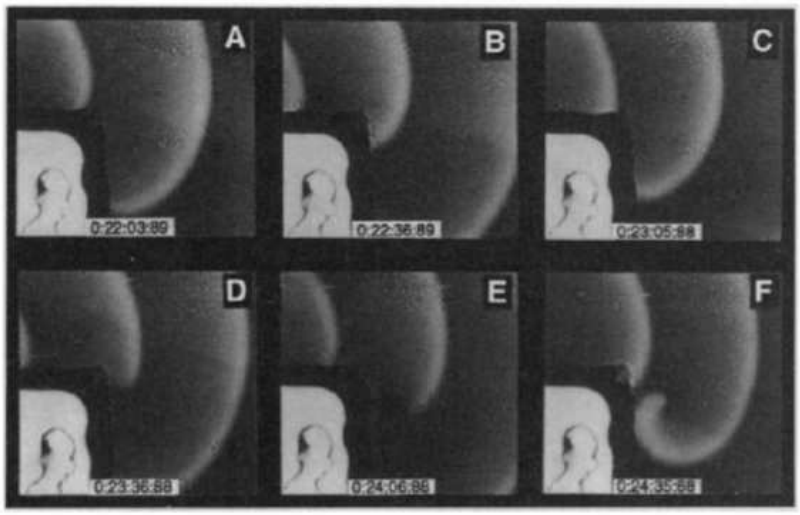

Figure 19. Principle of vortex shedding stemming from an upward traveling planar wave that is forced to follow a boundary. Example of a spiral wave developing at a corner in the boundary in an experiment of the Belousov-Zhabotinsky reaction. From [206]. Reprinted with permission from AAAS.

An interesting phenomena relevant to cardiology, is also the formation of spiral waves at sharp changes such as corners or sudden extensions in a boundary, which was observed in experiments and simulations related to the Belousov-Zhabotinsky reaction [206] (see Fig. 19) and to the catalytic CO oxidation on a platinum surface [207]. Cabo et al. pointed out that such a vortex shedding at obstacles to propagation may be behind formation of spirals in cardiac tissue [145].

Not only spiral initiation but also persistent spiral waves can be affected by geometries and in particular by boundary effects. This is relevant for rotors in cardiac tissue, because the spiral wavelength (i.e., distance between two consecutive pulses) is typically of the same order as the size of the heart. In other words, unlike in chemical reaction-diffusion systems one will rarely find spirals with many windings. For a typical example, see the rotating excitation in Fig. 13 above. Theory [208] as well as experiments and simulations [209] have focused on spirals in circular and spherical domains. Hartmann et al. report that the spiral frequency increases substantially if the size of the domains is smaller than half the spiral wavelength in a large domain

and that spirals cannot be sustained for domains smaller than one tenth of the spiral wavelength in a large domain [209]. Other interesting aspects recently found include boundary-induced meander [210] as well as the existence of discrete orbits for particular distances to the boundary [211] as well as changes in the stability of scroll waves near boundaries [212, 213].

4.3. Anisotropic tissue

Anisotropy alone in homogeneous two dimensions, or in thin homogeneous cardiac tissues, will only produce the deformation of the waves, without inducing any new instability. In three-dimensional media the shape of filaments of scroll waves adapts to the fiber anisotropy. In general, it is possible to show that in a 3D reaction-diffusion system with anisotropy the stationary shape of the filament is a geodesic of a Riemannian space, whose metric tensor is related to the inverse of the diffusion tensor [214,215]. The filaments align with the local fiber orientation [216], and they bend and adopt curved shapes following geodesic metrics [217]. The curvature of such filaments may induce the formation of twist which may destabilize the scroll waves and produce instabilities [78] or spiral breakup [73]. Furthermore, abrupt changes of anisotropy may induce oscillatory dynamics of the filament superposed to the normal rotation of the scroll wave around the filament [218].

The implementation of relatively complex models in realistic geometries of the ventricles requires the use of an adequate description of the orientation of the fibers and the correct values for the anisotropy governing the wave propagation through fiber directions [219]. They are nowadays implemented in all modern electrophysiological models of the heart [30]

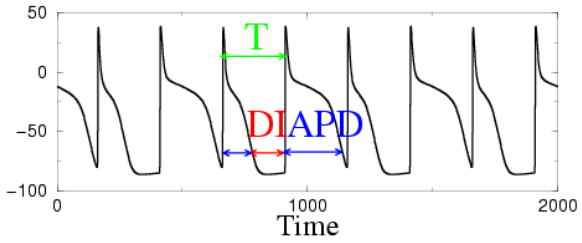

Figure 20. Sequence of action potentials with alternating action potential durations (APD) in a cell paced at constant stimulation period, exemplifying the phenomenon of cardiac alternans. The action potential duration (APD) is usually defined as the time from the steepest increase of the transmembrane potential V to a repolarization of 90 percent. The duration between two consecutive action potentials is called diastolic interval (DI).

5. Cardiac alternans

Among the cardiac instabilities known to give rise to arrhythmia and fibrillation one of the most studied is that of cardiac alternans. It was first described under the name of pulsus alternans by Ludwig Traube in 1872 as the alternation of strong and weak arterial pulses. Later on it was discovered and studied by Hering in 1908 [220] and Sir Thomas Lewis in 1911 [221] that this alternation had an electrophysiological origin. It corresponded to a beat-to-beat change in the duration of the action potential at the single cell level (Fig. 20), that resulted in beats of weaker and stronger contraction of the heart. This abnormal electrical activity was recognized as an alteration of the ECG by Kalter and Schwartz [222] in 1948. Specifically, as a change in the amplitude or position of the T-wave of the ECG, related to a change in repolarization (see Fig. 3). Since then, the appearance of T-wave alternans has been recognized as a indicator

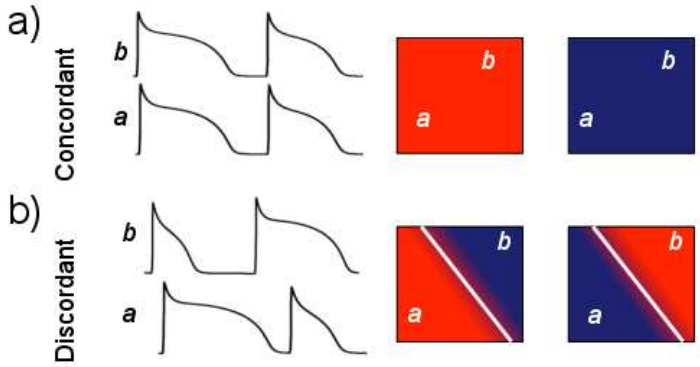

Figure 21. Schematic illustration of concordant and discordant alternans. The alternation in the APD can be in phase over all the tissue (concordant alternans) or create out of phase regions (discordant alternans), separated by a nodal line, where the value of the APD remains constant at consecutive beats.

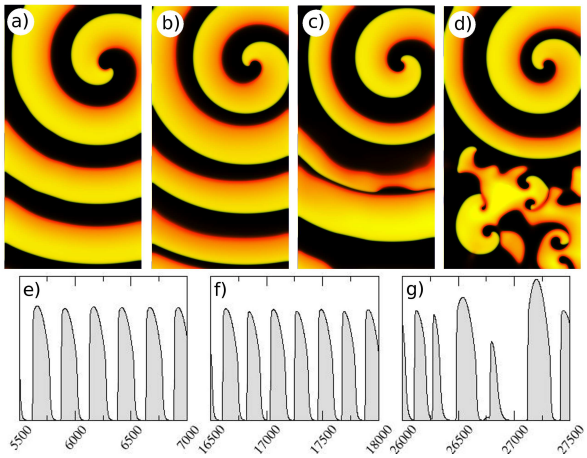

Figure 22. Spiral break-up due to alternans. Dynamics of a spiral wave in the Fenton-Karma model (top panels) and membrane potential at a point of the system (bottom panels) after a slow change on the parameter τ_d in Eqs. (33). Rigid rotation of a spiral wave (a), spiral wave with alternans in the propagation (b), spiral wave with a conduction block which will generate the breakup of the spiral (c), spiral wave together with spiral breakup produced by alternans (d). The local membrane potential shows for (a) a regular propagation (e), for (b) an alternating APD and amplitude (f) and for (d) a more complex dynamics (g).

of suffering sudden cardiac death (SCD) [223]. Due to this, T-wave alternans has been proposed as a risk stratifier of SCD. An electrophysiological explanation of this link was given by Pastore et al [224] that found that, in tissue, action potential alternans could be either in phase (termed concordant alternans) or out of phase in differents parts of tissue (discordant alternans), as shown in Figure 21. This latter case was found to be very proarrhythmic, since it gives rise to dispersion of repolarization that can result in localized block, and the initiation of reentry and fibrillation. The role of alternans on spiral stability had been studied previously by A. Karma [84, 225], who showed that alternans can produce break-up of the waves emitted by a spiral (Fig. 22), due to localized conduction blocks. At fast pacing rates, the instability reaches the spiral core and produces a disordered state, where vortices are continuously created and destroyed, similarly to what is observed during ventricular fibrillation in the heart.

5.1. Dynamics

From a theoretical point of view, alternans at the single cell level were studied using a cobweb construction (see Figure 23) by Nolasco and Dahlen [226], that also introduced the concept of AP restitution, i.e., the experimentally observed fact that the action potential duration (APD) at a given beat depends on the time elapsed between the end of the previous action potential and the beginning of the current one (known as diastolic interval, DI). Although more complex effects may appear, resulting in memory when the APD depends on the past history of the system, this basic map is still the basis of many studies of alternans. It was in fact used by Guevara *et al* [227] to show

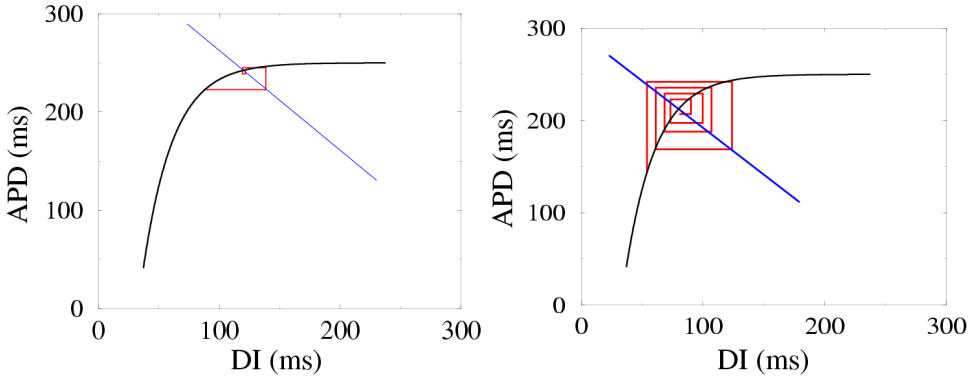

Figure 23. Cobweb diagram used for the study of alternans. The fixed point is given by the intersection of the curves $APD = f(DI)$ and $T = APD + DI$. Under consecutive iterations it can be stable (a) or give rise to a period-doubled solution (b), depending on the slope of the restitution curve df/dDI at the fixed point.

that alternans appears as a period doubling bifurcation of the periodic train of APs at a constant stimulation period.

The basic approach to alternans for a single cell starts from a restitution relationship $APD_{n+1} = f(DI_n)$ relating the DI at a given beat with the duration of the AP in the following stimulation, where it is assumed that the action potential duration depends only on the preceding diastolic interval. Then, we can describe the dynamics of a cell paced with a constant period $T = APD_n + DI_n$ by means of a one-dimensional discrete map

$$APD_{n+1} = f(T - APD_n). \tag{50}$$

The pacing period T acts as the bifurcation parameter. A fixed point of this map corresponds to a sequence of constant action potential durations. Whether the fixed point is attractive or unstable is determined by the slope the function $f(T - APD)$ at the fixed point (Fig. 23). The fixed point becomes unstable at a period doubling bifurcation if the slope of the APD-restitution curve $f(DI)$ exceeds one [226]. This is known as the restitution hypothesis [228]. However, there is contradictory evidence regarding its validity [229, 230]. In effect, various authors reported severe shortcomings of the mentioned criteria [231, 232]. More complex dynamics, including the effect of memory $APD^{n+1} = f(DI^n, DI^{n-1}, \ldots)$ result in higher dimensional maps [233–235]. Then, instead of a restitution curve one can talk about a restitution portrait [236, 237] and the condition for the appearance of alternans is related to the responses of the system under different stimulation protocols. There is now increasing evidence that often the failure of the simple restitution curve is due to alternans originating as an instability of intracellular calcium cycling [230, 238], that is independent of transmembrane voltage kinetics, as shown in experiments under AP clamp conditions [239, 240].

In tissue, the dynamical behavior becomes richer. For a pulse circulating in a ring (similar to anatomical reentry in which the action potential circulates a nonexcitable obstacle) the topology of the problem imposes that, once alternans develop, they are

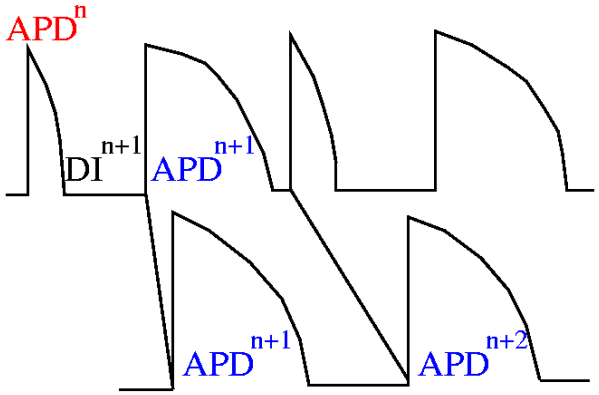

Figure 24. Schematic view of the effect of CV-restitution. A pulse after a long DI at the pacing point will have a fast conduction velocity, so the stimulation arrives early to the other end of the cable. The next pulse, by the other hand, will follow a short DI, and have a slow conduction velocity. This will increase the stimulation period at one end of the cable with respect to the pacing point, inducing a change in the phase of oscillation.

always discordant. In effect, the ring geometry imposes periodic boundary conditions for the APD, i.e., $APD^{n+1}(0) = APD^n(L)$. Then, in order for an APD to go from being long to short at a given point in the ring in two consecutive excitations, the value of the APD has to change continuously from one value to the other as one moves along the ring, implying the presence of at least one node. By means of an analysis of coupled maps, Courtemanche *et al* [241, 242] showed that the instability to discordant alternans was a Hopf bifurcation, resulting in quasiperiodic oscillations. This point was confirmed in an ionic model given by the modified Beeler-Reuter model by Bauer *et al* [243], performing an stability analysis of the periodic traveling solution in the ring using continuation methods (see section 5.2.3).

The original experiments by Pastore *et al* [224], however, were in a patch of tissue paced at one point. In that case, the transition from concordant to discordant alternans was hypothezied to be due to preexisting heterogeneities in tissue. In fact, gradients of electrophysiological properties can give rise to discordant alternans [244]. However, numerical simulations of homogeneous tissue [245, 246], showing the transition from concordant to discordant alternans, showed that heterogeneity was not an essential factor. Rather, the transition was dynamical. In fact, the key ingredient is that, due to the dispersion relation (dependency of the speed of the pulse on the diastolic interval), the local stimulation period varies from point to point in the tissue. This heterogeneity, dynamically created, is what prompts the transition from concordant to discordant alternans (see Fig. 24). This point can be understood using a kinematic description to study the dynamics of alternans (see Section 5.2.1).

5.2. Theory and Methods

Alternans in a one-dimensional geometry, either with periodic boundary conditions (a pulse circulating in a ring), or in a paced cable, can be studied using a kinematic description that provides the local values of the pacing period and APD in terms of the restitution properties of the tissue. This provides a description of the system that is valid even in the nonlinear regime, so it can be used to study, for instance, conduction blocks. Close to the onset of alternans it is possible to derive amplitude equations for the spatio-temporal dynamics of alternans. Even if these equations can be derived from the kinematic equations, they can also be written down based on general symmetry properties of the bifurcation to alternans and, therefore, reproduce generic properties of the dynamics. Besides, one can analyze the bifurcation to alternans through a full linear stability analysis of the cable equations. For this one can exploit the symmetry properties of a pulse circulating in a ring. A full linear stability analysis for the paced case is, at this moment, missing.

5.2.1. Kinematic description of alternans. Let us consider the case of a cable paced at one end $x = 0$ with period T_0. Then, we characterize the time at which the wavefront and the waveback pass through a given point of tissue x by:

$$t_f(x) = t_f(0) + \int_0^x \frac{dx'}{c(x')}, \tag{51}$$

$$t_b(x) = t_f(x) + APD(x); \tag{52}$$

where $c(x)$ is the velocity of the wavefront at position x. Knowing $c(x)$ and $APD(x)$ at every point in space, then the system is completely determined. From the restitution curves, we know that these variables will depend on position through the value of the diastolic interval DI at that point, so $c(x) = CV[DI(x)]$, $APD(x) = f[DI(x)]$. Besides, at each point we have that local period of stimulation corresponding to the beat n is $T^n(x) = APD^n(x) + DI^n(x)$, so

$$DI^n(x) = T^n(x) - f[DI^{n-1}(x)], \tag{53}$$

but

$$T^{n+1}(x) = t_f^{n+1}(x) - t_f^n(x) = T_0 + \int_0^x \frac{dx'}{CV[DI^{n+1}(x')]} - \int_0^x \frac{dx'}{CV[DI^n(x')]}; \tag{54}$$

where $T_0 = t_f^{n+1}(0) - t_f^n(0)$ is the pacing period at the origin.

Eqs. (53)-(54) constitute a closed set of discrete time equations (maps) that can be used to study the stability of a pulse in tissue. However, there is a missing point that happens to be crucial, this is, that the restitution curve of a given cell in tissue is actually affected by electrotonic current coming from neighboring cells. During pulse propagation, the electrotonic current coming from the left and right neighboring cells is different, meaning that the change in the restitution curve must break the left-right symmetry. The easiest way to include this effect is to consider diffusion plus a first derivative, that breaks this symmetry (for a more rigorous derivation, see [247]). Then

$$f_{tissue}(DI^n) = f_{cell}(DI^n) - w\partial_x DI^n + \xi^2 \partial_x^2 DI^n. \tag{55}$$

The two spatial derivatives on the r.h.s of this equation originate from the resistive electrical coupling between cells during repolarization, which tends to smooth out spatial variations of APD. Both first and second derivative terms are present because action potentials propagate in the $+x$ direction from the paced end of the cable towards the opposite end, and this propagation breaks the inherent parity symmetry $x \to -x$ that would be present if, for example, all the cells in the cable were activated simultaneously. It follows that the coefficient of the first derivative term, which explicitly breaks this symmetry, must vanish when the conduction velocity is infinite, and all the cells are effectively activated simultaneously, which implies the scaling $w \sim D/CV$. Furthermore, since the second derivative term originates from the parity symmetric diffusive coupling in the cable equation, it is sensible to assume that ξ is related to the diffusion length, i.e., the length over which the membrane potential can diffuse on the characteristic time scale of repolarization. Recalling that the solution of the one-dimensional diffusion equation with a boundary fixed at a value V_0 is $V(x,t) = V_0 \mathrm{erfc}(x/2\sqrt{Dt})$, then one obtains that $\xi \sim (D \times APD)^{1/2}$. For typical parameters of cardiac tissue, ξ is a few mm and w is even smaller.

Including this effect, and substituting in Eq. (53), the final equation is, therefore:

$$DI^{n+1} = T_0 + \int_0^x \frac{dx'}{CV[DI^{n+1}(x')]} - \int_0^x \frac{dx'}{CV[DI^n(x')]} - f_{cell}(DI^n) + w\partial_x DI^n - \xi^2 \partial_x^2 DI^n; \tag{56}$$

which provides a mesoscopic description of pulse propagation, that has been useful in describing conduction blocks [248], the effect of electrophysiological gradients [244], electromechanical coupling [249], etc.

5.2.2. Amplitude equations. Close to the onset of alternans one can consider a reduced description of the dynamics, based on amplitude equations [250]. These have been very successful in examining the dynamics in a multitude of physical systems, such as convection in fluids, chemical reactions, etc. In the current setting they can be obtained considering small modulations on top of the period doubling

$$DI^n = DI^* + (-1)^n a(x,t), \tag{57}$$

where the modulation is assumed to depend on a continuous time $t = nT_0$, since the beat to beat change is small once the rapid changes are factored out with the term $(-1)^n$. Then, from the second iteration of the map (56) one obtains the equation:

$$T_0 \partial_t a = \sigma a - w\partial_x a + \xi^2 \partial_x^2 a - g a^3 - \frac{1}{\Lambda} \int_0^x a(x')dx', \tag{58}$$

that provides a description of the spatio-temporal evolution of cardiac alternans. The last term in the equation corresponds to a nonlocal coupling. This appears from the need to integrate the wavefront speed along a trajectory to obtain the stimulation period at a given point. In fact, $1/\Lambda = (2/c^2)dc/dDI$, so the influence of this nonlocal term is greater when the CV-restitution curve is steep. It is important to notice that, due to

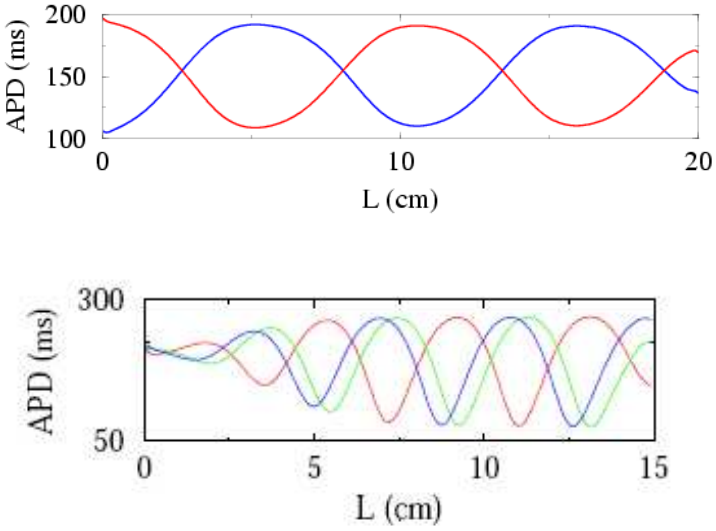

Figure 25. Distribution of the action potential duration in a long strand of tissue obtained simulating the Noble model (top panel), showing a standing wave pattern and a simple two-variable model (bottom panel), showing a traveling wave pattern. The red and blue lines correspond to two consecutive beats, while the green line in the bottom panel represents the APD ten beats later, showing that the pattern is traveling towards the pacing point. Adapted with permission from Ref. [247]. Copyrighted by the American Physical Society.

the presence of this term, a solution $a(x,t) = a_0$, corresponding to concordant alternans with a constant amplitude, does not satisfy equation (58). In a semi-infinite domain $x \in [0, \infty)$, the base state $a = 0$ always bifurcates to discordant alternans.

Using Eq. (58), in [247, 251] it was shown that discordant alternans appears either in the form of standing waves, with fixed node positions (points at which the oscillation vanishes, i.e. $a = 0$), or traveling waves, where the nodes appear periodically at the end of the cable, and disappear at the pacing point (see Fig. 25). The transition from one to the other type of solution occurs as the slope of CV-restitution is increased. From the spectra (Fig. 26) associated to the linearized version of Eq. (58) one can observe that the traveling waves correspong to modes of the absolute spectrum while the standing waves correspond to isolated eigenvalues, probably appearing because of the breaking of translational symmetry due to the pacing point. From the dispersion relation associated to Eq. (58) it can be estimated that the wavelengths for standing and traveling waves are given by $\lambda = 2\pi(w\Lambda)^{1/2}$ and $\lambda = 4\pi(2\xi^2\Lambda)^{1/3}/\sqrt{3}$, respectively, with associated frequencies $\Omega_i = 0$, $\Omega_i = (3\sqrt{3}/2)(\xi/2\Lambda)^{2/3}$ [247, 251]. The solution with the smaller wavelength is the one that bifurcates first.

The amplitude equation formalism can be applied to diverse situations, as gradients of electrophysiological properties [244], anomalous dispersion [252], control of alternans [253–257], or coupling with intracellular calcium [258,259]. It also provides us with some insight into another important problem, not jet completely understood: the influence of alternans on the stability of spiral waves. The distribution in the amplitude of alternans

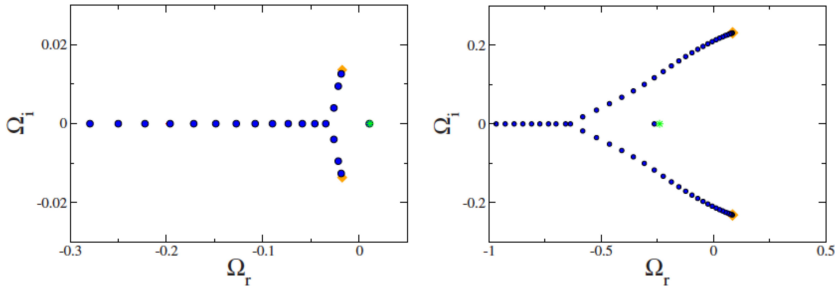

Figure 26. Spectra corresponding to the amplitude equations (58), obtained solving the associated linear eigenvalue problem, with $a(x,t) = \Phi(x)e^{\Omega t/T_0}$. The analytical predictions given in the text correspond to the diamonds, for the stationary mode, and the stars, for the standing waves. The parameters of the amplitude equations correspond to the Noble model (left) and a simple two-variable model (right). Depending on the parameters the first mode to bifurcate is a stationary mode, corresponding to an isolated eigenvalue or to an eigenmode of the continuous branch. Adapted with permission from Ref. [247]. Copyrighted by the American Physical Society.

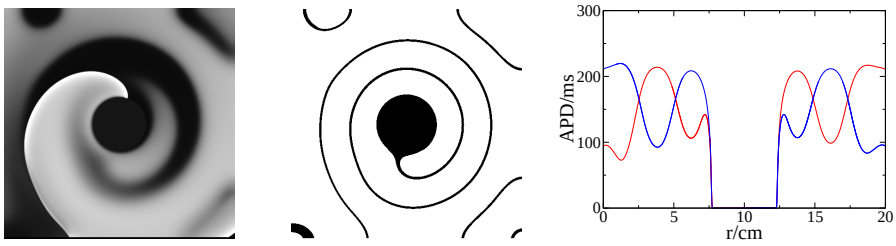

Figure 27. Spiral, nodal line and APD at two consecutive beats in the radial direction, in the modified Beeler-Reuter (MBR) model. The nodal line adopts the form of a spiral and the APD presents nodes, as in the one-dimensional paced case (see Figure 25), that travel towards the center of the spiral. Adapted with permission from Ref. [252]. Copyrighted by the American Physical Society.

will determine where conduction block (i.e. the break-up of the waves of the spiral) occurs. As in the ring geometry, for topological reasons, alternans on top of a spiral wave always present a nodal line (or an odd number of them), separating regions with opposite APD alternation. Since, in the far field, the waves emanating from the spiral asymptote to plane waves, one would expect to obtain a distance between nodal lines similar to the paced case and, therefore, a spiraling nodal line (see Figure 27). In [260] it was shown that, depending on parameters, the dynamics of the nodal line is dominated, either by the core, or by the far field.

5.2.3. Numerical bifurcation and stability analysis. The kinematic description based on coupled maps provides a phenomenological account of the transition to alternans. A more accurate determination of this transition can be made performing a numerical stability analysis. Apart from direct numerical simulations of heart models, mathematical analysis based on dynamical systems tools like bifurcation theory [261]

have added important contributions to the understanding of cardiac arrhythmias [11,262]. The latter methods (continuation and stability analysis in 1D) can be applied to models with modified ion channel kinetics [243]. This allows not only for a fast and efficient computation of action potential (AP) forms and APD and CV restitution, but also enables a quick assessment of the changes of the alternans instability with changing model properties.

One approach along these lines is to compare direct simulations of propagation on a one-dimensional (1D) ring, where one can take advantage of the translation symmetry of the problem, and numerical stability analysis in this set-up. We start from the equations describing a one-dimensional electrophysiological model of the spatial profile of the transmembrane voltage $V(x)$ and the vector of corresponding spatial profiles of the gating variables $\vec{w}(x)$:

$$\begin{aligned} \frac{\partial V}{\partial t} &= \nabla \cdot (D \nabla V) - \frac{I_{ion}(V, \vec{w})}{C_m}, \\ \frac{\partial \vec{w}}{\partial t} &= \vec{g}(V, \vec{w}). \end{aligned} \tag{59}$$

The stability analysis is based on the continuation of periodic solutions in the above equation. The stability of pulses or pulse trains in a ring is obtained via the solution of the linear stability problem by numerical computation of pulse spectra. This yields not only a much more accurate determination of the onset of alternans than the direct numerical integration of electrophysiological model equations, but also a numerical test of the validity of simplified theories like the restitution hypothesis introduced above for a specific model. In an exemplary study [243], the membrane ionic dynamics were described by the Beeler-Reuter Drouhard-Roberge model [70, 263] for mammalian ventricular tissue.

The calculations necessary for a numerical bifurcation analysis of propagating action potentials in the one-dimensional system can be described in two steps. First, one can calculate the shape and velocity of a traveling pulse in a ring. Second, the stability of the pulse is investigated. A traveling pulse in a ring which moves with fixed velocity c and maintains its shape is stationary in a co-moving frame of reference with coordinate $\xi = x - ct$. A transformation of the 1D version of Eqs. (59) to this co-moving frame yields

$$\begin{aligned} \frac{\partial V}{\partial t} &= -\frac{I_{ion}(V, \vec{w})}{C_m} + c\frac{\partial V}{\partial \xi} + D\frac{\partial^2 V}{\partial \xi^2}, \\ \frac{\partial \vec{w}}{\partial t} &= \vec{g}(V, \vec{w}) + c\frac{\partial \vec{w}}{\partial \xi}. \end{aligned} \tag{60}$$

Traveling wave solutions $(V_0(\xi), \vec{w}_0(\xi))$ can be found assuming the condition of stationary $\partial V/\partial t = 0$, $\partial \vec{w}/\partial t = 0$, so Eqs. (60) becomes a traveling wave ordinary differential equation (ODE). This allows to study properties of nonlinear waves by using well established dynamical systems methods like bifurcation analysis and continuation [264]. Propagating periodic action potential sequences can be calculated by continuation

of limit cycle in this ODE system, e.g., employing the continuation and bifurcation software for ODEs [265].

One can perform a linear stability analysis of the traveling pulse $(V_0(\xi), \vec{w}_0(\xi))$ [266, 267], by linearizing the co-moving frame reaction-diffusion equations (60) with respect to small deviations from the steady traveling pulse $(\delta V(\xi,t), \delta\vec{w}(\xi,t))$. The separation ansatz

$$(\delta V(\xi,t), \delta\vec{w}(\xi,t)) = e^{\lambda t} \cdot (\Phi(\xi), \vec{W}(\xi)), \tag{61}$$

results in an eigenvalue equation

$$\lambda \begin{pmatrix} \Phi(\xi) \\ \vec{W}(\xi) \end{pmatrix} = \mathcal{L} \begin{pmatrix} \Phi(\xi) \\ \vec{W}(\xi) \end{pmatrix} \tag{62}$$

with

$$\mathcal{L}(\Phi, \vec{W}) = J_{(V_0,\vec{w}_0)}(\Phi, \vec{W}) + c\frac{d\Phi}{d\xi} + D\frac{d^2\Phi}{d\xi^2}; \tag{63}$$

The Jacobian matrix $J_{(V_0,\vec{w}_0)}(\Phi, \vec{W})$ contains periodical functions of ξ with spatial period L as elements. The real part of a given eigenvalue λ decides on temporal growth or decay of a corresponding eigenfunction, compare Eq. (61). We are looking for $L-$periodic solutions of the eigenvalue equation (62) with regard to the pulse in a ring. Since one wants to solve Eq. (62) by continuation, one needs to consider a more general problem first: For each complex number λ, Eq. (62) represents a second order linear ODE with periodic coefficients which can be rewritten as a first order ODE. Its general solution is given by the Floquet theorem. We adjust the complex number λ so that the system (62) possesses a Floquet multiplier $e^{i2\pi\gamma}$ of absolute value one ($\gamma \in \mathbb{R}$), which corresponds to the existence of a solution of Eq. (62) on the domain $(0, L)$ with boundary condition

$$(\Phi, \vec{W}, \frac{d\Phi}{d\xi})(L) = e^{i\,2\pi\gamma}\ (\Phi, \vec{W}, \frac{d\Phi}{d\xi})(0), \qquad \gamma \in \mathbb{R}. \tag{64}$$

Following the methods described above, one can compute profiles and velocities c of pulses on a ring for different ring lengths L. The resulting dispersion relation or conduction velocity (CV) restitution curve $c(L)$ shows for large L a plateau (to be exact, this model presents weak anomalous dispersion, i.e., negative slope [268], see Fig. 28(a). Anomalous dispersion in the context of cardiac models is known as supernormal conductivity [40]).

Numerical bifurcation analysis allows us to test the hypothesis regarding the relation between the onset of alternans and the form of APD-restitution curve. The family of traveling pulses parameterized by L defines an APD-restitution curve $f(DI)$, shown in Fig. 28(b). This APD-restitution curve is a well defined function for traveling pulses but might fail to apply for the dynamics of non-steady states. The onset of alternans can be determined with the linear stability analysis defined by Eq. (62). The eigenvalue zero belongs always to the spectrum of the traveling pulse due to the translation invariance. The traveling pulse is stable if all eigenvalues except $\lambda = 0$ are

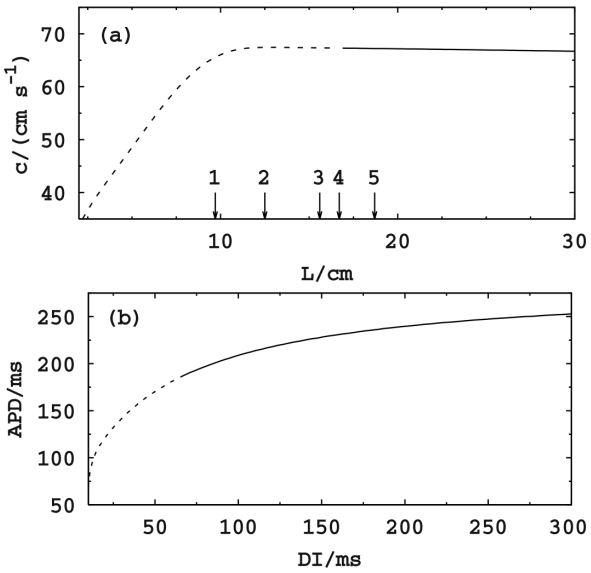

Figure 28. (a): Dispersion relation - conduction velocity c vs. ring perimeter L. Solid (dashed) line indicates a stable (unstable) pulse. For labeled pulses Fig. 29 shows spectra. (b): APD-restitution curve for the traveling pulse. Reprinted with permission from [243]. Copyright 2007, AIP Publishing LLC.

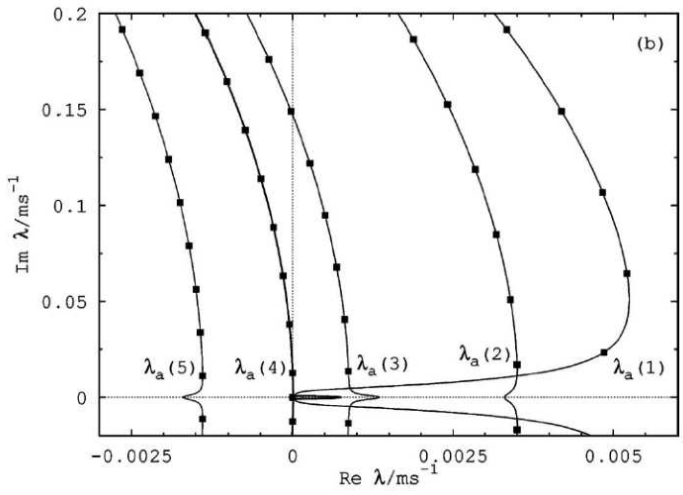

Figure 29. Critical curves of essential spectra. Squares depict eigenvalues with respect to the pulse in a ring. Labels refer to Fig. 28. The instability appears through a pair of complex conjugate eigenvalues λ_a. Successively pairs of eigenvalues with higher frequency (= larger imaginary parts) cross the imaginary axis. Reprinted with permission from [243]. Copyright 2007, AIP Publishing LLC.

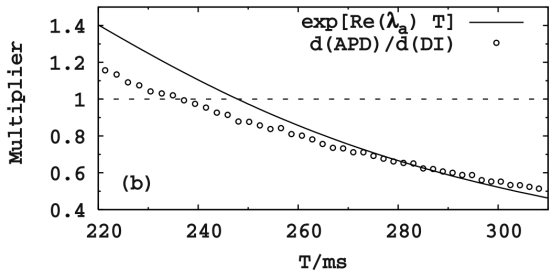

Figure 30. Slope of the APD-restitution curve for the traveling pulse (circles) and multiplier $e^{Re[\lambda_a(T)]\cdot T}$ (solid line) that is associated with the pair of critical eigenvalues. The APD restitution slope at the onset of alternans determined by numerical linear stability analysis is 1.2. Reprinted with permission from [243]. Copyright 2007, AIP Publishing LLC.

located in the left complex half-plane away from the imaginary axis. It is unstable if at least one eigenvalue has a positive real part.

Eigenvalues for pulses that belong to different ring lengths are shown in Fig. 29(b) by squares. Associated pulses are marked on the dispersion relation in Fig. 28(a). Decreasing the size of the ring below a given critical value L^{crit} a pair of complex conjugate eigenvalues λ_a and its complex conjugate cross the imaginary axis from the left to the right, with $\mathrm{Re}(\lambda_\mathrm{a}^\mathrm{crit}) = 0$ giving the condition for the onset of alternans. The imaginary part contains a period $2\pi/\mathrm{Im}(\lambda_\mathrm{a})$ which would be twice the pulse period if the bifurcation would correspond to a perfect period doubling. The condition for alternans determines the critical size of the ring L^{crit} and the related pulse and conduction velocity c^{crit}. The circumferences L^{crit} obtained by the continuation method are in line with those found in numerical simulations. The associated eigenfunctions to λ_a^{crit} show a broad amplitude at the back of the pulse [243] indicating the variations of the APD that occur in alternans. One can evaluate the restitution condition from the results of the numerical stability analysis, see Fig. 30. Comparing the slope of the $APD-$restitution curve to the multiplier $e^{\mathrm{Re}[\lambda_\mathrm{a}(\mathrm{T})]\cdot\mathrm{T}}$ one finds for the modified Beeler-Reuter model that the slope of the restitution curve is 0.85 at the onset of alternans giving a sizable deviation of the prediction of a slope 1 [226].

The mentioned frequency ratio of two indicates that the solution of the eigenvalue equation (62) and the resulting spectra reflect the alternans instability. The results for various choices of parameters governing the ion channel kinetics of the modified Beeler-Reuter model and the related 1D simulation results regarding alternans are given for the example studied in [243]. The described methods were also analyze the stability of pulse trains of two and more action potentials on a ring [252] yielding results in line with those found earlier for FitzHugh-Nagumo model with anomalous dispersion.

6. Spiral wave dynamics

Rotating excitations (rotors) are often found in cardiac experiments and corresponding simulations. A special case of two-dimensional rotors are spiral waves, that are discussed in this section. Their three-dimensional equivalent are scroll waves that will be reviewed separately in the next section. Spirals can become unstable (spiral breakup), which leads typically to a state of irregular, chaotic activity. The description of reentry in cardiac tissue in terms of a rotating wave around an obstacle forming a spiral wave dates back to a classical paper by Wiener and Rosenblueth in 1946 [269]. Later, it was shown in chemical media (i.e., in the Belousov-Zhabotinsky (BZ) reaction [270]) that such rotors can be autonomous and circulate around an unexcited area referred to as the spiral core. An obstacle is thus not necessary to sustain spiral waves in excitable media. In the cardiac literature this latter case is refered to as functional reentry, and contrasted with anatomical reentry when the spiral wave is anchored to an obstacle and rotates around a region of heterogeneous tissue. In any of these cases, the rotors impose a frequency that is much larger than the natural sinus rhythm frequency of the heart and are therefore widely discussed as building block of ventricular tachycardias and fibrillation, see e. g. [20]. To exist, sustained rotating spirals need a minimum system size of 20 percent of the spiral wavelength in an unbounded domain. So one may expect that rotors are not found in small animals. Recent studies, however, reveal that (stable and unstable) spirals and the related signature of ventricular fibrillation (VF) appear even in mice and rats. A comparative analysis of typical VF frequencies ν_{VF} in animals from mice and rats via cats, dogs and pigs to humans and horses displays a characteristic power law scaling with $\nu_{VF} \propto BM^{-1/4}$, where BM is the body mass [271]. Similarly, the rotor core diameter R scales with $R \propto BM^{1/4}$, while the action potential velocity is practically constant. In absolute numbers, characteristic fibrillation frequencies decrease from 38 Hz in mice to 6.8 Hz in humans. Since the extension L of the heart roughly scales with $L \propto BM^{1/4}$, the characteristic ratio of system size L to rotor size R is only weakly dependent on the size of the animal and apart from the characteristic scaling of frequencies and lengths comparable rotor dynamics may be observed in many different species.

Theoretical analysis and numerical simulations of spirals in cardiac propagation were often motivated by the rich variety of experimentally observed spiral dynamics. Stationary and drifting spirals were discovered, e. g., in slices of ventricular muscle from dog and sheep [16, 17]. Later on, improved imaging techniques allowed the visualization of spiral dynamics on the surface of isolated rabbit hearts [135], wherein nonstationary reentrant spiral dynamics was identified as a mechanism for polymorphic tachycardia. Optical imaging of electrical activity in isolated, perfused dog hearts enabled the observation of transiently erupting rotors and frequent wavefront collisions and wavebreak generation in the early phase of ventricular fibrillation-like activity [272]. In parallel, a method to obtain spatial phase maps (i.e., representation of the dynamical phase of the local excitations, see Fig.2) was developed that allowed to identify the

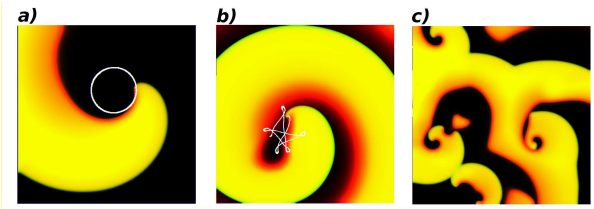

Figure 31. Types of spiral wave dynamics in numerical simulations of the Fenton-Karma model together with the trajectory of the spiral tip, and its relation to cardiac arrhythmia: Monomorphic ventricular tachycardia related with a rigid rotating spiral wave (a), polymorphic ventricular tachycardia related with a meandering spiral wave (b) and ventricular fibrillation related with spiral breakup (c).

multiple spiral tips (i.e., phase singularities), as sources of fibrillatory activity and rotating, reentrant excitations and to follow their temporal evolution with emphasis on formation and termination of such rotors [273].

Depending on the dynamics of the tip and the type of wave interaction between consecutive pulses of the same spiral wave, different types of behavior are observed, see Fig. 31 for three representative examples:

- *Rigidly rotating spiral waves*: the tip of the spiral wave rotates rigidly around a circular unexcited region, the core (Fig. 31(a)). Under some conditions such dynamics is associated with monomorphic ventricular tachycardia where the ECG shows a fast characteristic frequency [17]. Two limiting cases can be distinguished: the large core regime, when the core size is larger than the typical spiral wavelength and there is not interaction between consecutive pulses, and the small core regime, where the core size is much smaller than the wavelength [274].
- *Meandering spiral waves*: the motion of the tip is not circular but it performs a more complex motion. These spiral waves would produce the appearance of several frequencies in the ECG and, therefore, they are associated to polymorphic ventricular tachycardia. In the simplest case two frequencies are combined to produce epicycloid or hypocycloid dynamics [275]. The appearance of additional frequencies produces complex spiral motion [276]. In effect, the typical spiral waves observed in models of cardiac tissue present elongated cores. In these, the tip follows a relatively large straight motion along the refractory tail of the previous pulse combined with rapid turns (Fig. 31(b)) [277]. Variation of parameters in cardiac models yields a variety of meander patterns [74].
- *Spiral break-up*: the interaction between pulses can produce the breaking of the spiral in different pieces that automatically rotate and produce new spiral waves. Then, the new spirals break again, producing a cascade effect (Fig. 31(c)). A final chaotic dynamic state of pieces of rotating spirals fills out the whole system [91,278]. Such a state has been proposed to underlie ventricular and atrial fibrillation [80,279].

6.1. Meandering

The term meandering spiral waves was firstly used by Winfree in the description of chemical spirals in the BZ reaction [280]. In this, the rotation of some spiral tips is not rigid but a cycloid motion resulting from the combination of two frequencies and giving rise to a flower-like dynamics, see Fig. 32. Such experimental results were posteriorly explained by numerical simulations in different simple reaction-diffusion models [132,281,282], which were able to define the tip of the spiral and to calculate its trajectory.

The meandering motion of the spiral waves appears due to the interaction of the wavefront with the refractory tail of the previous excitation. Therefore, it can be interpreted as a time-delay feedback in the active medium [283]. The analysis of the dynamics of spiral meandering revealed that it appears through an oscillatory, Hopf bifurcation. This was first demonstrated numerically by Barkley, Kness and Tuckerman [86]. At the same time, Karma [284] showed that meander occurs via a Hopf bifurcation of circularly rotating spiral-wave solutions when the excitability of the model is sufficiently high. A complete stability analysis of the spiral wave solution has been performed in a simple reaction-diffusion model, identifying the eigenvalues and the unstable modes corresponding to the Hopf bifurcation [285]. The ensuing dynamics has been studied using a reduction of the whole reaction-diffusion system to a low-dimensional model in terms of a normal form analysis, that captures the interaction between the original rotating state and the new modes appearing at the Hopf bifurcation [286,287].

Meandering spiral waves are commonly observed in simple and complex models of cardiac tissue. Close to the bifurcation three cases can be distinguished depending on the motion of the tip: inward and outward meandering, and drift. Depending on the relation between the characteristic rotation frequency of the spiral and the frequency of the Hopf bifurcation, epicycloid (Fig. 32(b)) and hypocycloid (Fig. 32(d)) dynamics can be observed, which produce meandering with inward and outward petals, respectively. In the case of resonance between the two frequencies, a linear drift is obtained, see Fig. 32(c).

Far from the bifurcation threshold, cardiac models usually present complex meandering motion, as meandering with linear cores [288], a combination of a fast half rotation with a slow linear motion along the refractory tail [289], or hypermeander [276], a randomly motion associated to highly meander spiral waves.

Associated with meander (or hypermeander) is the Doppler effect, by which the wavelength of the spiral shortens ahead of the tip in the direction of its movement and enlarges in the opposite direction. When this effect is large it can give rise to spiral breakup [91,290]. Even if it is stable, it results in complex dynamics, that in the ECG is manifested as polymorphic VT, sometimes indistinguishable from those obtained during VF [122].

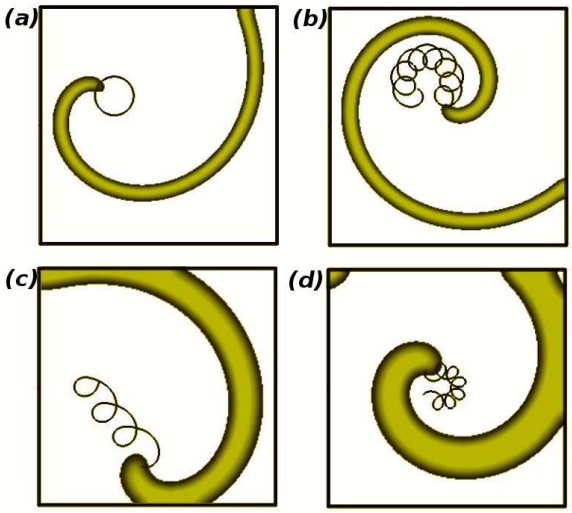

Figure 32. Numerical simulations with the Barkley model of different meandering of spiral waves in cardiac tissue close ot the bifurcation: Rigid rotation with large core (a), inward meandering spiral (b), drifting meandering spiral (c), outward meandering spiral (d).

6.2. Spiral breakup

An important motivation for the study of excitable media has been the quest for the cause of irregular high-frequency electrical activity in cardiac muscle typically observed during ventricular and atrial fibrillation [15]. The reason for the onset of ventricular fibrillation as well as possible treatments remain subjects of intense experimental and theoretical research [291]. Early experiments in thin sheets of heart tissue displayed only stable spirals in contrast with the irregular activity seen in experiments with whole hearts [17]. In addition, it was argued that hearts with small mass and, in particular, small wall thicknesses do not support irregular spiral turbulence-like electrical dynamics. Consequently, A. T. Winfree suggested that irregular activity in the heart might be a genuinely 3D phenomenon [121]. Thus realistic three-dimensional, anisotropic models of the heart and excitable media have been investigated and revealed various sources of irregular activity on the surface including intricate dynamics of scroll waves [78, 292] and the analogue of breakup in three dimensions [293, 294], for further elaboration on complex 3D dynamics, see Section 7. In parallel, the phenomenon of spiral breakup has emerged as a candidate mechanism for ventricular and atrial fibrillation and shall be reviewed in this section.

In reaction-diffusion media, three fundamentally different mechanisms of spiral breakup have been observed:

- *Lateral instabilities*, observed in chemical reaction-diffusion equations, spirals can break because the waves emitted from the spiral's centre (core) are destabilized by transverse perturbations that appear only for fast inhibitor diffusion [295–298], but this mechanism is not relevant for electrophysiological models. Zykov et al. showed

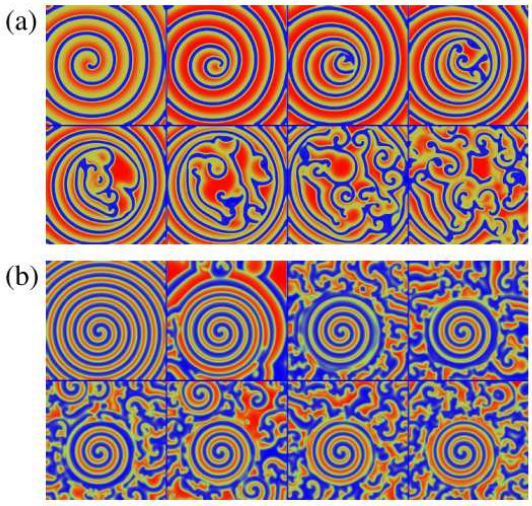

Figure 33. Examples for time evolution of (a) core breakup for excitable conditions and (b) a far-field breakup for oscillatory conditions in the Bär-Eiswirth model Eqs. (41), for details, see [301, 304]. Reprinted figure from [304] with permission of IOP Publishing & Deutsche Physikalische Gesellschaft, CC BY-NC-SA.

that inhibitor diffusion is needed to obtain instability of transversal modes [298]. In contrast, cardiac models have diffusion only in the activator variable, i.e. spatial coupling is provided exclusively by the coupling of transmembrane potential, while diffusion of ions is absent or can be neglected on the scale of the tissue.

- *Radial instabilities*, observed in cardiac models, typically unstable modes in the radial direction [71, 84, 91, 225, 241, 242, 278, 279, 299–301] cause spiral instability and possibly breakup. If, instead, transversal modes would be the main cause of spiral instability and breakup, excitation waves should display corrugations as seen in models with fast inhibitor diffusion, see e.g. the images displayed in the corresponding references [295–298].
- *Meandering-induced instabilities*, this possibility can arise from the destabilization of the core's location through meandering [285, 286, 302] that was described above in Section 6.1.

In what follows, we shall concentrate mostly on destabilization against modes in the radial direction, since these are the most relevant ones for cardiac dynamics exhibiting spiral breakup. Strong spiral meandering stemming from an instability of the spiral core can, however, enhance these instabilities since it effectively corresponds to a moving wave source, where a nonlinear Doppler effect leads to modulation of the wavelength, for a detailed discussion see [91, 303].

It is crucial to note that in all examples of radial spiral breakup in reaction-diffusion models and related experiments two different scenarios are observed: spirals may break first close to their core or alternatively far away from the core [301], see Fig. 33. The core breakup in Fig. 33(a) is accompanied by a meander instability, which

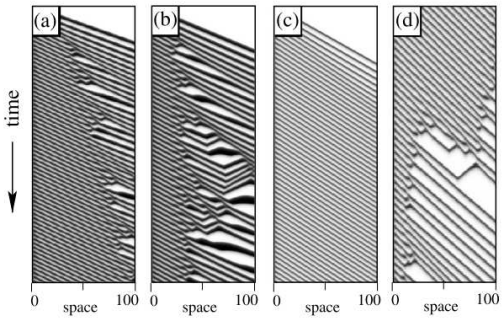

Figure 34. Examples for time evolution of the radial dynamics corresponding to (b) a core breakup for excitable conditions and (d) a far-field breakup for oscillatory conditions in the Bär-Eiswirth model Eqs. (41), for details see [301, 304]. The simulations have been run with a suitable Dirichlet boundary condition at the left end and a zero-flux Neumann boundary conditions at the right end of the domain. Reprinted figure from [304] with permission of IOP Publishing & Deutsche Physikalische Gesellschaft, CC BY-NC-SA.

introduces a Doppler effect into the waves emitted from the spiral core. Breakup near the core is found in simulations in excitable media [84, 91, 278] and in experiments with a chemical reaction [290], whereas breakup far away from the core is typically seen under oscillatory conditions both in chemical experiments [305] and in simulations of the complex Ginzburg-Landau equation (CGLE) [306, 307]. Interestingly, core and far-field breakup occurs also in a 1D set-up, where the spiral core is mimicked by a suitable Dirichlet boundary condition (see Fig. 34). It was found [301, 304] in simulation of the Bär-Eiswirth model of Eqs. (41) that using the values of u and v of an additional unstable focus in the local dynamics of this model (for details see [304]) selects wavelength and frequencies similar to the ones found in 2D spirals in simulations of the same model. At the same time the effect of meandering on the radially outgoing wavetrain is absent. The emergence of breakup like dynamics in the 1D setup (see Fig. 33b,d) shows that meandering may not be necessary to obtain core-breakup. This stipulation has been verified in 2D simulations of spirals and spiral break-up presented in [308].

To summarize, one can distinguish four distinct phenomenologies of spiral breakup:

- *Far-field breakup without meandering* as seen in Fig.33(b), the CGLE and the Belousov-Zhabotinsky reaction, typically associated with long-wavelength modulation caused by the Eckhaus instability.
- *Core breakup without meandering* as reported in the Bär-Eiswirth model by Sandstede and Scheel [308].
- *Far-field breakup with meandering* as seen in chemical experiments by Zhou and Ouyang [309, 310], in simulations of calcium waves by Falcke et al [311]. For a theoretical analysis, see the work of Brusch et al [303].
- *Core breakup with meandering* as seen in Fig. 33(a), in many cardiac models

[84, 279, 292] and in experiments with the Belousov-Zhabotinsky reaction [310]. This route is often termed Doppler-induced instability.

For models of cardiac tissue, usually core-breakup and strong meandering of the spiral core is observed [279].

7. Scroll wave dynamics

In the ventricles, one has to take into account that the wall thickness is not negligible, making the tissue fully three-dimensional. The natural extension of spiral waves in two dimensions corresponds to scroll waves in three dimensions.

Straight scroll waves may rotate with constant frequency. However, under certain conditions the filament of the scroll is not straight but takes a helical shape under meandering, see Section 7.1, or when an external twist is imposed, see Section 7.2; or it may produce complex unstable dynamics if the tension of the filament is negative, see Section 7.3. Finally, the breakup of spiral and of scroll waves are discussed in Section 7.4.

7.1. Meandering

The natural extension of two-dimensional meandering to more realistic three-dimensional tissue is the meandering of scroll waves [312]. The first explicit simulations of scroll meandering were obtained with simple models and its dynamics employed to explain relevant properties of the ECG under arrhythmic conditions [135].

In the first numerical simulations an equivalent behavior to two-dimensional meandering was assumed. However, it was observed that scroll curvature modifies the meander Hopf instability, resulting in a short wavelength instability that saturates. Then, one obtains helicoidal meandering scrolls [313] because the meandering of the filament of the scroll wave promotes the bending of the filament [73].

The linear stability analysis of scroll waves shows that the branch of meander modes can become unstable for finite wavelength perturbations along the filament, see Sec. 8.2.2, even if it is stable in two dimensions, so three-dimensional effects make the scroll unstable where the spiral was stable [139,314]. The final nonlinear state depends on the boundary conditions, so the amplitude of meander is constant along the direction of the filament z for periodic boundary conditions, but varies with z for non-flux boundary conditions.

Spiral meander in the presence of an external field can be studied using a normal form model [315], which can also be applied to a scroll wave, with filament curvature taking the place of the external field. This improves previous models [313] by considering the effect of scroll curvature both in the motion of the instantaneous filament and in the amplitude of the meander modes and explains the difference in curvature between the translation and meander modes.

Apart from the quasi two-dimensional periodic meander, complex aperiodic meander has also been described [316], which presents buckling of the scroll wave, an instability typically associated to negative filament tension, see Sec.7.3.2.

7.2. Sproing

Three dimensional waves rotate around the center filament. If, moving along the filament, there is a rotation resulting in a shift in the position of the wavefronts, then one talks about twisted scroll waves. Such rotation produces a change in the frequency of the rotors in each plane perpendicular to the scroll filament.

A twisted filament in a homogeneous system relaxes to an untwisted configuration [317]. However, there are several cases where twist can be imposed in the filaments, which may result in their destabilization:

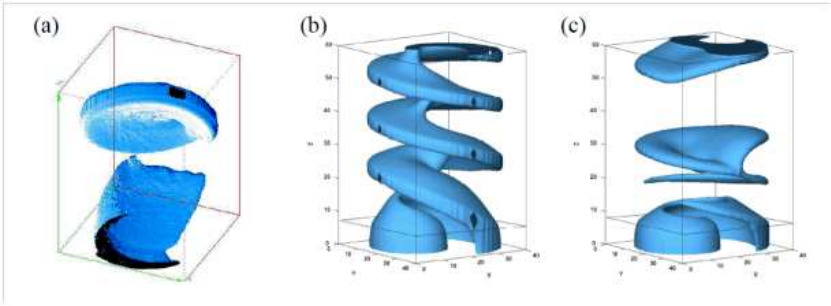

Figure 35. Experimental observation of sproing instability in the Belousov-Zhabotinsky reaction in an vertical oxygen gradient and simulations of (b) twisted scroll wave and (c) scroll breakup due to sproing in the Barkley model with a vertical gradient in excitability and zero-flux boundary conditions. Shown are surfaces of constant chemical concentrations, for more information see [318].

- *Periodic boundary conditions*: Straight scroll waves connecting two boundaries with periodic boundary conditions cannot eliminate the twist due to topological restrictions. It produces scroll waves with an integer number of rotations which depending on the total length of the system determines the twist of the filament. The twist can be controlled changing the number of rotations or the total length. Such condition is very useful for the realization of numerical simulations [319] and the analytic study [139] but unrealistic for comparison with experiments.
- *Heterogeneous system*: A change in the value of the excitability along the direction of the straight filament produces a change in the rotation frequency. For instance, if there is a constant gradient of excitability along the filament twist then forms homogeneously along this direction [160]. A step change in excitability produces twist in the slower part of the medium [160, 320]. More complex heterogeneities would change the local excitability of the medium and change the rotation frequency around the filament, inducing a distribution of twist (see Fig. 35).
- *Diffusion anisotropy*: If the scroll filament is aligned with the direction of transmural rotational anisotropy twist is induced along the filament [73,78,321,322].

In any of these cases, for small values of twist τ, the filament evolves to a straight twisted filament. However, if twist increases above a critical value ($\tau > \tau_c$), the straight

filament becomes unstable giving rise to a helical shape of the filament [139], in an instability known as sproing. The radius of the helix grows as the square root of the difference between the actual twist value and the critical value ($\sqrt{\tau - \tau_c}$), which suggests that it corresponds to a supercitical Hopf bifurcation.

7.3. Negative line tension

Even if the scroll filaments are just convenient mathematical entities, their dynamics permits to assign them physical magnitudes like tension. The first reference to the concept of filament tension of scroll waves is due to Yakushevich [323].

The first three-dimensional numerical simulations showed the dynamics of scroll waves with positive filament tension: straight filaments are stable while scroll rings shrink and disappear [324]. Then, numerical simulations were done showing not only shrink of scroll rings but also expansion [92]. Almost simultaneously, the first interpretations in terms of kinematic theory already predicted the existence of expanding scroll rings [325], implying that a straight scroll wave had to be also unstable.

The first clear numerical simulations of negative filament tension where done by Biktashev et al and the instability explained in terms of negative filament tension using a perturbation theory [93]. Recently, Dierckx et al [326] have calculated higher orders in the perturbation theory in generic models of excitable media.

Numerically, the full turbulent dynamics was studied some years later [140] and its possible appearance in ionic models of cardiac tissue was also discussed [75], where it is related to reduced conductances of sodium and slow inward currents. These low values are typically employed to model ischemic conditions of cardiac tissue [126].

Further understanding of this instability was obtained when, using a complete linear stability analysis of the scroll wave solution in a simple reaction-diffusion model, the unstable mode corresponding to the negative filament instability was identified as a translational mode, related to rigid body displacements in the direction perpendicular to the filament [314].

In simple models positive tension occurs for a medium with high excitability, i.e. a low excitation threshold, while negative tension occurs typically in media with low excitability [40, 140, 325]. However, more elaborate models show a region of the parameter space where scroll rings can slowly expand even if the medium is highly excitable [327], although turbulent dynamics was not observed in such simulations. Besides a change in the parameters of the model, the excitability of the medium can also be decreased replacing the partial differential equations by a discrete model, resulting in a change of filament tension when discreteness is increased [192].

The most detailed study of the onset of negative filament tension has been performed in the Barkley model Eqs. (40) [139,140,328]. In a large region of parameters Eqs. (40) produce stable scroll waves with positive tension and without any scroll breakup, see Fig. 36. Negative filament tension appears inside a broad region of parameters and closer to the non-excitable condition, where free edges retract, see

Fig. 36. Exactly at the boundary with non-excitability the spiral rotation period increases to infinity, note that this limit corresponds to the large core limit employed later for different analysis.

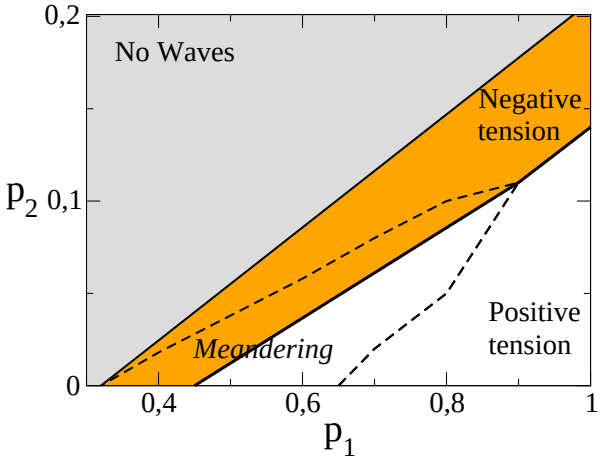

Figure 36. Phase diagram of the dynamics of scroll waves in the Barkley model as function of two parameters [328]. Four regions are shown in the diagram: No waves corresponds to unexcitable conditions, so scroll waves do not exist in this region; Negative and positive tension regions are conveniently noted in the diagram and the dashed line corresponds to three-dimensional meandering region. Note that both, positive and negative tension, are compatible with meandering.

Scroll waves with negative filament tension have been recently found in three-dimensional chemical BZ reaction [329, 330]. However, they have not been observed in experiments in cardiac tissue, so the relevance of this instability for the induction of fibrillation is disputed.

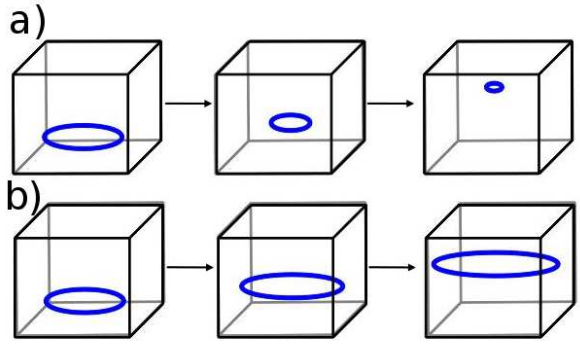

Figure 37. Sketch of the dynamics of a scroll ring: Positive (a) and negative (b) tension of the circular filament, giving rise to collapse and expansion respectively.

7.3.1. Expansion of scroll rings. A scroll wave in a thin slab, with its straight filament orthogonal to the boundaries, is a quasi 2D solution, as each section orthogonal to the

filament is the same and all spatial derivatives in the third direction parallel to the filament are zero. The first essential 3D effects occur when one considers either curved of twisted filaments. An ideal object to study the effect of curvature is a scroll ring that contains a circular filament, with constant curvature. The filament dynamics of scroll rings was studied in [92, 324, 331], showing that the rotation of a scroll ring is non-stationary, see Fig. 37. The position of its filament is not stable but drifts in space, with drift velocities proportional to the filament curvature:

$$c_n = -D_n\kappa, \qquad c_b = D_b\kappa; \tag{65}$$

where c_n and c_b are drift velocities in the normal (horizontal in Fig. 37) and binormal (vertical) directions, D_n and D_b are proportionality coefficients, and κ is the filament curvature. For scroll rings κ is equal to R^{-1}, where R is the radius of the ring, so Eqs. (65) take the simple form:

$$\dot{R} = -\frac{D_n}{R}, \qquad \dot{Z} = \frac{D_b}{R}. \tag{66}$$

Based on the sign of the normal component of the velocity two regimes of the scroll ring are distinguished. The first regime with positive D_n corresponds to a contraction of the scroll ring [324], see Fig. 37(a). When the ring filament reaches a critical radius, collapse of the scroll ring occurs. The second regime with $D_n < 0$ is the scroll ring extension [92] shown in Fig. 37(b). Under such conditions the radius of the scroll ring increases proportionally to its curvature. Expansion and collapse of scroll rings are typically accompanied by a vertical drift, see Fig. 37.

7.3.2. Buckling of scroll waves. Filament contraction decreases the filament length and thus is associated with positive line tension, while extension of the filament corresponds to the case of negative tension. A filament with positive line tension will either collapse (e.g. for the case of a scroll ring) or will attain a stable shape with the minimal possible length (e.g. for a straight scroll). Thus, an initially perturbed straight filament will recover the stable straight configuration. By the contrary, a filament with negative tension tends to increase its length. The instability due to negative filament tension and the resulting turbulence is a purely three-dimensional effect. For the same parameter values spiral waves are stable in two dimensions. It follows that there is a minimal thickness of the three-dimensional wall below which the effects of negative filament tension disappear. In Fig. 38 we show the results of some numerical simulations with the same parameter values but for different vertical thicknesses. When the tissue becomes very thin, the instability does not develop and the scroll wave rotates in a similar fashion as a spiral wave in two-dimensional media, see Fig. 38(a). For intermediate thickness the filament is unstable, however the length of the filament saturates. The filament bends and undergoes a complex meandering motion without breaking up, see Fig. 38(b). Such dynamics is known as buckling of scroll waves and produces buckled, precessing filaments, where the negative filament tension instability is arrested by the horizontal boundaries. The study of this bifurcation shows a critical thickness to obtain

a finite, saturated, buckling amplitude [332]. For thick three-dimensional tissue the negative tension instability develops, see Fig. 38(c), giving rise to a turbulent state.

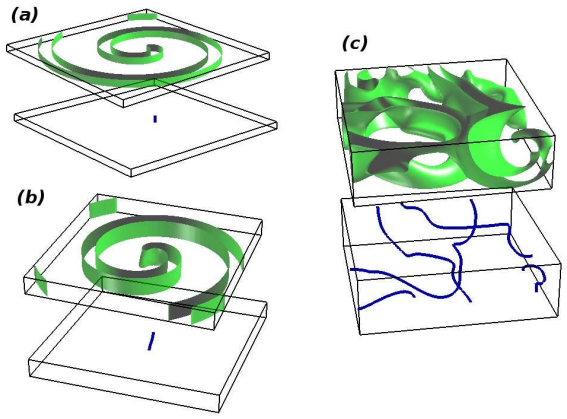

Figure 38. Numerical simulations of scroll waves with negative filament tension under different geometric constrains: Scroll wave is stable in a thin layer (a), slight bending of the filament for a slab of tissue (b) and negative filament tension in a thick system (c). Simulations done with the Luo-Rudy model. Adapted from [75] with permission of Springer.

7.3.3. Turbulence of scroll waves. In large systems, filaments with negative filament tension grow, creating loops. Then, if the filament touches a boundary, this results in the filament breaking into two pieces, leading to filament multiplication [40,56,93,140]. This regime has received different names from different authors, e.g. autowave turbulence [333], scroll wave turbulence [334] or Winfree turbulence [140].

An example of turbulent dynamics is shown in Fig. 39. First, a scroll wave rotates around its straight filament. As time goes on, transverse deformations in the filament develop (Fig. 39(a-b)). The length of the filament rapidly increases because it loops out and forms an irregular expanding tangle. The tangle initially still consists of a single connected filament until the moment it touches a boundary plane. After that, the filament gets fragmented into many pieces (Fig. 39(c)) that fill the medium and the resulting waves exhibit a turbulent appearance (Fig. 39(d)).

Upon onset of the instability the total length of the filament increases exponentially with time. The total length saturates when the outflow of filament through the boundaries is compensated by the increase of filament length generated by the instability [328]. The turbulent dynamics frequently presents an intermittent behavior between complex turbulence and a relatively organized state [334]. This occurs due to the stabilizing effect of filament interaction; filaments tend to bunch in groups of three or more filaments [334]. These filament bundles push the remaining individual pieces of filament outside the medium, and thereby counteract the effects of negative filament tension. This effect is associated with parameters for which formation of multi-armed

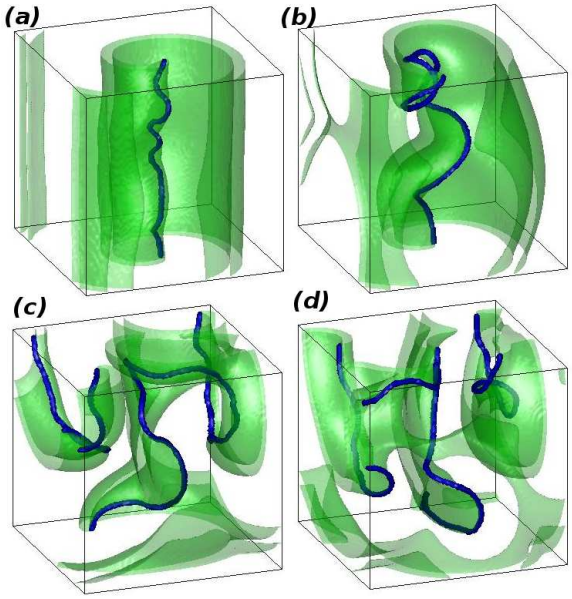

Figure 39. Numerical simulations of a scroll wave with negative filament tension: initial deformed filament (a), bending of the filament (b), breakup of the filament at the boundaries (c) and stationary chaotic dynamics (d). Simulations done with the Luo-Rudy model. Adapted from [75] with permission of Springer.

spiral waves in two spatial dimensions is found, which typically occurs at low excitability conditions [335].

7.4. Characterization of electrical turbulence.

An important issue is the quantitative characterization of the turbulent fibrillation dynamics in experiments and corresponding simulations. Since formation of a spiral or scroll due to reentry of electrical activity and subsequent breakup of this initial rotor is believed to be the most likely mechanism for fibrillation, we focus here on the characterization of irregular activity states in models and experiments exhibiting spiral breakup. Electrical turbulence in general can be classified as spatiotemporal chaos [336]. Indications for spatiotemporal chaos are spatial correlations that decay on scales much smaller than the system size, short temporal correlation, many positive Lyapunov exponents, and an extensive scaling of the attractor dimension (Kaplan-Yorke dimension) estimated from the spectrum of Lyapunov exponents with the system size (= area in 2D or volume in 3D). The computation of Lyapunov exponents is technically quite involved and has therefore not been carried out for realistic electrophysiological models. To our knowledge, the only example where the extensive scaling of the attractor dimension has been shown numerically for an excitable model with a turbulent dynamics stemming from spiral breakup is the work of Strain and Greenside on the Bär-Eiswirth model [337]. An alternative approach to characterize spatio-temporal spiral chaos on the basis of coherent structures was recently suggested by Byrne et al. [338].

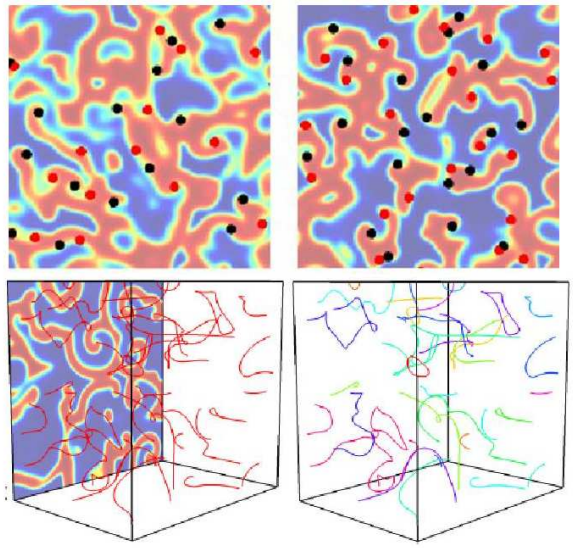

Figure 40. Comparison of turbulent states in the Bär-Eiswirth model: defect-mediated turbulence in 2D (top row) and filament turbulence in 3D (bottom row). Reprinted figure with permission from [339]. Copyright (2015) by the American Physical Society.

A second approach builds on the phenomenological classification of electrical turbulence in excitable media as defect-mediated turbulence. Defect-mediated turbulence refers to a state where new defects are created in pairs of opposite topological charge and existing defects are annihilated if they collide with defects of opposite topological charge. The sign of the topological charge at the center of a spiral or a spiral fragment characterizes its sense of rotation (clockwise or counterclockwise). The term was introduced originally for spatiotemporal chaos in the complex Ginzburg-Landau equation by Coullet et al. [340]. An illustration of defect-mediated turbulence resulting from spiral breakup in an excitable medium in 2D simulations is given in the top row of Fig. 40, where topological defects are marked by black and red circles. Gil et al. developed a simple theory for the defect statistics in defect-mediated turbulence by assuming a constant creation rate of defect pairs in competition with an annihilation rate proportional to the square of the defect number in the medium [341]. As a result, the defect number fluctuates in time according to a Poisson distribution and the variance of the defect number was predicted to be equal to its temporal mean [341]. Studies of the defect-statistics in the Bär-Eiswirth model [342, 343] revealed that spiral breakup leads to an initial fast transient increase of the defect number, but shows substantial deviations from the prediction of the model by Gil et al. In particular, the variance close to the breakup instability is much smaller than the mean, which is due to a strong anticorrelation between topological defects reminiscent of the spatial correlation of particles in a liquid. Further away from the breakup instability spatial correlations are much weaker and the defect statistics are in line with the prediction of the simple theory by Gil et al. [341].

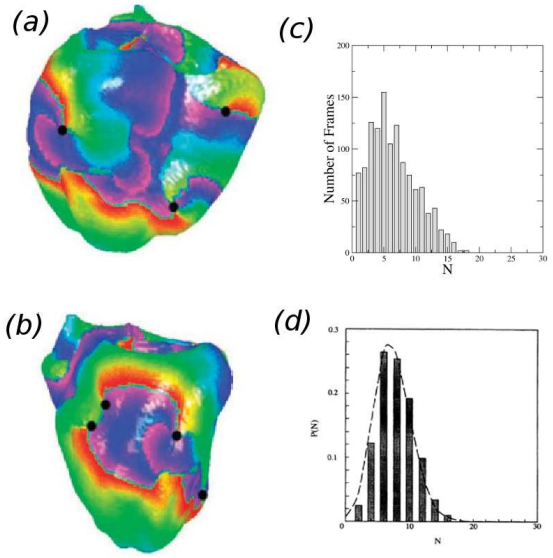

Figure 41. Phase singularities on the epicardial surface in a three-dimensional simulation with realistic electrophysiological model and heart anatomy (a) and (b) from [344] and typical temporal evolution (c) and epicardial phase singularities, see more details in [345] vs. Poissonian defect statistics (d) predicted from a simple theory [341]. Reprinted figure panels (a) and (b) with permission from [345]. Reprinted figure panels (d) with permission from [341]. Copyright (1990) by the American Physical Society.

Recent studies by Davidsen and coworkers have focused on the similarities and differences between defect statistics in 2D and filament statistics in 3D. For filament-induced turbulence emerging from a three-dimensional filament instability, they analyzed the statistics of defects (spirals) on the surface of their 3D simulation volume and found that the creation and annihilation rates of the surface defects follow essentially a linear dependence on the defect number in the medium with a constant offset [346] in contrast to 2D defect-mediated turbulence described above. This offers a possibility to determine the essential mechanism of electrical turbulence from experimental data on phase singularities. In a more recent study, the effect of the third dimension on the defect statistics in a system with genuine 2D spiral breakup instability was investigated showing no crucial differences in the defect statistics stemming from the dimension [339].

Defect statistics altogether offer an interesting and sufficiently simple tool to analyze electrical turbulence in the heart or in tissue cultures. TenTusscher, Panfilov and colleagues have indeed investigated the "organization" of ventricular fibrillation in the human heart both for realistic cardiac simulations [345] and for experimental data recorded in patients during heart surgery [344]. Their results are illustrated in Fig. 41, which shows a statistics roughly in line with the mean = variance prediction of Gil et al. [341]. The analysis of defect-statistics on the epicardial surface provides a useful tool to characterize electrical turbulence and evaluate the accuracy of predictions from

computational models with experimental data. A recent application, e.g., compares defect statistics and other metrics from homogeneous and heterogeneous models [347] and concludes that the influence of transmural and apicobasical electrophysiological heterogeneity in electrical turbulence is negligible and may, hence, be discarded in models. These heterogeneities were included by assigning different electrophysiological parameters to epicardial, midmyocardial and endocardial cell layers in [347].

8. Theory and methods for spiral and scroll wave instabilities

After the phenomenological description of the different instabilities affecting rotors in cardiac tissue presented in the previous two sections, we survey in this section theoretical approaches and numerical methods to study and analyze the instabilities responsible of complex dynamics in excitable media and cardiac models.

8.1. Kinematic description

In many situations a spiral or scroll wave can be considered as a rigid body, and its motion reduced to the motion of its tip (for a spiral) or its instantaneous or central filament (for a scroll). This is particularly valid in the limit of weak excitability, where this procedure can be performed rigorously using perturbation methods [348–350]. Cardiac tissue, under normal conditions, is highly excitable, so the kinematics equations in this case have to be considered as a phenomenological description of the motion of the spiral (or scroll) wave. Still, such a description has helped to understand important phenomena, as the origin of meander [351], the drift of spirals under an external field [352–354], or the influence of a periodic forcing [355]. This knowledge has helped to devise possible methods for defibrillation using low intensity electrical fields [356].

8.1.1. Spiral waves. This phenomenological approach starts by reducing the dynamics of a spiral wave to the motion of its tip [283,357]. In a Cartesian coordinate frame such equations are written as

$$\frac{dX}{dt} = -c\sin\alpha - g\cos\alpha, \qquad \frac{dY}{dt} = c\cos\alpha - g\sin\alpha; \tag{67}$$

where X and Y are the tip coordinates, α its angular variable, and c and g denote, respectively, the normal and tangential (respective to the spiral curve) tip velocities, see Fig. 42. These two velocities depend on curvature effects, parametrized by the instantaneous wavefront curvature at the tip, denoted κ, and are expressed by the eikonal equation for the normal velocity, and an analogous description for the tangential velocity:

$$c = c_0 - D\kappa, \qquad g = g_0 - \gamma\kappa; \tag{68}$$

in terms of the set of basic kinematic parameters c_0 , g_0 , D, and γ. In the limit of weak excitability the curvature correction to the normal velocity can be assumed negligible ($D\kappa \ll c_0$), so that c reduces to c_0.

The particular solution corresponding to a rigid rotating spiral is recovered by setting $\alpha = \omega_0 t$ and taking $g = 0$, which gives a critical curvature $\kappa_c = g_0/\gamma$. From the calculation of the curvature of a spiral wave rotating around an obstacle of radius R_0, one obtains $\kappa_c = (c_0/\xi^2 D R_0^2)^{1/3}$ [283], resulting from the limit of Wiener and Rosenblueth approach of spiral waves [269], with ξ being a numerical constant. Thus, the natural frequency of the rotating spiral is [283]

$$\omega_0 = \frac{c_0}{R_0} = \xi\sqrt{Dc_0}\sqrt{\kappa_c^3}, \tag{69}$$

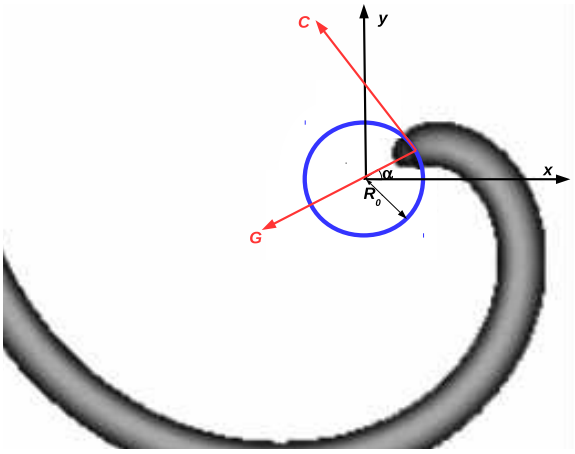

Figure 42. Sketch of the spiral wave motion. Wave corresponds to a snapshot of a rotating spiral wave in a generic model of excitable medium. The coordinates of the tip are x and y around the center of the core of the spiral, shown with a blue solid line. It is also shown the angular rotation of the tip around the core α, and the normal c and tangential g velocities of the tip, with respect of the wave front, giving rise to the final rotating motion.

In general, to obtain solutions for quasi-rigid rotating spirals, one needs to supplement Eqs. (67) with appropriate equations for the angle α and the curvature at the tip κ, both being assumed to be time-dependent quantities:

$$\frac{d\kappa}{dt} = \frac{\gamma\omega_0}{D}(\kappa_c - \kappa), \qquad \frac{d\alpha}{dt} = \omega_0 + \gamma(\kappa_c - \kappa)\kappa \tag{70}$$

where $D/(\gamma\omega_0)$ is the characteristic relaxation time of a perturbation in the tip curvature to the rigid rotating spiral solution. Note that if $D/\gamma \gg 1$ this time is larger than the rotation period. The change in the curvature of the tip modifies the tangential velocity and, therefore, the frequency of rotation.

The effect of the interaction between consecutive pulses can be incorporated into the kinematic description by considering the dependence of the normal and tangential velocities of the tip $c_0(T)$ and $g_0(T)$, on T, which is the rotation period for the rigid rotating spiral. This gives rise to a time-delay feedback. While for large T one recovers the usual rigid rotation description, Eqs. (67), since $c_0(T) \to c_0$ and $g_0(T) \to g_0$ in this limit; at rotation periods of the order of the recovery time, the velocities are modified:

$$c = c_0(T) - D\kappa, \qquad g = g_0(T) - \gamma\kappa; \tag{71}$$

where T is a spatially distributed function $T = T(x, y, t)$ of the previous wave. For the numerical calculation of the trajectories the whole wavefront has to be calculated, and it can be used for the study of the meandering of spiral waves, see [283].

In the limit of a weakly excitable medium (or large core limit) it is possible to study the onset of the meander instability by means of an asymptotic analysis [351, 358]. In this, a relation between the instantaneous radius of rotation R_i and the normal velocity of the wave with respect of the wave front at the tip c can be obtained, given by $R_i = (D/c_0)(b/(1 - c/c_0))^{3/2}$, being D the diffusion constant, c_0 the speed of a planar

front, and b a numerical constant [351,358]. Provided that c is known, then this sufficies to determine the motion and stability of the tip. In the case of meander, it was shown that the tip velocity c depends on the motion of the previous pulse due to the interaction of the wave front with its own recovery tail. Assuming a perturbation of the form: $p = [R_0 + q(t)]\exp(i\theta)$, with p the position of the tip in the complex plane and R_0 the radius of the circular core, it was shown that the radial perturbation satisfies a delay differential equation, given by [358]:

$$\frac{d^2q}{d\theta^2} + \omega^2 q = \omega^2 m F[q(t) - q(t - T_0)], \tag{72}$$

being T_0 the spiral period, m a parameter that depends on the properties of the medium and F a tanh-shaped function that can be calculated through asymptotics. A stability analysis of this equation shows that when the parameter m exceeds a certain threshold meander appears with a frequency ω_H that is half the frequency of the spiral. Thus, in this limit, meander is perfectly periodic. Calculations for smaller cores, show that as one leaves the large core limit the ratio becomes smaller that 1/2 and the motion becomes quasi-periodic, as is observed in numerical simulations [358].

8.1.2. Scroll wave rings. In a three-dimensional system, a scroll wave is approximated by an oriented traveling surface with an open edge corresponding to the filament [359]. Each element of the surface moves with a velocity proportional to the mean curvature H, i.e., the average of the principal curvatures, of the surface: $c = c_0 - 2DH$. The motion of the free edge of the surface depends on the mean curvature near the edge (H_0) and on the geodetic curvature κ of the edge line itself, and it grows ($g > 0$) or contracts ($g < 0$) with a velocity $g = g_0 - 2\gamma H_0 - \gamma'\kappa$, where g is the extension of the transversal velocity defined in Eqs. (68). The five kinematic parameters describing the evolution of a scroll wave (c_0, g_0, D, γ and γ') can be determined from the particular reaction-diffusion model [283].

The motion of the waves follows the dynamics of the free edge corresponding to the filament and, therefore, a quasi-steady approximation can be applied [283]. For the particular case of scroll rings the geodetic and mean curvatures can be expressed in terms of the angle of rotation around the filament α and the radius R of the scroll ring: $\kappa = -R^{-1}\cos(\alpha)$ and $H_0 = (\kappa - R^{-1}\sin(\alpha))/2$. As a result a set of four ordinary differential equations for the position of the free edge in cylindrical coordinates can be derived for the case of scroll rings with large radius [325, 359]:

$$\begin{aligned}
\dot{\kappa} &= \frac{\omega_0}{D}\left\{g_0 - \gamma\kappa + \frac{1}{R}\left[\gamma\sin\alpha + (\gamma' - D)\cos\alpha\right]\right\},\\
\dot{\alpha} &= \omega_0 + \kappa(g_0 - \gamma\kappa) + \frac{1}{R}\left[\gamma\sin\alpha + (\gamma' - D)\cos\alpha\right]\kappa,\\
\dot{\rho} &= -c_0\sin\alpha - \frac{1}{R}\left\{D + \left[\gamma\sin\alpha + (\gamma' - D)\cos\alpha\right]\cos\alpha\right\},\\
\dot{z} &= c_0\cos\alpha - \frac{1}{R}\left[\gamma\sin\alpha + (\gamma' - D)\cos\alpha\right]\sin\alpha,
\end{aligned} \tag{73}$$

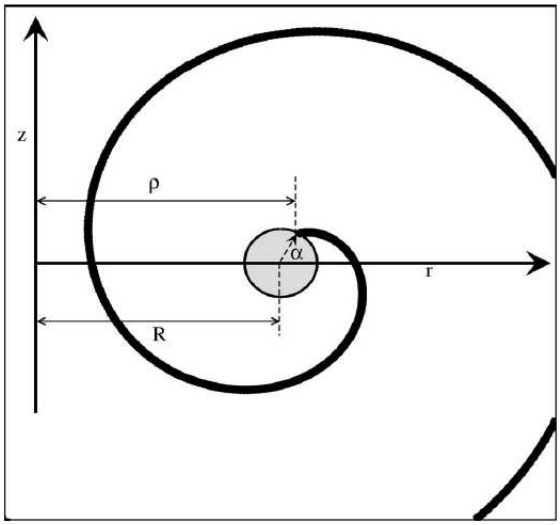

Figure 43. Sketch of the angular section of a scroll ring. Solid black line correponds to the angular section of the scroll wave and the grey cercle to the angular section of the ring filament. The coordinates of the edge are ρ for the radial direction and z for the vertical. It is also shown the angular rotation of the edge around the filament α, and the averaged radius R of the filament. Reprinted with permission from [360]. Copyright 2006, AIP Publishing LLC.

where where ω_0 corresponds to the rotation frequency of a spiral wave in two dimensions, ρ is the radial component and z the vertical position of the free edge, its local curvature (κ) and the angle of rotation (α), see a schematic representation in Fig.43. At first order in R^{-1}, and after the integration over one period of rotation, the dynamics of a scroll ring becomes [325, 360]:

$$\dot{R} = -\frac{D_n}{R}, \qquad \dot{Z} = \frac{D_b}{R}, \tag{74}$$

where the filament tension D_n and the vertical drift parameter D_b can be explicitly calculated in terms of the kinematic parameters [325, 359, 360]:

$$D_n = D - \frac{3}{4}\frac{c_0}{g_0}\frac{\gamma[D(\gamma' - D) + \gamma^2]}{\gamma^2 + D^2}, \tag{75}$$

$$D_b = \frac{3}{4}\frac{c_0}{g_0}\frac{\gamma^2(\gamma' - 2D)}{\gamma^2 + D^2}. \tag{76}$$

Depending on the value of the parameters the filament tension can change the sign. The decrease of g_0 in Eq. (75) may change the sign of D_n to negative values if g_0 is sufficiently small. Scroll waves in the kinematic approach can be formed only if $g_0 > 0$. If $g_0 < 0$ no steadily rotating scroll waves can form and the tip contracts in the course of time. Thus, decreasing the value of g_0 is equivalent to a reduction of the excitability and it means that filament tension becomes negative under conditions of weak excitability [360].

8.1.3. Equations for filament motion. The main idea of this approach is to assume that a scroll wave can be constructed by placing 2D spirals along a line (filament) slowly

varying in space. A periodic rigidly rotating spiral wave satisfies $V = V(r, \theta - \omega t)$. For the scroll wave, one can represent the three-dimensional space in the neighborhood of the filament using the coordinate representation $\mathbf{R} + p\mathbf{N} + q\mathbf{B}$, given by:

$$\frac{d\mathbf{R}}{ds} = \mathbf{T}, \qquad \frac{d\mathbf{T}}{ds} = \kappa\mathbf{N}, \qquad \frac{d\mathbf{N}}{ds} = -\kappa\mathbf{T} + \tau_g\mathbf{B}, \qquad \frac{d\mathbf{B}}{ds} = -\tau_g\mathbf{N}, \tag{77}$$

where $\mathbf{R}$ is the position of the filament, $\mathbf{T}$ is the tangent vector, $\mathbf{N}$ and $\mathbf{B}$ the normal and binormal unit vectors, s the arclength, κ the curvature and τ_g the torsion of the filament. Then, the filament dynamics is represented by coordinates along its length s and in normal p and binormal q directions yielding to $V(s, p, q, t) = V_0(r, \theta + \phi(s, t) - \omega t) + V_1 + ...$, (where r and θ are the polar coordinates in the plane p, q) [361].

Starting from the straight, untwisted scroll wave, one can obtain the motion of the mean filament and the equation for twist, making an expansion in terms of curvature and torsion, and projecting over the adjoints translational and rotational marginal eigenmodes (also known as response functions, see [137, 138]). At lowest order this results in the equations [93, 361]:

$$\frac{\partial\phi}{\partial t} = \frac{\partial\mathbf{N}}{\partial t} \cdot \mathbf{B} + b_1 \left(\frac{\partial^2\phi}{\partial s^2} - \frac{\partial\tau_g}{\partial s} \right) + a_1 \left(\frac{\partial\phi}{\partial s} - \tau_g \right)^2, \tag{78}$$

$$\frac{\partial\mathbf{R}}{\partial t} \cdot \mathbf{N} = b_2\kappa, \tag{79}$$

$$\frac{\partial\mathbf{R}}{\partial t} \cdot \mathbf{B} = c_3\kappa. \tag{80}$$

where it is imposed the gauge condition $\partial_t\mathbf{R} \cdot \mathbf{T} = 0$.

In the case of an untwisted scroll ring, $\kappa = R^{-1}$, and the former equations become simply [93]:

$$\dot{R} = -\frac{D_n}{R}, \qquad\qquad \dot{Z} = \frac{D_b}{R}, \tag{81}$$

where $\dot{R}$ and $\dot{Z}$ are, respectively, the velocities of the filament in the normal and binormal directions. The parameters $D_n = b_2$ and $D_b = c_3$ can be obtained by calculating the adjoint eigenfunctions of the linearization around a stable rotating scroll wave [361]. As in the previous section the theory predicts a linear dependence of the radius of the scroll ring on the curvature. Note, however, that the finding of the adjoint solution is not trivial and it has to be obtained using numerical methods [138].

The ribbon model (78)-(80) developed by Keener can be extended also to the case of twist induced instabilities. Defining $\mathbf{p}(\sigma, t)$, the unit vector pointing orthogonally from the center filament to the line of instantaneous scroll wave tips, the scroll wave twist can be defined as $\tau = (\mathbf{p} \times \partial_s\mathbf{p}) \cdot \mathbf{T}$. Then, a phenomenological extension of Eqs. (78)-(80) for a twisted scroll wave was developed in [160] (a more rigorous derivation can be found in [326]), giving

$$\begin{aligned}[\mathbf{R}_t]_\perp = {} & a_1\mathbf{R}_{ss} + a_2\mathbf{R}_s \times \mathbf{R}_{ss} + d_1\tau\mathbf{R}_s \times \mathbf{R}_{sss} - d_2\tau[\mathbf{R}_{sss}]_\perp \\ & - b_1[\mathbf{R}_{ssss}]_\perp - b_2\mathbf{R}_\mathbf{s} \times \mathbf{R}_{ssss}\end{aligned} \tag{82}$$

where the brackets denote the component of the enclosed vector orthogonal to the filament tangent. This equation has to complemented with an equation for the evolution of the ribbon twist. From the conservation of the linking number, one obtains the general expression

$$\frac{\partial}{\partial t}\left(\frac{\partial \tau}{\partial s}\right) = \frac{\partial \omega}{\partial s} + \left(\frac{\partial \mathbf{T}}{\partial s} \times \frac{\partial \mathbf{T}}{\partial t}\right) \cdot \mathbf{T} \tag{83}$$

that corresponds to the conversion of twist into writhe. To completely characterize the problem, one has to write down the dependence of scroll frequency ω on twist. Keeping the first twist corrections to the un-twisted scroll frequency:

$$\omega = \omega_0 + c\tau_w^2 + D\partial_s \tau + (\mathbf{T} \cdot \partial_t \mathbf{R})\tau \tag{84}$$

Eqs. (83), (84) are equivalent to Keener's phase equation (78).

To calculate the stability of a straight scroll wave one can consider small transverse deformations X, Y, perpendicular to the direction of the scroll z. Then, up to quadratic order for the complex deformation field $W(z,t) = X(z,t) + iY(z,t)$, Eqs. (82)-(84) become

$$\partial_t W = a\partial_z^2 W + id\tau\partial_z^3 W - b\partial_z^4 W, \tag{85}$$

$$\begin{aligned}\partial_t \tau &= \partial_z(D\partial_z\tau) + \partial_z(c\tau_w^2) + \partial_z\omega_0 \\ &\quad + \Re\left\{\left[\partial_z(\tau\partial_z\overline{W}) - i(\partial_z^2\overline{W})\partial_z\right]\partial_t W\right\}\end{aligned} \tag{86}$$

where a, b, d are complex coefficients ($a = a_1 + ia_2$, etc). For a contant twist the linear modes $W(z,t) = W_0 e^{ikz+\Omega t}$ correspond to helices of pitch k. The resulting dispersion relation

$$\Omega = -ak^2 + d\tau k^3 - bk^4 \tag{87}$$

gives an instability away from $k = 0$ when twist is larger than a critical value $\tau^c = 2\sqrt{a_1 b_1/d_1^2}$, corresponding to sproing, with pitch $k_c = \sqrt{a_1/b_1}$. For an initial helix in the unstable regime with pitch k, $W(z,t) = R(t)e^{ikz}$, and initial twist τ^0, the equation for the twist becomes

$$\partial_t \tau = -k^2(\tau + k)RR_t \tag{88}$$

that gives $\tau = \tau_0 - (\tau^0 + k)k^2R^2/2$, so twist decreases as the scroll acquires an helical form (twist is transformed into writhe). Introducing this in the equation of the center filament, one obtains the expression for a supercritical bifurcation

$$R_t = d_1 k^3\left[(\tau^0 - \tau^c)R - (\tau^0 + k)k^2R^3/2\right] \tag{89}$$

that results in a final helix radius $R = [2(\tau^0 - \tau^c)/(\tau^0 + k)k^2]^{1/2}$.

Numerically, the previous result can be obtained with simulations with periodic boundary conditions where the twist is fixed. In the more realistic case of non-flux boundary conditions, twist can be induced with a spatial change of excitability [160]. Interestly, Eqs. (83,84), give a very good prediction of the distribution of twist even for fast spatial changes of excitability. The onset of sproing in this case can be calculated from the absolute instability spectrum [160], giving rise to a spatial modulation in the amplitude of the helix resulting from sproing.

8.2. Linear stability analysis of spiral and scroll waves

8.2.1. Stability analysis of spiral waves. A rigid rotating spiral wave, stationary solution of the reaction-diffusion system, remains stationary in a frame rotating with the same frequency ω of the spiral. In such co-moving frame the reaction-diffusion equations take the form:

$$\left(\frac{\partial}{\partial t} - \omega\frac{\partial}{\partial \theta}\right) V = D\nabla^2 V + I(V,w),$$
$$\left(\frac{\partial}{\partial t} - \omega\frac{\partial}{\partial \theta}\right) w = R(V,w). \tag{90}$$

The steady state solution corresponding to a rigidly rotating spiral wave (defined by V_0 and w_0) is obtained by solving the expression:

$$0 = \omega\frac{\partial}{\partial \theta}V_0 + D\nabla^2 V_0 + I(V_0,w_0),$$
$$0 = \omega\frac{\partial}{\partial \theta}w_0 + R(V_0,w_0). \tag{91}$$

The stability of the solution V_0 and w_0 is obtained through a linear stability analysis, perturbing the solution $V = V_0 + V_1\exp(\sigma t)$ and $w = w_0 + w_1\exp(\sigma t)$, and evaluating the eigenvalues of the resulting eigenvalue problem [285]:

$$\sigma V_1 = \left[\omega\frac{\partial}{\partial \theta} + D\nabla^2_{2D} + k\frac{\partial I}{\partial V}(V_0,w_0)\right] V_1 + \left[\frac{\partial I}{\partial w}(V_0,w_0)\right] w_1,$$
$$\sigma w_1 = \left[\frac{\partial R}{\partial V}(V_0,w_0)\right] V_1 + \left[\omega\frac{\partial}{\partial \theta} + \frac{\partial R}{\partial w}(V_0,w_0)\right] w_1. \tag{92}$$

Besides the neutral modes associated to translational and rotational symmetries, given by eigenvalues $\sigma = 0$ and the complex-conjugate pair $\sigma_t = \pm i\omega$ (marked respectively as a star at the origin $Re(\sigma) = Im(\sigma) = 0$ and two stars at $Im(\sigma) = \pm\omega$ in Fig. 44), there is a pair of eigenvalues whose stability $Re(\sigma)$ changes with the control parameter of the corresponding model employed in Eqs. (90). The rigid rotating spiral wave becomes unstable through a Hopf bifurcation because these two eigenvalues are complex with no null imaginary part, as indicated by the arrows in Fig. 44. The complex part of the eigenvalue produces a secondary frequency ω_H. This new frequency induces the meandering of spiral waves, a cycloidal motion composed by two frequencies. If $\omega_H < \omega$ the meandering produces inward loops and if $\omega_H > \omega$, outward loops, which is actually the case shown in Fig. 44.

8.2.2. Linear stability analysis of untwisted straight scroll waves. Similarly to the case of the spiral, a linear stability analysis permits the detection of instabilities of the rigidly rotating scroll waves in a co-rotating reference frame, that will be used in the following. First, Eqs. (38) are transformed into cylindrical coordinates (r,θ,z), using $\theta = \theta_0 - \omega t$ where ω is the scroll wave rotation frequency:

$$\left(\frac{\partial}{\partial t} - \omega\frac{\partial}{\partial \theta}\right) V = D\left(\nabla^2_{2D} + \frac{\partial^2}{\partial z^2}\right) V + I(V,w),$$

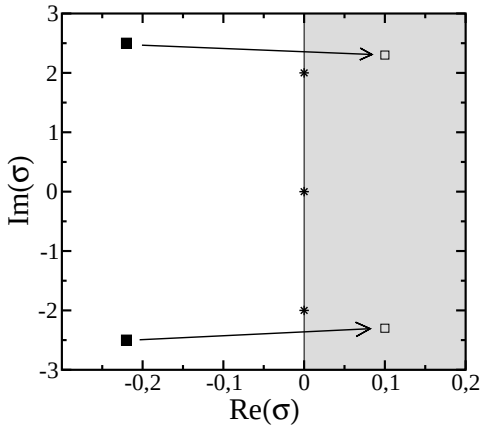

Figure 44. Sketch of the leading eigenvalue spectra of spiral waves close to the meandering instability. Crosses show eigenvalues on the imaginary axis due to symmetries. Solid and open squares show bifurcating eigenvalues before and after the instability. For the original data see [285].

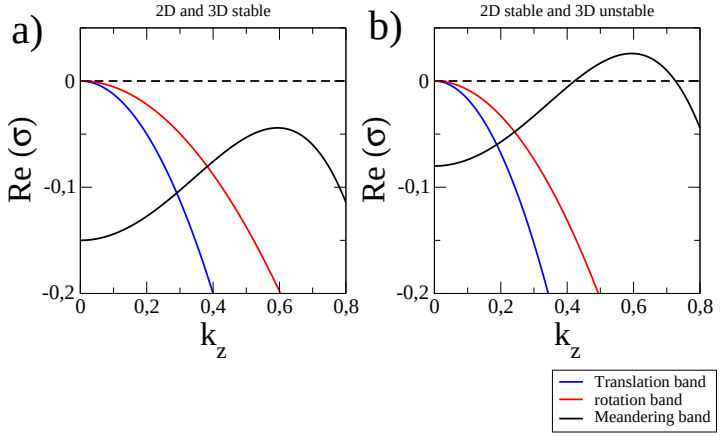

Figure 45. Sketch of the dependence of the real part of the growth rate on the wave number before (a) and after (b) the three-dimensional meandering instability. For the original data see [139].

$$\left(\frac{\partial}{\partial t} - \omega\frac{\partial}{\partial \theta}\right) w = R(V, w); \tag{93}$$

where, for simplicity, we do not considered the effects of the twist. The resulting equation for the steady state is obtained assuming that $V_0 = V_0(r, \theta)$ and $w_0 = w_0(r, \theta)$. These functions do not explicitly depend on the z-coordinate, so one recovers the basic solution for the spiral wave, given by Eqs. (91), that in this case corresponds to a straight scroll wave, without twist.

Next, the stability of this solution can be determined through a linear stability analysis considering small perturbations of the steady state: $V(r, \theta, z) = V_0(r, \theta) + V_1(r, \theta)\exp(\sigma t - ik_z z)$ and $w(r, \theta, z) = w_0(r, \theta) + w_1(r, \theta)\exp(\sigma t - ik_z z)$. Introducing these perturbations in Eqs. (93), one obtains the equations obeyed by V_1 and w_1 and

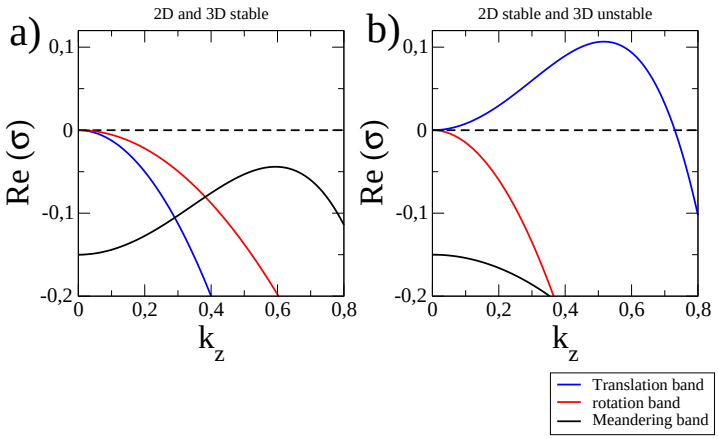

Figure 46. Sketch of the dependence of the real part of the growth rate on the wave number before (a) and after (b) the three-dimensional negative filament tension instability. For the original data see [139].

the growth rate σ:

$$\begin{aligned}\sigma V_1 &= \left[-Dk_z^2 + \omega\frac{\partial}{\partial\theta} + D\nabla_{2D}^2 + \frac{\partial I}{\partial V}(V_0, w_0)\right] V_1 + \left[\frac{\partial I}{\partial w}(V_0, w_0)\right] w_1, \\ \sigma w_1 &= \left[\frac{\partial R}{\partial V}(V_0, w_0)\right] V_1 + \left[\omega\frac{\partial}{\partial\theta} + \frac{\partial R}{\partial w}(V_0, w_0)\right] w_1. \end{aligned} \tag{94}$$

From these equations the corresponding dispersion relation can be calculated [139], i.e. the dependence of the different eigenvalues or growth rates σ on k_z. If the real part of one of the eigenvalues is positive ($Re(\sigma) > 0$) for a window of values of k_z, the rigidly rotating scroll wave is unstable.

As it was already noted in Sec. 6.1, the two-dimensional meander modes correspond to two complex conjugate eigenmodes, whose real part crosses zero at the two-dimensional meander instability line. The induction of the meander instability by three-dimensional effects is shown in Fig. 45. All modes in Fig. 45(a) have negative real parts so the scroll wave is stable. However, Fig. 45(b) shows that the real part of a finite band of modes has become positive indicating that the 3D scroll wave is unstable to meander, while the real part of 2D spiral meander mode at $k_z = 0$ is still negative and therefore the 2D spiral is stable.

One of the eigenvalue pairs obtained in the stability analysis of scroll waves corresponding to a perturbation with $k_z = 0$ is purely imaginary $\pm i\omega$ and is related to the translational invariance of the underlying reaction-diffusion equations. For nonzero values of k_z, the real part of this eigenvalue may become positive and it is maximal for a particular spatial wavenumber (Fig. 46). This instability corresponds to negative filament tension. From the dispersion relation one observes that the band of unstable wavenumbers has a maximum value k_z^{max}, which defines the minimum tissue size, or critical thickness, $L_{min} = 2\pi/k_{max}$, below which the negative line tension instability does not develop [139, 314], as discussed in Section 7.3.2.

8.2.3. Linear stability analysis of twisted straight scroll waves. In this case we employ Eqs. (93) in cylindrical coordinates (r,θ,z), where the amount of twist τ in the scroll wave is explicitly considered using $\theta = \theta_0 - \omega t - \tau z$:

$$\left(\frac{\partial}{\partial t} - \omega\frac{\partial}{\partial \theta}\right) V = D\left(\nabla^2_{2D} + \frac{\partial^2}{\partial z^2} - 2\tau\frac{\partial^2}{\partial\theta\partial z} + \tau^2\frac{\partial^2}{\partial\theta^2}\right) V + I(V,w),$$
$$\left(\frac{\partial}{\partial t} - \omega\frac{\partial}{\partial \theta}\right) w = R(V,w); \tag{95}$$

see for more details [314]. The resulting equation for the steady state is obtained assuming that $V_0 = V_0(r,\theta)$ and $w_0 = w_0(r,\theta)$. As in the previous case, the stability of this solution can be determined through a linear stability analysis introducing small perturbations of the steady state: $V(r,\theta,z) = V_0(r,\theta) + V_1(r,\theta)\exp(\sigma t - ik_z z)$ and $w(r,\theta,z) = w_0(r,\theta) + w_1(r,\theta)\exp(\sigma t - ik_z z)$ into Eqs. (95):

$$\begin{aligned}\sigma V_1 &= \left[-Dk_z^2 + \omega\frac{\partial}{\partial\theta} + D\tau^2\frac{\partial^2}{\partial\theta^2} + 2Di\tau k_z\frac{\partial}{\partial\theta} + D\nabla^2_{2D} + \frac{\partial I}{\partial V}(V_0,w_0)\right] V_1 \\ &+ \left[\frac{\partial I}{\partial w}(V_0,w_0)\right] w_1, \\ \sigma w_1 &= \left[\frac{\partial R}{\partial V}(V_0,w_0)\right] V_1 + \left[\omega\frac{\partial}{\partial\theta} + \frac{\partial R}{\partial w}(V_0,w_0)\right] w_1. \end{aligned} \tag{96}$$

For nonzero twist ($\tau \neq 0$) the dispersion relations obtained from Eq. (96) are not symmetric with respect k_z and therefore σ does not depend only in k_z^2 but also on odd powers of k_z.

8.3. Normal form analysis of the meander transition

8.3.1. Spiral waves. A simple phenomenological analysis of the transition to meander was developed by Barkley [286] and further formalized by Sandstede & Scheel [287]. In this, a normal form is derived for the bifurcation to meander, assuming that it occurs as a supercritical Hopf bifurcation, and taking into account Euclidean symmetry (rotation plus translations in the plane). Then, at the onset of the instability there are five marginal modes, corresponding to translational and rotational symmetry, and the modes emerging from the Hopf bifurcation. With this, the model reads:

$$\dot{\phi} = \omega \tag{97}$$
$$\dot{p} = e^{i\phi}(i\omega R_0 - \overline{z}) \tag{98}$$
$$\dot{z} = (\lambda_H - |z|^2)z \tag{99}$$

where ϕ is the phase of the circular motion of the spiral tip, and the complex functions $p = x + iy$ and $z = \rho e^{i\alpha}$ are the position of the tip and the (complex) amplitude of the Hopf modes. Besides, the Hopf and translational eigenvalues are given by $\lambda_H = \mu + i\omega_H$ and $\lambda_T = i\omega$, respectively (note that the equations are written in the original, not in the comoving, frame). When $\mu < 0$ the Hopf modes decay to zero, and the solution is

a rigidly rotating spiral $p(t) = R_0 e^{i\omega t}$. When $\mu > 0$, then, taking $z = \rho e^{i\alpha}$, for the Hopf mode one obtains:

$$\dot{\rho} = (\mu - \rho^2)\rho, \ \dot{\alpha} = \omega_H, \tag{100}$$

which, assuming that the amplitude decays fast to its steady state value, gives $\rho = \sqrt{\mu}$, $\alpha = \alpha_0 + \omega_H t$. Then, the motion of the tip of the spiral is given by:

$$\dot{p} = i\omega R_0 e^{i\omega t} - \sqrt{\mu} e^{-i\alpha_0 + i(\omega - \omega_H)t}. \tag{101}$$

When the frequency of the Hopf modes is the same as the original frequency of the spiral $\omega_H = \omega$, this equation results in a linear drift of the tip:

$$p(t) = R_0 e^{i\omega t} - \sqrt{\mu} t e^{-i\alpha_0}, \tag{102}$$

If the frequencies are different, $\omega_H \neq \omega$ then, the solution reads:

$$p(t) = R_0 e^{i\omega t} + \frac{i\sqrt{\mu}}{\omega - \omega_H} e^{-i\alpha_0 + i(\omega - \omega_H)t}, \tag{103}$$

that results in outward or inward petals depending on the relative values of ω and ω_H.

These type of normal forms can also be used, for instance, to study the resonant drift of the spirals under the effect of a periodic forcing [362].

8.3.2. Scroll waves. The normal form of a spiral wave under meandering (97)-(99) has to be modified in order to take into account the effects of a small curvature of slightly curved filaments of a 3D scroll wave [315].

$$\begin{aligned} \frac{d\phi}{dt} &= \omega, \\ \frac{\partial p}{\partial t} &= e^{i\phi}(i\omega R_0 - z) + \beta \frac{\partial^2 p}{\partial z^2}, \\ \frac{\partial z}{\partial t} &= (\mu - i\omega_H - |z|^2)z + \gamma e^{-i\phi} \frac{\partial^2 p}{\partial z^2}. \end{aligned} \tag{104}$$

Using a perturbation of the form $p = R_0 e^{i\omega t} + p_1 e^{i\phi} e^{\sigma t + i k_z z}$ and $z = z_1 e^{\sigma t + i k_z z}$, where $R_0 e^{i\omega t}$ is the steady scroll wave solution, one obtains the eigenvalues corresponding to the meander and translation bands. The eigenvalue for meandering becomes:

$$\sigma_H = \mu - i\omega_H - \left[\frac{\gamma}{\mu + i(\omega - \omega_H)} \right] k_z^2; \tag{105}$$

so σ_H depends on k_z, and therefore the bifurcation line of 3D meander may be different than 2D meandering. The eigenvalue corresponding to the translation band is:

$$\sigma_t = -i\omega + \left[\beta + \frac{\gamma}{\mu + i(\omega - \omega_H)} \right] k_z^2; \tag{106}$$

which indicates that the real value of σ depends on k_z, and for large enough values of γ the eigenvalue may become positive. The curvature at the origin of the translation band is the same as the drift velocity of a spiral in the presence of a electric field. It is also equal to the opposite of the curvature of the meander band shifted by a factor β [315]. The specific form of the coefficients γ and β can be found in [315].

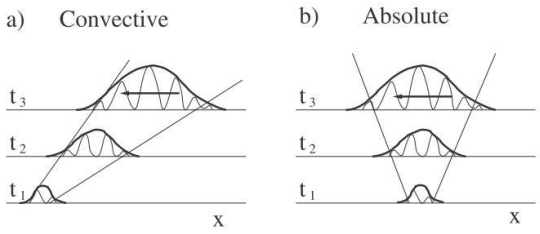

Figure 47. The difference between convective and absolute instabilities is illustrated by the response to a localized perturbation - the solid line indicates the difference between a state that evolves from a large local perturbation to a reference state (e. g. a periodic wavetrain resp. a periodic train of action potentials in electrophysiological context) and the reference state before the perturbation.

8.4. Linear stability analysis of spirals near breakup.

A theoretical analysis of spiral breakup can be based on a numerical linear stability analysis of stable rotating spirals in a rotating frame [285] (see section 8.2.1) or on the stability analysis of 1D wavetrains that are governing the radial dynamics in the spiral waves [301, 304]. In the latter case one can compute the set of eigenvalues giving rise to the essential (for unbounded system or systems with periodic boundary conditions) or the absolute spectrum (for finite bounded systems) [363]. Similarly, the continuous spectrum of spirals in large but bounded finite domains is different from the continuous spectrum of spirals in unbounded domains. For more details, we refer to work by Sandstede and Scheel [308, 363]. In practice, instabilities of the absolute spectrum often indicate an absolute instability of wavetrains, where a given perturbation grows locally, i.e., at the point it was applied Fig. 47(b), whereas instabilities of the essential spectra capture also convective instabilities, where the growing perturbations travel towards one of the system boundaries (Fig. 47(a)). A typical example for the radial dynamics of a spiral where the asymptotic wave-train in the far-field is convectively unstable is given in Fig. 34 (a) in Section 6 above. It is worth noting that absolute and essential spectra of a given wavetrain are obtained from the same linearized equation. The differences between absolute and essential spectra are caused only by the different boundary conditions that in turn lead to different eigenfunctions; for a simple example, see the discussion on a Ginzburg-Landau equation with an advection term in [364].

To understand the mechanisms of spiral breakup, it is instructive to consider the basic arguments in spiral stability analysis. A stable rotating spiral in an excitable medium selects, for a given set of parameters, a particular wavelength λ_0 and a related temporal period T_0. At the same moment, there exists a one-parameter family of periodic wave solutions with varying speed c, temporal period T and wavelength $\lambda = c(\lambda)T$. The one-parameter family is described by a conduction velocity (CV) dispersion curve $c(\lambda)$. At small wavelength, the wavetrains either exhibit an instability (modulation of Eckhaus instability in the complex Ginzburg-Landau equation(CGLE) resp. alternans in many cardiac tissue models that are most relevant here) or cease to exist (saddle-node or

drift pitchfork bifurcations in FitzHugh-Nagumo systems [365, 366]). If the wavelength selected by the spiral is smaller than this minimum value, it will be unstable. These minimum stable wavelengths and periods shall be called λ_{min}, respectively T_{min}, in the following. Only in a few cases (e.g. for the CGLE describing oscillatory media [367], or the Rinzel-Keller model of an excitable medium [368]), it is possible to compute the instabilities or bifurcations analytically. In other cases, simpler kinematic theories (see above section on alternans) or approximations by singular perturbation theory (excitable media) may yield useful information on the nature of this instability. For the models employed in cardiac dynamics, none of these methods are sufficient to yield an understanding of the instability at λ_{min}. This calls again for alternative methods, namely numerical stability analysis of traveling waves, introduced above in Section 5.2.3.

8.4.1. Linear stability analysis of periodic traveling waves. One has to numerically compute the 1D wave solutions and their linear stability along the dispersion curve. Continuation software as AUTO can be used to obtain the spatial profiles $U_0(z)$ of periodic waves as stationary solutions in a co-moving frame $z = r - ct$ [369]. Consequently, one needs to compute periodic orbits that correspond to a single wavelength with periodic boundary conditions. The evolution of small perturbations of a spatially periodic travelling wave $U_0(z)$ in the reaction diffusion equations is described by $W_{jn}(z)e^{\omega_{jn}t}$, where $W_{jn}(z)$ and ω_{jn} are eigenvectors and eigenvalues of the linearized equations. For continuum models such as the reaction-diffusion equations used in electrophysiology, there are infinitely many eigenvalues and eigenfunctions as the system length $L \to \infty$. Consequently, the ω_{jn} are located on continuous curves in the complex plane. A wavetrain solution is stable when all eigenvalues ω_{jn} have non-positive real parts. If the wavelength λ is used as a bifurcation parameter, the described method yields accurate information on the minimum stable wavelength λ_{min} for a given model and parameter set, where the eigenvalue spectra and the eigenfunctions describe the dynamics of perturbations to the wavetrains.

If one considers periodic travelling waves with constant shape $U_0(z)$ and constant speed c in 1D, a few facts on the eigenvalues and the eigenfunctions are known a priori. If the cardiac model is spatially homogeneous, any translation of a given periodic solution is also a valid solution with identical stability properties. This translational symmetry of the wavetrains is reflected by an eigenvector $W_{00} = dU_0/dz$ with zero eigenvalue $\omega_{00} = 0$ (Goldstone mode). Symmetry arguments require the eigenfunctions of the periodic operator, obtained by linearization around a wavetrain with wavelength λ, to be Bloch functions $W_{jn}(z) = e^{i(2\pi n/L)z}\phi_{jn}(z) = e^{ikz}\phi_{jn}(z)$ with $\phi_{jn}(z) = \phi_{jn}(z + \lambda)$ and $n = 0, \ldots, N-1$ [370]. The above Bloch form can be used in an ansatz that reduces the stability problem for the infinite domain to a stability problem in a domain of length λ with the wavenumber $k = 2\pi n/L$ as an additional parameter. If one assumes a purely imaginary exponent ikz in the prefactor of the Bloch eigenfunctions, one obtains the so-called essential spectrum. To assess the stability of spirals in finite domains, one needs, however, to compute also the absolute spectrum. This can be done by employing

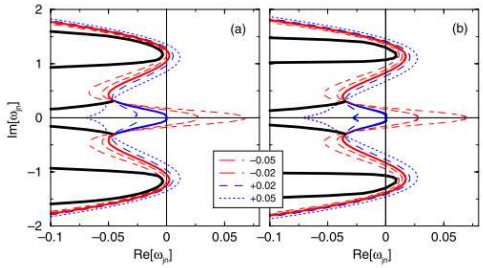

Figure 48. Examples for absolute (thick black lines) and essential spectra (thick red and blue lines) for a wavetrain with a given wavelength and changing parameter ϵ in a modified Barkley model just below (left panel) and above (right panel) the instability responsible for a breakup dynamics in the radial dynamics. The thin lines are obtained by using the exponential weights μ given in the inset. These spectra indicated outward moving perturbation for long-wavelength Eckhaus-type modes (blue part of essential spectrum) and inward moving perturbation for finite-wavelength modes (red part of essential spectrum). Reprinted figure from [304] with permission of IOP Publishing & Deutsche Physikalische Gesellschaft, CC BY-NC-SA.

an ansatz $W_{jn}(z) = e^{(\mu+ik)z}\phi_{jn}(z)$ for the eigenfunction that yields spectra depending on the exponential weight, i.e. $\omega_{jn} = \omega_{jn}(\mu)$. The group velocities of the associated modes are then $v_g = \partial Im(\omega_{jn}(\mu))/\partial k = \partial Re(\omega_{jn}(\mu))/\partial\mu$. The sign of the group velocities indicates in which direction modes are travelling. In addition, one can compute the most relevant parts of the absolute spectra $\omega_{jn}(\mu)$ by requiring $\partial Re(\omega_{jn}(\mu))/\partial\mu|_{\mu=\mu^*} = 0$ and verifying the pinching condition, see [308]. In this fashion, one can obtain the growth rates and frequency of the modes with zero group velocity that constitute the absolute spectrum and determine the stability in a finite system. A result of the application of this procedure for a model near parameters for spiral breakup is shown in Fig. 48.

The result of an application of the described procedure for different parameters in the vicinity of spiral breakup found in 2D simulations, is shown in Fig. 49, which demonstrates that spiral breakup in this case of an excitable medium can be explained from an absolute instability of the 1D wavetrain with the same wavelength as the asymptotic wavelength in the far-field of the spiral. Remarkably, the studies from which Fig. 48 and Fig. 49 were taken, both relate spiral breakup near the core in a situation where meandering is absent to an absolute linear instability of the 1D wavetrain. Interestingly, the critical modes in Fig. 48 are short (i.e. finite) wavelength whereas the instability in Fig. 49 results from a long-wavelength Eckhaus instability.

8.4.2. Spiral instabilities and breakup phenomenologies. Potential discrepancies between 2D simulation and stability analysis of the 1D radial dynamics may arise from nonlinear behaviour not captured by the linear stability analysis or instabilities of the discrete spectrum, like spiral meandering [286, 302] discussed in Subsection 6.1. Such instabilities do not have a counterpart in one dimension and require a numerical stability analysis in two dimensions that is computationally more expensive and in

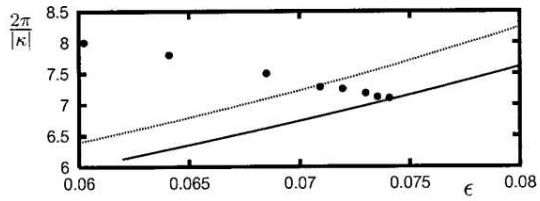

Figure 49. Example for comparison of essential (dotted line) and absolute instabilities (solid line) of 1D wavetrains in the Bär-Eiswirth model for excitable conditions and different. Plotted is the spatial period (wavelength) $\lambda = 2\pi/k$ of a 1D wavetrain vs. the parameter ϵ. Spiral breakup is observed in simulations for the parameter chosen here at $\epsilon = 0.074$. The full circles show the wavelength selected by a spiral obtained from 2D simulations. For breakup condition $\epsilon > 0.074$, the selected spiral wavelength is in the absolutely unstable region. Reprinted figure with permission from [308]. Copyright (2000) by the American Physical Society.

practice often restricted to rather small domain sizes (typically up to system sizes of a few spiral wavelengths) as well as to the iterative computation of the largest eigenvalues. Wheeler and Barkley have carried out a full 2D numerical stability analysis for a spiral in a circular domain and a co-rotating frame of reference and obtained a reasonable approximation of the continuous and discrete spectra for spirals in large domains [371]. This approach is conceptually even simpler and more complete than the reduction of the spiral stability analysis to the analysis of stability of 1D wavetrains presented above, but is computationally much more expensive and may be difficult to apply to many-variable cardiac models.

One can analyze the phenomenon of spiral breakup by comparing numerical simulations with a stability analysis of periodic wavetrains. It is thereby possible to link distinct phenomenologies of spiral breakup, e.g. core breakup and far-field breakup (see Fig. 33), with different instabilities of the radial wavetrains or rotating spirals. Additional factors like meander instability, which is often quite pronounced in realistic models, make the analysis more difficult.

A study of simple reaction-diffusion systems [304] revealed that the instabilities of 1D wavetrains in a ring geometry are usually of convective nature (see section 3.2). To obtain breakup in stationary sources, respectively non-meandering spirals, however, an absolute instability of the plane waves in the far-field is required [367], which requires additional consideration. Several studies [304, 308, 371] have found that spiral breakup in simulations is often clearly correlated with absolute linear instabilities of plane waves in the far-field. Stability analysis also showed a relation between the characteristics of the instability and the phenomenology of breakup in simulations. Linear stability analysis of waves yields information on the group velocity of the unstable modes, which sometimes gives a hint on the phenomenology of spiral breakup in the present context. Hence, the sign of the group velocity may decide if breakup occurs near or far-away from the core. It is important to note that nevertheless (i) core breakup can result

from different types of instability and that (ii) the same instability scenario may lead to phenomenologically different appearances. In other words, the form of the linearly unstable modes is not sufficient to determine the full nonlinear spatiotemporal dynamics. Moreover, a particular phenomenology found in simulations does not necessary allow a conclusion on the specific nature of the linear instability presumably behind it. To obtain the full information, direct simulations and an independent linear stability are hence necessary. In many cardiac models, core breakup is presumably caused by an alternans instability of the wavetrains emitted from the spiral core [225, 279, 292, 372].

The influence of meandering and the resulting Doppler effect in core breakup has been verified in simulations [91] and experiments with the Belousov-Zhabotinsky reaction [290]. Far-field breakup of (presumably) meandering spirals with a non-decaying modulation of the wavetrain in the far-field ('superspirals' [287, 373]) has been studied in the same reaction [309, 310]. Here, an interpretation of the breakup in terms of the non-linear consequences of the Eckhaus instability has been given [303]. Most of results for the stability analysis of spirals near the onset of breakup were obtained for simple reaction-diffusion systems. The analysis and numerical procedures described here may be applied to simple cardiac models like the Aliev-Panfilov model [79] or the variant of the Noble model studied by Karma [84]. This should enable researchers to elucidate the mechanisms behind the rich phenomenology of spiral breakup found in cardiac models [40]. Finally, the hypothesis that alternans is the crucial instability behind spiral breakup maybe tested and possible alternatives may be uncovered.

9. Discussion and outlook

Cardiac arrhythmias are potential triggers of sudden cardiac death, which is the main cause of death in the developed world [374], and a plethora of other health risks. The transition between healthy and pathological tissue dynamics may have different causes, e.g., myocardial ischemia, infarction or genetic predisposition. Similarly, the dynamical mechanisms governing such a transition are not unique and often not well understood. As a result mathematical modeling of action potential propagation in the heart has become a major research topic during the last two decades. Realistic models of cardiac tissue include hundred of dynamical coupled equations evolving in complex and asymmetrical geometries.

A huge growth of computational capabilities and numerical algorithms in the last years has enabled direct numerical simulations, employing these models, to reproduce the main properties of cardiac arrhythmia and the associated dynamical transitions. However, mechanistic interpretations of the transition are often difficult and missing for realistic cardiac models. Therefore, we have reviewed here often findings in simplified models of cardiac tissue to analyze the different mechanisms of instabilities in cardiac dynamics and provided simplified theoretical descriptions.

Altogether, cardiac modeling has emerged as one of the prime application areas of theories and methods of nonlinear physics originally developed for pattern formation in extended nonequilibrium media. Rotors are believed to be formed in reentry and are crucial for the appearance of arrhythmias like ventricular tachycardia (VT) as well as atrial and ventricular fibrillation (AF,VF). Therefore, a substantial part of this review is focused on the dynamics and potential instabilities of such structures.

We have reviewed the related advances in theory, the different numerical and analytical methods that have been developed in recent years and their application to cardiac dynamics. According to Jalife [4] in particular rotors are crucial:"*AF and VT/VF are by far the most significant cardiac arrhythmias faced by the physician. Owing to their highly complex electrocardiographic appearance, both AF and VF are commonly thought of as being the result of exceptionally complex and disorganized cardiac activation, in which electrical waves propagate through the atria or ventricles chaotically and unpredictably. In fact, during fibrillation the electrical activation sequence is profoundly abnormal; electrical wave fronts do not follow the usual paths. The atrial or ventricular rates accelerate to the extreme and electrical waves assume a complex vortex-like behavior that looks a lot like eddy formation and turbulence in water. Recent evidence strongly suggesting that rotors are critical in sustaining both atrial and ventricular fibrillation (AF, VF) in the human heart, which may have critical implications for treatment with radio-frequency ablation.*" This passage illustrates the fruitful exchange between the nonlinear physics and the cardiology communities that has been the main theme of this review article.

What has been achieved is a detailed understanding of a few central phenomena. Often this has been done initially for largely simplified cardiac model equations. The

findings and the associated methods described here can, however, also be applied to more realistic electrophysiological models and may in the future help the analysis of newly developed computational models. The starting point for a nonlinear dynamics treatment of cardiac propagation is a periodic sequence of action potentials corresponding to (a somewhat idealized) normal sine rhythm. This rhythm is parametrized by its frequency and the wavelength of subsequent action potentials and corresponding velocities.

A key instability that already occurs in the local dynamics of paced cardiac cells is cardiac alternans (Section 5), which is a period doubling of the oscillation in the membrane potential of a single cardiac cell occurring at sufficiently large pacing frequency. In a single cell the onset of alternans can be predicted from the action potential duration (APD) restitution curve that describes the dependency of the time a specific AP lasts on the diastolic interval The map approach, amplitude equations as well as numerical linear analysis of APD trains allow accurate predictions for the onset of alternans. Many of these theories are not rigorous and therefore need comparison with direct numerical simulations. In tissue, alternans may occur in two different forms, namely discordant and concordant alternans. Discordant alternans is particularly relevant and may lead to further complications like APD block and formation of rotors. The mechanism of its occurrence has been worked out nicely in the framework of amplitude equations.

The dynamics of rotors invokes many complicated phenomena. Rotors in cardiac tissues behave usually in a complicated manner. This is a result of various dynamical instabilities of the spirals rigid rotation (Section 6). These may act upon the core region near the tip or in the far-field of periodic waves of a spiral or affect both aspects. Most electrophysiological models display strong meandering, a well understood phenomenon stemming from an oscillatory instability of the tip motion. Instabilities in the far-field lead typically to the destruction of coherent spiral patterns and to formation of new rotors by spiral breakup.

Scroll waves are subject to many new instabilities like negative filament line tension and sproing that were described in Section 7, that also contains a discussion on the state-of-the art characterization of electrical turbulence. Finally, Section 8 deals with approaches to analyze the instabilities behind the complex dynamical phenomenologies found in simulations of cardiac dynamics and corresponding experiments. A main result is that changes in behavior of rotors are often associated with linear instabilities. Numerical stability analysis can then give an accurate determination of critical parameters, nature of instabilities and bifurcation and their spatiotemporal signatures.

A popular view cited in many talks and publications, see e.g. [15, 40] is that the mechanism for ventricular fibrillation may develop from a rotor that occurs from a perturbation of the regular sine rhythm. The rotor is the center of a spiral wave that typically has a much higher frequency than the sine rhythm in cardiac tissue and therefore occurs as tachycardia. If this spiral is unstable a more irregular pattern appears that bears the signature of fibrillation. Alternative explanations for the irregular dynamics observed in fibrillation have featured a single drifting or wildly moving

(meandering) rotor or electrical turbulence forming at some distance from a spiral (mother rotor) center. All these scenarios can be traced back to the different instabilities described in this review and are, in principle, possible in perfectly homogeneous tissue. Since healthy tissue usually is not subject to the cascade of events leading to fibrillatory activity, functional reentry may occur as a result of pathological changes in the electrophysiological properties of the myocytes.

While this review mostly has dealt with cardiac propagation in homogeneous and isotropic media, the true heart has a couple of other important features that need to be incorporated into a realistic modeling with the goal to obtain quantitative predictions and sufficient agreement with experiments. In the following we briefly address some of these possible model extensions.

- *Models including heterogeneities and anisotropy*: Heterogeneities (see Section 4.2) and anisotropy (see Section 3.5) are often relevant in the formation and maintenance of arrhythmias. In such a case, one sometimes speaks of anatomical reentry. While investigations of spatially homogeneous models show that heterogeneities are not always necessary to generate complex, irregular activity in the heart, they may largely enhance the probability of such effects and alter substantially the appearance of irregular electrical activity in the tissue. A striking example are the complex fractionated atrial electrograms, see e. g. [375], that show very short correlations in space that cannot be reproduced in simulation of homogeneous tissue models and are therefore often associated with microfibrosis or other variations of conductive properties at the level of individual cardiac muscle cells. As a result more and more models incorporate detailed information on structural heterogeneities or the anatomy of fiber orientation that determines the anisotropic conduction properties in the heart and try to assess the impact of tissue anatomy on cardiac dynamics, for a short review, see e. g. [32]. In ageing tissue the amount of heterogeneity, e.g. due to fibrosis, as well as the prevalence of arrhythmias like AF and VF is strongly increased. Therefore, it will be necessary to include structural details possibly obtained from imaging of specific patient into quantitative modeling of cardiac disease. A good understanding of the role of heterogeneity,a classical subject on cardiac modeling research with contributions already in the sixties [376], shall nevertheless be coupled to an analysis of an averaged homogeneous model. If the averaged parameters place the dynamics in the tissue close to an instability, the influence of heterogeneities may be crucial to trigger malfunction. For larger heterogeneities and smoothly varying parameters, again stability analysis and bifurcation theory can be directly applied to cardiac as has been done previously for simple generic reaction-diffusion equations of FitzHugh-Nagumo type [377–380]. Modeling of heterogeneities is also necessary for a better understanding and development of therapeutic strategies in atrial and ventricular fibrillation. To prevent these arrhythmias, already now ablation procedures are employed that assume that the source of these abnormal cardiac dynamics can be localized and isolated. This implicitly assumes that they stem from areas where ischaemia or

fibrosis have altered the dynamics of the tissue towards a potentially damaging form. Another relevant area where heteregoneities of another type have recently be implicated is defibrillation of tissue with chaotic, irregular activity. Luther et al. have provided experimental evidence that suggests that defibrillation may work to a large extent by wave initiation at larger non-conducting heterogeneities in cardiac tissue, namely blood vessels that exceed a certain critical size [54, 55]. Their work has sparked a lively discussion among experimentalist and modelers. A recent contribution is the work by Caldwell et al. who provide experimental data on wave initiation by applying external field to tissue and provide an alternative explanation [381]. The final word in this debate is, however, not yet spoken and will require a much larger effort in modeling and detailed experiments that should aim at understanding the mechanism of defibrillation and on optimizing the defibrillation strategies, e. g. by following and critically testing ideas like Luther et al. who showed that application of a sequence of smaller shocks may provide much more efficient than the standard protocol of defibrillation based on one single large shock [54].

A topic related to the inclusion of heterogeneities is the correct description of anisotropy. Despite large progress during the last years in computational modeling the extension of the analysis of instabilities to anisotropic conditions, more complete geometries and more elaborate models is still in progress. For example the characteristic Eikonal equation can be generalized to the case of anisotropic tissue to produce a modified curvature relation for wave fronts in anisotropic generic models of excitable media [382]. The use of complex metrics adapting the anisotropic properties of the media, for example using analytical models of fiber structure [383], to the metrics and generalize the analytical solutions in cartesian coordinates to the new metrics has already given first promising results.

- *Models with electro-mechanical coupling and mechano-electric feedback*: An important improvement in the instability theories of cardiac tissue has been already begun with the incorporation of the effects of the deformation of the tissue in the study of the different instabilities. The effect of a deforming metrics in wave propagation has been studied in simulations in a medium with a varying oscillatory metric [384, 385] and indicate that the mechanical deformation could play an important role on the stability of spiral waves. An oscillatory change of metrics in one of the directions, results effectively in time-varying anisotropic diffusion that changed the local curvature of the waves emitted by the spiral. If, at a given point, the local curvature became too small to support propagation, block and spiral break-up resulted. On the other hand, the influence of the stretch activated channels in action potential morphology and propagation has been shown to give rise to spontaneous oscillations [104,386,387], ectopic beats [388], initiation of spiral waves [389,390], spiral break-up [105,391], instability of scroll waves [392], or transition from concordant to discordant alternans [249].
- *Stochastic models*: Throughout this review, we have discussed deterministic models.

Since, however, the importance of fluctuations and stochastic dynamics ihas been established for important aspect of cardiac muscle cell physiology, in particular for intracellular calcium cycling [26], stochastic elements have entered more advanced physiological models and have become a topic of increasing interest to cardiac modelers. This aspect was recently covered by a longer review article [27].
Often these models describe the fluctuation at the level of a single cell. It remains a largely unsolved problem, how fluctuations at the level of the single cell can be incorporated in tissue models. Moreover, it is not yet clear if and how such fluctuations will become critical for the dynamics at the tissue or organ level. A first step maybe to employ discrete models of cardiac tissue that represent the dynamics of individual cells and are simple enough to be computationally feasible, see e. g. [170–172], with additional noise terms or a stochastic dynamics derived from detailed cellular models.

In summary, we have reviewed here a collection of important results regarding the dynamics of cardiac propagation in one-, two- and three-dimensional cardiac tissue and introduced tools for the analysis of crucial instabilities that have been previously applied to generic models of excitable media and to simple cardiac models. Such knowledge may motivate other researchers to extend the current techniques into more elaborate frameworks, where it may be used for more complex and realistic physiological models of cardiac tissue and eventually contribute to a complete understanding and classification of cardiac arrhythmias, which should be helpful for the subsequent development of efficient defibrillation protocols or preventive drug therapies.

Acknowledgments

We like to thank Thomas Niedermayer and two anonymous referee for a careful reading of the manuscript and making numerous suggestions, which helped to improve the manuscript. We acknowledge financial support from the German Science Foundation (DFG) within the framework of SFB 910 Control of self-organizing nonlinear systems; from the Ministerio de Ciencia e Innovación of Spain under grant numbers FIS2011-28820-C02-01 and SAF2014-58286-C2-2-R and MINECO of Spain under the Ramon y Cajal program with the grant number RYC-2012-11265.

References

[1] Shanthi Mendis, Pekka Puska, Bo Norrving, et al. *Global atlas on cardiovascular disease prevention and control.* World Health Organization, 2011.

[2] Mohsen Naghavi, Haidong Wang, Rafael Lozano, Adrian Davis, Xiaofeng Liang, Maigeng Zhou, Stein Emil Vollset, Ayse Abbasoglu Ozgoren, Safa Abdalla, Foad Abd-Allah, et al. Global, regional, and national age-sex specific all-cause and cause-specific mortality for 240 causes of death, 1990-2013: a systematic analysis for the global burden of disease study 2013. *Lancet*, 385(9963):117–171, 2015.

[3] D. Zipes and J. Jalife. *Cardiac Electrophysiology: From Cell to Bedside.* Elsevier, 2013.

[4] José Jalife. Introduction to the series on computational approaches to cardiac arrhythmias translation into diagnostics and therapy. *Circulation Research*, 112(5):831–833, 2013.

[5] Peter J Hunter, Andrew J Pullan, and Bruce H Smaill. Modeling total heart function. *Annual Review of Biomedical Engineering*, 5(1):147–177, 2003.

[6] Peter J Hunter and Thomas K Borg. Integration from proteins to organs: the physiome project. *Nature Reviews Molecular Cell Biology*, 4(3):237–243, 2003.

[7] Zhilin Qu, Alan Garfinkel, James N Weiss, and Melissa Nivala. Multi-scale modeling in biology: how to bridge the gaps between scales? *Progress in Biophysics and Molecular Biology*, 107(1):21–31, 2011.

[8] Salvatore Torquato. *Random heterogeneous materials: microstructure and macroscopic properties*, volume 16. Springer Science & Business Media, 2002.

[9] JC Neu and W Krassowska. Homogenization of syncytial tissues. *Critical Reviews in Biomedical Engineering*, 21(2):137–199, 1992.

[10] Paul E Hand, Boyce E Griffith, and Charles S Peskin. Deriving macroscopic myocardial conductivities by homogenization of microscopic models. *Bulletin of Mathematical Biology*, 71(7):1707–1726, 2009.

[11] James P Keener and James Sneyd. *Mathematical physiology*, volume 1. Springer, 1998.

[12] Grégoire Nicolis. *Introduction to nonlinear science*. Cambridge University Press, 1995.

[13] Steven H Strogatz. *Nonlinear dynamics and chaos: with applications to physics, biology, chemistry, and engineering*. Westview press, 2014.

[14] Leon Glass and Michael C Mackey. *From clocks to chaos: the rhythms of life*. Princeton University Press, 1988.

[15] Arthur T Winfree. *When time breaks down: the three-dimensional dynamics of electrochemical waves and cardiac arrhythmias*. Princeton University Press Princeton, 1987.

[16] Jorge M Davidenko, Arcady V Pertsov, Remy Salomonsz, William Baxter, and José Jalife. Stationary and drifting spiral waves of excitation in isolated cardiac muscle. *Nature*, 355(355):349–351, 1992.

[17] Arkady M Pertsov, Jorge M Davidenko, Remy Salomonsz, William T Baxter, and Jose Jalife. Spiral waves of excitation underlie reentrant activity in isolated cardiac muscle. *Circulation Research*, 72(3):631–650, 1993.

[18] AT Winfree. Stably rotating patterns of reaction and diffusion. *Prog Theor Chem*, 4:1–51, 1978.

[19] David A Kessler, Herbert Levine, and William N Reynolds. Spiral core in singly diffusive excitable media. *Physical review letters*, 68(3):401, 1992.

[20] Sandeep V Pandit and José Jalife. Rotors and the dynamics of cardiac fibrillation. *Circulation Research*, 112(5):849–862, 2013.

[21] G K Moe, W C Rheinboldt, and J A Abildskov. A computer model of atrial fibrillation. *Am Heart J*, 67:200–20, 1964.

[22] José Jalife, Omer Berenfeld, and Moussa Mansour. Mother rotors and fibrillatory conduction: a mechanism of atrial fibrillation. *Cardiovascular Research*, 54(2):204–16, 2002.

[23] Andrew J Pullan, Leo K Cheng, and Martin L Buist. *Mathematically modelling the electrical activity of the heart: From cell to body surface and back again*. World Scientific, 2005.

[24] Flavio H Fenton and Elizabeth M Cherry. Models of cardiac cell. *Scholarpedia*, 3(8):1868, 2008.

[25] André G Kléber and Yoram Rudy. Basic mechanisms of cardiac impulse propagation and associated arrhythmias. *Physiological Reviews*, 84(2):431–488, 2004.

[26] Martin Falcke. Reading the patterns in living cells: the physics of ca2+ signaling. *Advances in Physics*, 53(3):255–440, 2004.

[27] Zhilin Qu, Gang Hu, Alan Garfinkel, and James N Weiss. Nonlinear and stochastic dynamics in the heart. *Physics Reports*, 543(2):61–162, 2014.

[28] Gernot Plank, Rebecca AB Burton, Patrick Hales, Martin Bishop, Tahir Mansoori, Miguel O Bernabeu, Alan Garny, Anton J Prassl, Christian Bollensdorff, Fleur Mason, et al. Generation of histo-anatomically representative models of the individual heart: tools and application.

Philosophical Transactions of the Royal Society A: Mathematical, Physical and Engineering Sciences, 367(1896):2257–2292, 2009.

[29] Martin J Bishop, Gernot Plank, Rebecca AB Burton, Jürgen E Schneider, David J Gavaghan, Vicente Grau, and Peter Kohl. Development of an anatomically detailed mri-derived rabbit ventricular model and assessment of its impact on simulations of electrophysiological function. *American Journal of Physiology-Heart and Circulatory Physiology*, 298(2):H699–H718, 2010.

[30] RH Clayton, Olivier Bernus, EM Cherry, Hans Dierckx, FH Fenton, L Mirabella, AV Panfilov, FB Sachse, G Seemann, and H Zhang. Models of cardiac tissue electrophysiology: progress, challenges and open questions. *Progress in Biophysics and Molecular Biology*, 104(1):22–48, 2011.

[31] Bruce H Smaill, Jichao Zhao, and Mark L Trew. Three-dimensional impulse propagation in myocardium arrhythmogenic mechanisms at the tissue level. *Circulation Research*, 112(5):834–848, 2013.

[32] Pablo Lamata, Ramón Casero, Valentina Carapella, Steve A Niederer, Martin J Bishop, Jürgen E Schneider, Peter Kohl, and Vicente Grau. Images as drivers of progress in cardiac computational modelling. *Progress in Biophysics and Molecular Biology*, 115(2):198–212, 2014.

[33] Flavio H Fenton, Elizabeth M Cherry, and Leon Glass. Cardiac arrhythmia. *Scholarpedia*, 3(7):1665, 2008.

[34] James N Weiss, Alain Karma, Yohannes Shiferaw, Peng-Sheng Chen, Alan Garfinkel, and Zhilin Qu. From pulsus to pulseless the saga of cardiac alternans. *Circulation Research*, 98(10):1244–1253, 2006.

[35] James N Weiss, Michael Nivala, Alan Garfinkel, and Zhilin Qu. Alternans and arrhythmias from cell to heart. *Circulation Research*, 108(1):98–112, 2011.

[36] James N Weiss, Zhilin Qu, Peng-Sheng Chen, Shien-Fong Lin, Hrayr S Karagueuzian, Hideki Hayashi, Alan Garfinkel, and Alain Karma. The dynamics of cardiac fibrillation. *Circulation*, 112(8):1232–1240, 2005.

[37] James N Weiss, Alan Garfinkel, Hrayr S Karagueuzian, Thao P Nguyen, Riccardo Olcese, Peng-Sheng Chen, and Zhilin Qu. Perspective: A dynamics-based classification of ventricular arrhythmias. *Journal of Molecular and Cellular Cardiology*, 82:136–152, 2015.

[38] Alain Karma. Physics of cardiac arrhythmogenesis. *Annual Review of Condensed Matter Physics*, 4(1):313–337, 2013.

[39] Jaakko Malmivuo and Robert Plonsey. *Bioelectromagnetism: principles and applications of bioelectric and biomagnetic fields*. Oxford University Press, 1995.

[40] Flavio H Fenton, Elizabeth M Cherry, Harold M Hastings, and Steven J Evans. Multiple mechanisms of spiral wave breakup in a model of cardiac electrical activity. *Chaos: An interdisciplinary journal of Nonlinear Science*, 12(3):852–892, 2002.

[41] A L Hodgkin and A F Huxley. A quantitative description of membrane current and its application to conduction and excitation in nerve. *The Journal of Physiology*, 117(4):500–44, 1952.

[42] JP Keener. Homogenization and propagation in the bistable equation. *Physica D: Nonlinear Phenomena*, 136(1):1–17, 2000.

[43] Yan Wang and Yoram Rudy. Action potential propagation in inhomogeneous cardiac tissue: safety factor considerations and ionic mechanism. *American Journal of Physiology-Heart and Circulatory Physiology*, 278(4):H1019–H1029, 2000.

[44] Thomas Desplantez, Deborah Halliday, Emmanuel Dupont, and Robert Weingart. Cardiac connexins cx43 and cx45: formation of diverse gap junction channels with diverse electrical properties. *Pflügers Archiv*, 448(4):363–375, 2004.

[45] Habo J Jongsma and Ronald Wilders. Gap junctions in cardiovascular disease. *Circulation Research*, 86(12):1193–1197, 2000.

[46] Nicholas J Severs, Alexandra F Bruce, Emmanuel Dupont, and Stephen Rothery. Remodelling of gap junctions and connexin expression in diseased myocardium. *Cardiovascular Research*, 80(1):9–19, 2008.

[47] Stefan Dhein, Thomas Seidel, Aida Salameh, Joanna Jozwiak, Anja Hagen, Martin Kostelka, Gerd Hindricks, and Friedrich-Wilhelm Mohr. Remodeling of cardiac passive electrical properties and susceptibility to ventricular and atrial arrhythmias. *Frontiers in Physiology*, 5, 2014.

[48] Harold VM van Rijen, Dominik Eckardt, Joachim Degen, Martin Theis, Thomas Ott, Klaus Willecke, Habo J Jongsma, Tobias Opthof, and Jacques MT de Bakker. Slow conduction and enhanced anisotropy increase the propensity for ventricular tachyarrhythmias in adult mice with induced deletion of connexin43. *Circulation*, 109(8):1048–1055, 2004.

[49] Hiroshi Satoh, LM Delbridge, Lothar A Blatter, and Donald M Bers. Surface: volume relationship in cardiac myocytes studied with confocal microscopy and membrane capacitance measurements: species-dependence and developmental effects. *Biophysical Journal*, 70(3):1494–1504, 1996.

[50] Joakim Sundnes, Bjørn Fredrik Nielsen, Kent Andre Mardal, Xing Cai, Glenn Terje Lines, and Aslak Tveito. On the computational complexity of the bidomain and the monodomain models of electrophysiology. *Annals of Biomedical Engineering*, 34(7):1088–1097, 2006.

[51] Natalia Trayanova, Kirill Skouibine, and Felipe Aguel. The role of cardiac tissue structure in defibrillation. *Chaos: An Interdisciplinary Journal of Nonlinear Science*, 8(1):221–233, 1998.

[52] Natalia A Trayanova and Lukas J Rantner. New insights into defibrillation of the heart from realistic simulation studies. *Europace*, 16(5):705–713, 2014.

[53] John P Wikswo Jr, Shien-Fong Lin, and Rashida A Abbas. Virtual electrodes in cardiac tissue: a common mechanism for anodal and cathodal stimulation. *Biophysical Journal*, 69(6):2195, 1995.

[54] Stefan Luther, Flavio H Fenton, Bruce G Kornreich, Amgad Squires, Philip Bittihn, Daniel Hornung, Markus Zabel, James Flanders, Andrea Gladuli, Luis Campoy, et al. Low-energy control of electrical turbulence in the heart. *Nature*, 475(7355):235–239, 2011.

[55] Flavio H Fenton, Stefan Luther, Elizabeth M Cherry, Niels F Otani, Valentin Krinsky, Alain Pumir, Eberhard Bodenschatz, and Robert F Gilmour. Termination of atrial fibrillation using pulsed low-energy far-field stimulation. *Circulation*, 120(6):467–476, 2009.

[56] RA Gray and J Jalife. Ventricular fibrillation and atrial fibrillation are two different beasts. *Chaos: An Interdisciplinary Journal of Nonlinear Science*, 8(1):65–78, 1998.

[57] Elizabeth M Cherry, Harold M Hastings, and Steven J Evans. Dynamics of human atrial cell models: restitution, memory, and intracellular calcium dynamics in single cells. *Progress in Biophysics and Molecular Biology*, 98(1):24–37, 2008.

[58] Matteo E Mangoni and Joël Nargeot. Genesis and regulation of the heart automaticity. *Physiological Reviews*, 88(3):919–82, 2008.

[59] Ronald Wilders. Computer modelling of the sinoatrial node. *Medical & Biology Engineering & Computing*, 45(2):189–207, 2007.

[60] Denis Noble. A modification of the hodgkinhuxley equations applicable to purkinje fibre action and pacemaker potentials. *The Journal of Physiology*, 160(2):317–352, 1962.

[61] Philip Stewart, Oleg V Aslanidi, Denis Noble, Penelope J Noble, Mark R Boyett, and Henggui Zhang. Mathematical models of the electrical action potential of purkinje fibre cells. *Philosophical Transactions of the Royal Society A: Mathematical, Physical and Engineering Sciences*, 367(1896):2225–2255, 2009.

[62] Penelope J Noble and Denis Noble. A historical perspective on the development of models of rhythm in the heart. In *Heart Rate and Rhythm*, pages 155–173. Springer, 2011.

[63] Denis Noble and Yoram Rudy. Models of cardiac ventricular action potentials: iterative interaction between experiment and simulation. *Philosophical Transactions of the Royal Society of London. Series A: Mathematical, Physical and Engineering Sciences*, 359(1783):1127–1142, 2001.

[64] C H Luo and Y Rudy. A model of the ventricular cardiac action potential. depolarization, repolarization, and their interaction. *Circulation Research*, 68(6):1501–26, 1991.

[65] KHWJ Ten Tusscher, D Noble, PJ Noble, and AV Panfilov. A model for human ventricular tissue.

American Journal of Physiology-Heart and Circulatory Physiology, 286(4):H1573–H1589, 2004.

[66] Kirsten HWJ Ten Tusscher, Olivier Bernus, Rok Hren, and Alexander V Panfilov. Comparison of electrophysiological models for human ventricular cells and tissues. *Progress in biophysics and molecular biology*, 90(1):326–345, 2006.

[67] Robert K Amanfu and Jeffrey J Saucerman. Cardiac models in drug discovery and development: a review. *Critical Reviews in Biomedical Engineering*, 39(5):379–95, 2011.

[68] Joakim Sundnes, Glenn Terje Lines, Xing Cai, Bjørn Frederik Nielsen, Kent-Andre Mardal, and Aslak Tveito. *Computing the electrical activity in the heart*, volume 1. Springer Science & Business Media, 2007.

[69] GT Lines, ML Buist, P Grottum, AJ Pullan, J Sundnes, and A Tveito. Mathematical models and numerical methods for the forward problem in cardiac electrophysiology. *Computing and Visualization in Science*, 5(4):215–239, 2003.

[70] Go W Beeler and H Reuter. Reconstruction of the action potential of ventricular myocardial fibres. *The Journal of Physiology*, 268(1):177–210, 1977.

[71] Marc Courtemanche and Arthur T Winfree. Re-entrant rotating waves in a beeler–reuter based model of two-dimensional cardiac electrical activity. *International Journal of Bifurcation and Chaos*, 1(02):431–444, 1991.

[72] Ro E McAllister, D Noble, and RW Tsien. Reconstruction of the electrical activity of cardiac purkinje fibres. *The Journal of physiology*, 251(1):1–59, 1975.

[73] Zhilin Qu, Jong Kil, Fagen Xie, Alan Garfinkel, and James N Weiss. Scroll wave dynamics in a three-dimensional cardiac tissue model: roles of restitution, thickness, and fiber rotation. *Biophysical Journal*, 78(6):2761–2775, 2000.

[74] Zhilin Qu, Fagen Xie, Alan Garfinkel, and James N Weiss. Origins of spiral wave meander and breakup in a two-dimensional cardiac tissue model. *Annals of Biomedical Engineering*, 28(7):755–771, 2000.

[75] Sergio Alonso and Alexander V Panfilov. Negative filament tension in the luo-rudy model of cardiac tissue. *Chaos: An Interdisciplinary Journal of Nonlinear Science*, 17(1):015102, 2007.

[76] C H Luo and Y Rudy. A dynamic model of the cardiac ventricular action potential. i. simulations of ionic currents and concentration changes. *Circulation Research*, 74(6):1071–96, 1994.

[77] VI Krinskii and Yu M Kokoz. Analysis of excitable membranes equations. 3. purkinje fiber membrane-reduction of noble equations to 2nd order system-analysis of automaticity on nullclines plots. *Biofizika*, 18(6):1067–1073, 1973.

[78] Flavio Fenton and Alain Karma. Vortex dynamics in three-dimensional continuous myocardium with fiber rotation: Filament instability and fibrillation. *Chaos: An Interdisciplinary Journal of Nonlinear Science*, 8(1):20–47, 1998.

[79] Rubin R Aliev and Alexander V Panfilov. A simple two-variable model of cardiac excitation. *Chaos, Solitons & Fractals*, 7(3):293–301, 1996.

[80] Alain Karma. Electrical alternans and spiral wave breakup in cardiac tissue. *Chaos: An Interdisciplinary Journal of Nonlinear Science*, 4(3):461–472, 1994.

[81] Alfonso Bueno-Orovio, Elizabeth M Cherry, and Flavio H Fenton. Minimal model for human ventricular action potentials in tissue. *Journal of Theoretical Biology*, 253(3):544–60, 2008.

[82] Angelina Peñaranda, Inma R Cantalapiedra, Jean Bragard, and Blas Echebarria. Cardiac dynamics: a simplified model for action potential propagation. *Theoretical Biology and Medical Modelling*, 9(50):1–18, 2012.

[83] FJ Van Capelle and Dirk Durrer. Computer simulation of arrhythmias in a network of coupled excitable elements. *Circulation Research*, 47(3):454–466, 1980.

[84] Alain Karma. Spiral breakup in model equations of action potential propagation in cardiac tissue. *Physical Review Letters*, 71(7):1103, 1993.

[85] Richard FitzHugh. Impulses and physiological states in theoretical models of nerve membrane. *Biophysical Journal*, 1(6):445–466, 1961.

[86] Dwight Barkley, Mark Kness, and Laurette S Tuckerman. Spiral-wave dynamics in a simple

model of excitable media: The transition from simple to compound rotation. *Physical Review A*, 42(4):2489, 1990.

[87] EC Zeeman. Differential equations for the heartbeat and nerve impulse. *Towards a theoretical biology*, 4:8–67, 1972.

[88] Jinichi Nagumo, Suguru Arimoto, and Shuji Yoshizawa. An active pulse transmission line simulating nerve axon. *Proceedings of the IRE*, 50(10):2061–2070, 1962.

[89] Matthew Dowle, Rolf Martin Mantel, and Dwight Barkley. Fast simulations of waves in three-dimensional excitable media. *International Journal of Bifurcation and Chaos*, 7(11):2529–2545, 1997.

[90] Dwight Barkley. A model for fast computer simulation of waves in excitable media. *Physica D: Nonlinear Phenomena*, 49(1):61–70, 1991.

[91] M Bär and M Eiswirth. Turbulence due to spiral breakup in a continuous excitable medium. *Physical Review E*, 48(3):R1635, 1993.

[92] AV Panfilov and AN Rudenko. Two regimes of the scroll ring drift in the three-dimensional active media. *Physica D: Nonlinear Phenomena*, 28(1):215–218, 1987.

[93] VN Biktashev, AV Holden, and H Zhang. Tension of organizing filaments of scroll waves. *Philosophical Transactions of the Royal Society of London. Series A: Physical and Engineering Sciences*, 347(1685):611–630, 1994.

[94] Colleen C Mitchell and David G Schaeffer. A two-current model for the dynamics of cardiac membrane. *Bulletin of Mathematical Biology*, 65(5):767–793, 2003.

[95] P Kohl, C Bollensdorff, and A Garny. Effects of mechanosensitive ion channels on ventricular electrophysiology: experimental and theoretical models. *Experimental Physiology*, 91(2):307, 2006.

[96] NHL Kuijpers, HMM ten Eikelder, PHM Bovendeerd, S Verheule, T Arts, and PAJ Hilbers. Mechanoelectric feedback leads to conduction slowing and block in acutely dilated atria: a modeling study of cardiac electromechanics. *American Journal of Physiology- Heart and Circulatory Physiology*, 292(6):H2832, 2007.

[97] F Ravelli. Mechano-electric feedback and atrial fibrillation. *Progress in Biophysics and Molecular Biology*, 82(1-3):137–149, 2003.

[98] PJ Hunter, AD McCulloch, and HEDJ ter Keurs. Modelling the mechanical properties of cardiac muscle. *Progress in Biophysics and Molecular Biology*, 69(2-3):289–331, 1998.

[99] DA Nordsletten, SA Niederer, MP Nash, PJ Hunter, and NP Smith. Coupling multi-physics models to cardiac mechanics. *Progress in biophysics and molecular biology*, 104(1):77–88, 2011.

[100] Martyn P Nash and Peter J Hunter. Computational mechanics of the heart. *Journal of elasticity and the physical science of solids*, 61(1-3):113–141, 2000.

[101] Louis D Weise and Alexander V Panfilov. A discrete electromechanical model for human cardiac tissue: effects of stretch-activated currents and stretch conditions on restitution properties and spiral wave dynamics. *PloS one*, 8(3):e59317, 2013.

[102] Martyn P Nash and Alexander V Panfilov. Electromechanical model of excitable tissue to study reentrant cardiac arrhythmias. *Progress in Biophysics and Molecular Biology*, 85(2):501–522, 2004.

[103] P Kohl, A D Nesbitt, P J Cooper, and M Lei. Sudden cardiac death by commotio cordis: role of mechano-electric feedback. *Cardiovascular Research*, 50(2):280–9, 2001.

[104] A V Panfilov, R H Keldermann, and M P Nash. Self-organized pacemakers in a coupled reaction-diffusion-mechanics system. *Physical Review Letters*, 95(25):258104, 2005.

[105] A. V Panfilov, R. H Keldermann, and M. P Nash. Drift and breakup of spiral waves in reaction-diffusion-mechanics systems. *Proceedings of the National Academy of Sciences*, 104(19):7922–7926, 2007.

[106] Weizhen Niu and Frederick Sachs. Dynamic properties of stretch-activated k+ channels in adult rat atrial myocytes. *Progress in Biophysics and Molecular Biology*, 82(1):121–135, 2003.

[107] GCL Bett and F Sachs. Activation and inactivation of mechanosensitive currents in the chick

heart. *The Journal of Membrane Biology*, 173(3):237–254, 2000.

[108] Bryan J Caldwell, Mark L Trew, Gregory B Sands, Darren A Hooks, Ian J LeGrice, and Bruce H Smaill. Three distinct directions of intramural activation reveal nonuniform side-to-side electrical coupling of ventricular myocytes. *Circulation: Arrhythmia and Electrophysiology*, 2(4):433–440, 2009.

[109] R Christian Penland, David M Harrild, and Craig S Henriquez. Modeling impulse propagation and extracellular potential distributions in anisotropic cardiac tissue using a finite volume element discretization. *Computing and Visualization in Science*, 4(4):215–226, 2002.

[110] Jeroen G Stinstra, Bruce Hopenfeld, and Rob S MacLeod. On the passive cardiac conductivity. *Annals of Biomedical Engineering*, 33(12):1743–1751, 2005.

[111] Alexander V Panfilov and James P Keener. Re-entry in three-dimensional fitzhugh-nagumo medium with rotational anisotropy. *Physica D: Nonlinear Phenomena*, 84(3):545–552, 1995.

[112] Daniel D Streeter, Henry M Spotnitz, Dali P Patel, John Ross, and Edmund H Sonnenblick. Fiber orientation in the canine left ventricle during diastole and systole. *Circulation Research*, 24(3):339–347, 1969.

[113] PM Nielsen, IJ Le Grice, BH Smaill, and PJ Hunter. Mathematical model of geometry and fibrous structure of the heart. *American Journal of Physiology-Heart and Circulatory Physiology*, 260(4):H1365–H1378, 1991.

[114] Andrew E Pollard, Mary Jo Burgess, and Kenneth W Spitzer. Computer simulations of three-dimensional propagation in ventricular myocardium. effects of intramural fiber rotation and inhomogeneous conductivity on epicardial activation. *Circulation Research*, 72(4):744–756, 1993.

[115] DA Nordsletten, SA Niederer, MP Nash, PJ Hunter, and NP Smith. Coupling multi-physics models to cardiac mechanics. *Progress in Biophysics and Molecular Biology*, 104(1):77–88, 2011.

[116] Natalia A Trayanova. Whole-heart modeling applications to cardiac electrophysiology and electromechanics. *Circulation Research*, 108(1):113–128, 2011.

[117] Frederick J Vetter and Andrew D McCulloch. Three-dimensional analysis of regional cardiac function: a model of rabbit ventricular anatomy. *Progress in Biophysics and Molecular Biology*, 69(2):157–183, 1998.

[118] Carey Stevens, Espen Remme, Ian LeGrice, and Peter Hunter. Ventricular mechanics in diastole: material parameter sensitivity. *Journal of Biomechanics*, 36(5):737–748, 2003.

[119] Gunnar Seemann, Christine Höper, Frank B Sachse, Olaf Dössel, Arun V Holden, and Henggui Zhang. Heterogeneous three-dimensional anatomical and electrophysiological model of human atria. *Philosophical Transactions of the Royal Society of London A: Mathematical, Physical and Engineering Sciences*, 364(1843):1465–1481, 2006.

[120] Charles Antzelevitch, Serge Sicouri, Silvio H Litovsky, Anton Lukas, Subramaniam C Krishnan, Jose M Di Diego, Gary A Gintant, and Da-Wei Liu. Heterogeneity within the ventricular wall. *Circ Res*, 69(1):427, 1991.

[121] AT Winfree. Electrical turbulence in three-dimensional heart muscle. *Science*, 266(5187):1003–1006, 1994.

[122] Richard A Gray, José Jalife, Alexandre V Panfilov, William T Baxter, Candido Cabo, Jorge M Davidenko, Arkady M Pertsov, AV Panfilov, P Hogeweg, and AT Winfree. Mechanisms of cardiac fibrillation. *Science*, 270(5239):1222–1225, 1995.

[123] Natalia A Trayanova. Mathematical approaches to understanding and imaging atrial fibrillation significance for mechanisms and management. *Circulation Research*, 114(9):1516–1531, 2014.

[124] Olivier Bernus, Christian W Zemlin, Roman M Zaritsky, Sergey F Mironov, and Arkady M Pertsov. Alternating conduction in the ischaemic border zone as precursor of reentrant arrhythmias: a simulation study. *Europace*, 7(s2):S93–S104, 2005.

[125] Kathleen S McDowell, Hermenegild J Arevalo, Mary M Maleckar, and Natalia A Trayanova. Susceptibility to arrhythmia in the infarcted heart depends on myofibroblast density.

Biophysical Journal, 101(6):1307–1315, 2011.

[126] Robin M Shaw and Yoram Rudy. Electrophysiologic effects of acute myocardial ischemia: a theoretical study of altered cell excitability and action potential duration. *Cardiovascular Research*, 35(2):256–272, 1997.

[127] Nathalie Virag, Vincent Jacquemet, CS Henriquez, Steeve Zozor, Olivier Blanc, J-M Vesin, Etienne Pruvot, and Lukas Kappenberger. Study of atrial arrhythmias in a computer model based on magnetic resonance images of human atria. *Chaos: An Interdisciplinary Journal of Nonlinear Science*, 12(3):754–763, 2002.

[128] Pedro Brugada and Josep Brugada. Right bundle branch block, persistent {ST} segment elevation and sudden cardiac death: A distinct clinical and electrocardiographic syndrome: A multicenter report. *Journal of the American College of Cardiology*, 20(6):1391 – 1396, 1992.

[129] Gan-Xin Yan and Charles Antzelevitch. Cellular basis for the electrocardiographic j wave. *Circulation*, 93(2):372–379, 1996.

[130] Inma R Cantalapiedra, Angelina Peñaranda, Lluis Mont, Josep Brugada, and Blas Echebarria. Reexcitation mechanisms in epicardial tissue: Role of i to density heterogeneities and i na inactivation kinetics. *Journal of Theoretical Biology*, 259(4):850–859, 2009.

[131] Inma R Cantalapiedra, Angelina Peñaranda, Blas Echebarria, and Jean Bragard. Phase-2 reentry in cardiac tissue: role of the slow calcium pulse. *Physical Review E*, 82(1):011907, 2010.

[132] Vladimir Sergeevich Zykov. *Simulation of wave processes in excitable media*. Manchester University Press, 1987.

[133] AM Pertsov, M Wellner, and J Jalife. Eikonal relation in highly dispersive excitable media. *Physical review letters*, 78(13):2656, 1997.

[134] Elizabeth M Cherry and Flavio H Fenton. Visualization of spiral and scroll waves in simulated and experimental cardiac tissue. *New Journal of Physics*, 10(12):125016, 2008.

[135] Richard A Gray, José Jalife, Alexandre Panfilov, William T Baxter, Cándido Cabo, Jorge M Davidenko, and Arkady M Pertsov. Nonstationary vortexlike reentrant activity as a mechanism of polymorphic ventricular tachycardia in the isolated rabbit heart. *Circulation*, 91(9):2454–2469, 1995.

[136] Zhilin Qu, Alan Garfinkel, and James N Weiss. Vulnerable window for conduction block in a one-dimensional cable of cardiac cells, 1: single extrasystoles. *Biophysical Journal*, 91(3):793–804, 2006.

[137] IV Biktasheva, Dwight Barkley, VN Biktashev, GV Bordyugov, and AJ Foulkes. Computation of the response functions of spiral waves in active media. *Physical Review E*, 79(5):056702, 2009.

[138] IV Biktasheva, D Barkley, VN Biktashev, and AJ Foulkes. Computation of the drift velocity of spiral waves using response functions. *Physical Review E*, 81(6):066202, 2010.

[139] Hervé Henry and Vincent Hakim. Scroll waves in isotropic excitable media: Linear instabilities, bifurcations, and restabilized states. *Physical Review E*, 65(4):046235, 2002.

[140] Sergio Alonso, Francesc Sagués, and Alexander S Mikhailov. Taming winfree turbulence of scroll waves in excitable media. *Science*, 299(5613):1722–1725, 2003.

[141] M Courtemanche, W Skaggs, and Arthur T Winfree. Stable three-dimensional action potential circulation in the fitzhugh-nagumo model. *Physica D: Nonlinear Phenomena*, 41(2):173–182, 1990.

[142] Alain Pumir, V Nikolski, M Hörning, A Isomura, K Agladze, K Yoshikawa, R Gilmour, E Bodenschatz, and Valentin Krinsky. Wave emission from heterogeneities opens a way to controlling chaos in the heart. *Physical Review Letters*, 99(20):208101, 2007.

[143] Seiji Takagi, Alain Pumir, D Pazo, Igor Efimov, V Nikolski, and Valentine Krinsky. Unpinning and removal of a rotating wave in cardiac muscle. *Physical Review Letters*, 93(5):058101, 2004.

[144] Philip Bittihn, Gisela Luther, Eberhard Bodenschatz, Valentin Krinsky, Ulrich Parlitz, and Stefan Luther. Far field pacing supersedes anti-tachycardia pacing in a generic model of excitable media. *New Journal of Physics*, 10(10):103012, 2008.

[145] Candido Cabo, Arkady M Pertsov, Jorge M Davidenko, William T Baxter, Richard A Gray, and Jose Jalife. Vortex shedding as a precursor of turbulent electrical activity in cardiac muscle. *Biophysical Journal*, 70(3):1105–1111, 1996.

[146] Alexander V Panfilov and James P Keener. Effects of high frequency stimulation on cardiac tissue with an inexcitable obstacle. *Journal of Theoretical Biology*, 163(4):439–448, 1993.

[147] Cándido Cabo, Arkady M Pertsov, Jorge M Davidenko, and José Jalife. Electrical turbulence as a result of the critical curvature for propagation in cardiac tissue. *Chaos: An Interdisciplinary Journal of Nonlinear Science*, 8(1):116–126, 1998.

[148] Stephan Rohr, Jan P Kucera, Vladimir G Fast, and André G Kléber. Paradoxical improvement of impulse conduction in cardiac tissue by partial cellular uncoupling. *Science*, 275(5301):841–844, 1997.

[149] Christian W Zemlin and Arkady M Pertsov. Anchoring of drifting spiral and scroll waves to impermeable inclusions in excitable media. *Physical Review Letters*, 109(3):038303, 2012.

[150] Evgeny P Anyukhovsky, Eugene A Sosunov, and Michael R Rosen. Regional differences in electrophysiological properties of epicardium, midmyocardium, and endocardium in vitro and in vivo correlations. *Circulation*, 94(8):1981–1988, 1996.

[151] Wojciech Zareba, Arthur J Moss, and Saskia le Cessie. Dispersion of ventricular repolarization and arrhythmic cardiac death in coronary artery disease. *The American Journal of Cardiology*, 74(6):550–553, 1994.

[152] Mark Restivo, Edward B Caref, Dmitry O Kozhevnikov, and Nabil El-Sherif. Spatial dispersion of repolarization is a key factor in the arrhythmogenicity of long qt syndrome. *Journal of Cardiovascular Electrophysiology*, 15(3):323–331, 2004.

[153] Peter Milberg, Nico Reinsch, Kristina Wasmer, Gerold Mönnig, Jörg Stypmann, Nani Osada, Günter Breithardt, Wilhelm Haverkamp, and Lars Eckardt. Transmural dispersion of repolarization as a key factor of arrhythmogenicity in a novel intact heart model of lqt3. *Cardiovascular Research*, 65(2):397–404, 2005.

[154] C Antzelevitch and A Oliva. Amplification of spatial dispersion of repolarization underlies sudden cardiac death associated with catecholaminergic polymorphic vt, long qt, short qt and brugada syndromes. *Journal of Internal Medicine*, 259(1):48–58, 2006.

[155] Charles Antzelevitch. Role of spatial dispersion of repolarization in inherited and acquired sudden cardiac death syndromes. *American Journal of Physiology-Heart and Circulatory Physiology*, 293(4):H2024–H2038, 2007.

[156] Takeshi Aiba, Wataru Shimizu, Ichiro Hidaka, Kazunori Uemura, Takashi Noda, Can Zheng, Atsunori Kamiya, Masashi Inagaki, Masaru Sugimachi, and Kenji Sunagawa. Cellular basis for trigger and maintenance of ventricular fibrillation in the brugada syndrome model: high-resolution optical mapping study. *Journal of the American College of Cardiology*, 47(10):2074–2085, 2006.

[157] Anton Lukas and Charles Antzelevitch. Phase 2 reentry as a mechanism of initiation of circus movement reentry in canine epicardium exposed to simulated ischemia. *Cardiovascular Research*, 32(3):593–603, 1996.

[158] KHWJ Ten Tusscher and Alexander V Panfilov. Reentry in heterogeneous cardiac tissue described by the luo-rudy ventricular action potential model. *American Journal of Physiology-Heart and Circulatory Physiology*, 284(2):H542–H548, 2003.

[159] Candido Cabo and Penelope A Boyden. Heterogeneous gap junction remodeling stabilizes reentrant circuits in the epicardial border zone of the healing canine infarct: a computational study. *American Journal of Physiology-Heart and Circulatory Physiology*, 291(6):H2606–H2616, 2006.

[160] Blas Echebarria, Vincent Hakim, and Hervé Henry. Nonequilibrium ribbon model of twisted scroll waves. *Physical Review Letters*, 96(9):098301, 2006.

[161] Michael Vinson, Sergey Mironov, Scott Mulvey, and Arkady Pertsov. Control of spatial orientation and lifetime of scroll rings in excitable media. *Nature*, 386:477–480, 1997.

[162] VG Fast and AM Pertsov. [drift of vortex in the myocardium]. *Biofizika*, 35(3):478–482, 1989.

[163] Ezana M Azene, Natalia A Trayanova, and Eddy Warman. Wave front–obstacle interactions in cardiac tissue: A computational study. *Annals of Biomedical Engineering*, 29(1):35–46, 2001.

[164] AV Panfilov and BN Vasiev. Vortex initiation in a heterogeneous excitable medium. *Physica D: Nonlinear Phenomena*, 49(1):107–113, 1991.

[165] GB Makkes van der Deijl and AV Panfilov. Formation of fast spirals on heterogeneities of an excitable medium. *Physical Review E*, 78(1):012901, 2008.

[166] Rikkert H Keldermann, Kirsten HWJ ten Tusscher, Martyn P Nash, Rok Hren, Peter Taggart, and Alexander V Panfilov. Effect of heterogeneous apd restitution on vf organization in a model of the human ventricles. *American Journal of Physiology-Heart and Circulatory Physiology*, 294(2):H764–H774, 2008.

[167] Angelina Penaranda, Inma R Cantalapiedra, and Blas Echebarria. Slow pulse due to calcium current induces phase-2 reentry in heterogeneous tissue. In *Computing in Cardiology, 2010*, pages 661–664. IEEE, 2010.

[168] Sergio Alonso, Raymond Kapral, and Markus Bär. Effective medium theory for reaction rates and diffusion coefficients of heterogeneous systems. *Physical Review Letters*, 102(23):238302, 2009.

[169] Sergio Alonso, Markus Baer, and Raymond Kapral. Effective medium approach for heterogeneous reaction-diffusion media. *The Journal of Chemical Physics*, 131(21):214102, 2009.

[170] Daniel T Kaplan, Joseph M Smith, Bo EH Saxberg, and Richard J Cohen. Nonlinear dynamics in cardiac conduction. *Mathematical biosciences*, 90(1):19–48, 1988.

[171] Sergio Alonso and Markus Bär. Reentry near the percolation threshold in a heterogeneous discrete model for cardiac tissue. *Physical Review Letters*, 110(15):158101, 2013.

[172] Bruno Gouvêa de Barros, Rodrigo Weber dos Santos, Marcelo Lobosco, and Sergio Alonso. Simulation of ectopic pacemakers in the heart: multiple ectopic beats generated by reentry inside fibrotic regions. *Biomedical Research International*, page 713058, 2015.

[173] Jakob Löber, Markus Bär, and Harald Engel. Front propagation in one-dimensional spatially periodic bistable media. *Physical Review E*, 86(6):066210, 2012.

[174] Dong Fan, Abhijit Takawale, Jiwon Lee, and Zamaneh Kassiri. Cardiac fibroblasts, fibrosis and extracellular matrix remodeling in heart disease. *Fibrogenesis Tissue Repair*, 5(1):15–15, 2012.

[175] Stephan Rohr. Role of gap junctions in the propagation of the cardiac action potential. *Cardiovascular Research*, 62(2):309–322, 2004.

[176] Stephan Rohr. Arrhythmogenic implications of fibroblast-myocyte interactions. *Circulation: Arrhythmia and Electrophysiology*, 5(2):442–452, 2012.

[177] Frank B. Sachse, A. P. Moreno, G. Seemann, and J. A. Abildskov. A Model of Electrical Conduction in Cardiac Tissue Including Fibroblasts. *Annals of Biomedical Engineering*, 37(5):874–889, 2009.

[178] Peter Kohl, Patrizia Camelliti, Francis L Burton, and Godfrey L Smith. Electrical coupling of fibroblasts and myocytes: relevance for cardiac propagation. *Journal of Electrocardiology*, 38(4):45–50, 2005.

[179] K Andrew MacCannell, Hojjat Bazzazi, Lisa Chilton, Yoshiyuki Shibukawa, Robert B Clark, and Wayne R Giles. A mathematical model of electrotonic interactions between ventricular myocytes and fibroblasts. *Biophysical Journal*, 92(11):4121–4132, 2007.

[180] Yuanfang Xie, Alan Garfinkel, James N Weiss, and Zhilin Qu. Cardiac alternans induced by fibroblast-myocyte coupling: mechanistic insights from computational models. *American Journal of Physiology-Heart and Circulatory Physiology*, 297(2):H775, 2009.

[181] Yuanfang Xie, Alan Garfinkel, Patrizia Camelliti, Peter Kohl, James N Weiss, and Zhilin Qu. Effects of fibroblast-myocyte coupling on cardiac conduction and vulnerability to reentry: a computational study. *Heart Rhythm*, 6(11):1641–1649, 2009.

[182] Darren A Hooks, Karl A Tomlinson, Scott G Marsden, Ian J LeGrice, Bruce H Smaill, Andrew J Pullan, and Peter J Hunter. Cardiac microstructure implications for electrical propagation

and defibrillation in the heart. *Circulation Research*, 91(4):331–338, 2002.

[183] Darren A Hooks, Mark L Trew, Bryan J Caldwell, Gregory B Sands, Ian J LeGrice, and Bruce H Smaill. Laminar arrangement of ventricular myocytes influences electrical behavior of the heart. *Circulation Research*, 101(10):e103–e112, 2007.

[184] Kirsten HWJ Ten Tusscher and Alexander V Panfilov. Influence of diffuse fibrosis on wave propagation in human ventricular tissue. *Europace*, 9(suppl 6):vi38–vi45, 2007.

[185] Matthias W Keller, Armin Luik, Mohammad Soltan Abady, Gunnar Seemann, Claus Schmitt, and Olaf Dossel. Influence of three-dimensional fibrotic patterns on simulated intracardiac electrogram morphology. In *Computing in Cardiology Conference (CinC), 2013*, pages 923–926. IEEE, 2013.

[186] Fernando Otaviano Campos, Thomas Wiener, Anton J Prassl, R Weber Dos Santos, Damián Sánchez-Quintana, Helmut Ahammer, Gernot Plank, and Ernst Hofer. Electroanatomical characterization of atrial microfibrosis in a histologically detailed computer model. *Biomedical Engineering, IEEE Transactions on*, 60(8):2339–2349, 2013.

[187] Marjorie Letitia Hubbard and Craig S Henriquez. A microstructural model of reentry arising from focal breakthrough at sites of source-load mismatch in a central region of slow conduction. *American Journal of Physiology-Heart and Circulatory Physiology*, 306(9):H1341–H1352, 2014.

[188] Marjorie Letitia Hubbard, Joshua Xu, and Craig S Henriquez. The effect of random cell decoupling on electrogram morphology near the percolation threshold in microstructural models of cardiac tissue. In *Computing in Cardiology Conference (CinC), 2014*, pages 65–68. IEEE, 2014.

[189] Kim Christensen, Kishan A Manani, and Nicholas S Peters. Simple model for identifying critical regions in atrial fibrillation. *Physical Review Letters*, 114(2):028104, 2015.

[190] Elizabeth M Cherry, Joachim R Ehrlich, Stanley Nattel, and Flavio H Fenton. Pulmonary vein reentry—properties and size matter: insights from a computational analysis. *Heart Rhythm*, 4(12):1553–1562, 2007.

[191] Michel Haissaguerre, Pierre Jaïs, Dipen C Shah, Atsushi Takahashi, Mélèze Hocini, Gilles Quiniou, Stéphane Garrigue, Alain Le Mouroux, Philippe Le Métayer, and Jacques Clémenty. Spontaneous initiation of atrial fibrillation by ectopic beats originating in the pulmonary veins. *New England Journal of Medicine*, 339(10):659–666, 1998.

[192] Sergio Alonso, Markus Bär, and Alexander V Panfilov. Effects of reduced discrete coupling on filament tension in excitable media. *Chaos: An Interdisciplinary Journal of Nonlinear Science*, 21(1):013118, 2011.

[193] Zhilin Qu. Dynamical effects of diffusive cell coupling on cardiac excitation and propagation: a simulation study. *American Journal of Physiology-Heart and Circulatory Physiology*, 287(6):H2803–H2812, 2004.

[194] AV Panfilov. Spiral breakup in an array of coupled cells: the role of the intercellular conductance. *Physical Review Letters*, 88(11):118101, 2002.

[195] Shu-ichi Kinoshita, Mayuko Iwamoto, Keita Tateishi, Nobuhiko J Suematsu, and Daishin Ueyama. Mechanism of spiral formation in heterogeneous discretized excitable media. *Physical Review E*, 87(6):062815, 2013.

[196] Gil Bub, Alvin Shrier, and Leon Glass. Spiral wave generation in heterogeneous excitable media. *Physical Review Letters*, 88(5):058101, 2002.

[197] Benjamin E Steinberg, Leon Glass, Alvin Shrier, and Gil Bub. The role of heterogeneities and intercellular coupling in wave propagation in cardiac tissue. *Philosophical Transactions of the Royal Society A: Mathematical, Physical and Engineering Sciences*, 364(1842):1299–1311, 2006.

[198] AM Pertsov, EA Ermakova, and EE Shnol. On the diffraction of autowaves. *Physica D: Nonlinear Phenomena*, 44(1):178–190, 1990.

[199] Boris Y Kogan, Walter J Karplus, Brian S Billett, and William G Stevenson. Excitation wave propagation within narrow pathways: geometric configurations facilitating unidirectional block and reentry. *Physica D: Nonlinear Phenomena*, 59(4):275–296, 1992.

[200] Agota Toth, Vilmos Gaspar, and Kenneth Showalter. Signal transmission in chemical systems: propagation of chemical waves through capillary tubes. *The Journal of Physical Chemistry*, 98(2):522–531, 1994.

[201] G Haas, M Bär, IG Kevrekidis, PB Rasmussen, H-H Rotermund, and G Ertl. Observation of front bifurcations in controlled geometries: From one to two dimensions. *Physical Review Letters*, 75(19):3560, 1995.

[202] Nils Hartmann, Yannis Kevrekidis, and Ronald Imbihl. Pattern formation in restricted geometries: the no+ co reaction on pt (100). *Journal of Chemical Physics*, 112(15):6795–6803, 2000.

[203] Candido Cabo, Arkady M Pertsov, William T Baxter, Jorge M Davidenko, Richard A Gray, and Jose Jalife. Wave-front curvature as a cause of slow conduction and block in isolated cardiac muscle. *Circulation Research*, 75(6):1014–1028, 1994.

[204] Peter Schütz and Mathias Bode. Discrete coupling and propagating signals. *International Journal of Bifurcation and Chaos*, 6(10):1891–1900, 1996.

[205] S Martens, J Löber, and H Engel. Front propagation in channels with spatially modulated cross section. *Physical Review E*, 91(2):022902, 2015.

[206] Konstantin Agladze, James P Keener, Stefan C Müller, and Alexander Panfilov. Rotating spiral waves created by geometry. *Science*, pages 1746–1746, 1994.

[207] M Bär, AK Bangia, IG Kevrekidis, G Haas, H-H Rotermund, and G Ertl. Composite catalyst surfaces: Effect of inert and active heterogeneities on pattern formation. *The Journal of Physical Chemistry*, 100(49):19106–19117, 1996.

[208] VS Zykov and Stefan C Müller. Spiral waves on circular and spherical domains of excitable medium. *Physica D: Nonlinear Phenomena*, 97(1):322–332, 1996.

[209] N Hartmann, M Bär, IG Kevrekidis, K Krischer, and R Imbihl. Rotating chemical waves in small circular domains. *Physical Review Letters*, 76(8):1384, 1996.

[210] Markus Bär, Anil K Bangia, and Ioannis G Kevrekidis. Bifurcation and stability analysis of rotating chemical spirals in circular domains: Boundary-induced meandering and stabilization. *Physical Review E*, 67(5):056126, 2003.

[211] VN Biktashev, D Barkley, and IV Biktasheva. Orbital motion of spiral waves in excitable media. *Physical Review Letters*, 104(5):058302, 2010.

[212] Jan F Totz, Harald Engel, and Oliver Steinbock. Spatial confinement causes lifetime enhancement and expansion of vortex rings with positive filament tension. *arXiv preprint arXiv:1401.6550*, 2014.

[213] Arash Azhand, Rico Buchholz, Florian Buchholz, Jan Totz, and Harald Engel. No-flux boundaries stabilize scroll rings in excitable media with negative filament tension. *arXiv preprint arXiv:1401.8119*, 2014.

[214] Robert J Young and Alexander V Panfilov. Anisotropy of wave propagation in the heart can be modeled by a riemannian electrophysiological metric. *Proceedings of the National Academy of Sciences*, 107(34):15063–15068, 2010.

[215] Henri Verschelde, Hans Dierckx, and Olivier Bernus. Covariant stringlike dynamics of scroll wave filaments in anisotropic cardiac tissue. *Physical Review Letters*, 99(16):168104, 2007.

[216] Omer Berenfeld and Arkady M Pertsov. Dynamics of intramural scroll waves in three-dimensional continuous myocardium with rotational anisotropy. *Journal of theoretical biology*, 199(4):383–394, 1999.

[217] Marcel Wellner, Omer Berenfeld, José Jalife, and Arkady M Pertsov. Minimal principle for rotor filaments. *Proceedings of the National Academy of Sciences*, 99(12):8015–8018, 2002.

[218] Christian W Zemlin, Frency Varghese, Marcel Wellner, and Arkady M Pertsov. Refraction of scroll-wave filaments at the boundary between two reaction-diffusion media. *Physical review letters*, 114(11):118303, 2015.

[219] RH Clayton and AV Panfilov. A guide to modelling cardiac electrical activity in anatomically detailed ventricles. *Progress in Biophysics and Molecular Biology*, 96(1):19–43, 2008.

[220] H. Hering. Experimentelle studien an saugentieren uber das electro- cardiogram. *Z Exper Med*, 7:363, 1909.

[221] Thomas Lewis. Notes upon alternation of the heart. *Quart J Med*, 4:141–144, 1910.

[222] H H Kalter and M L Schwartz. Electrical alternans. *New York State Journal of Medicine*, 48(10):1164–6, 1948.

[223] David S Rosenbaum, Lance E Jackson, Joseph M Smith, Hasan Garan, Jeremy N Ruskin, and Richard J Cohen. Electrical alternans and vulnerability to ventricular arrhythmias. *New England Journal of Medicine*, 330(4):235–241, 1994.

[224] Joseph M Pastore, Steven D Girouard, Kenneth R Laurita, Fadi G Akar, and David S Rosenbaum. Mechanism linking t-wave alternans to the genesis of cardiac fibrillation. *Circulation*, 99(10):1385–1394, 1999.

[225] Alain Karma. Electrical alternans and spiral wave breakup in cardiac tissue. *Chaos: An Interdisciplinary Journal of Nonlinear Science*, 4(3):461–472, 1994.

[226] J B Nolasco and R W Dahlen. A graphic method for the study of alternation in cardiac action potentials. *Journal of Applied Physiology*, 25(2):191–6, 1968.

[227] MR Guevara, G Ward, A Shrier, and L Glass. Electrical alternans and period doubling bifurcations. *IEEE Comp Cardiol*, 562:167–170, 1984.

[228] Alan Garfinkel, Young-Hoon Kim, Olga Voroshilovsky, Zhilin Qu, Jong R Kil, Moon-Hyoung Lee, Hrayr S Karagueuzian, James N Weiss, and Peng-Sheng Chen. Preventing ventricular fibrillation by flattening cardiac restitution. *Proceedings of the National Academy of Sciences*, 97(11):6061–6066, 2000.

[229] Etienne J Pruvot, Rodolphe P Katra, David S Rosenbaum, and Kenneth R Laurita. Role of calcium cycling versus restitution in the mechanism of repolarization alternans. *Circulation Research*, 94(8):1083–1090, 2004.

[230] Joshua I. Goldhaber, Lai-Hua Xie, Tan Duong, Christi Motter, Kien Khuu, and James N. Weiss. Action potential duration restitution and alternans in rabbit ventricular myocytes: The key role of intracellular calcium cycling. *Circulation Research*, 96(4):459–466, 2005.

[231] Eric Cytrynbaum and James P Keener. Stability conditions for the traveling pulse: Modifying the restitution hypothesis. *Chaos: An Interdisciplinary Journal of Nonlinear Science*, 12(3):788–799, 2002.

[232] Elizabeth M Cherry and Flavio H Fenton. Suppression of alternans and conduction blocks despite steep apd restitution: electrotonic, memory, and conduction velocity restitution effects. *American Journal of Physiology-Heart and Circulatory Physiology*, 286(6):H2332–H2341, 2004.

[233] Jeffrey J. Fox, Eberhard Bodenschatz, and Robert F. Gilmour. Period-doubling instability and memory in cardiac tissue. *Physical Review Letters*, 89:138101, 2002.

[234] Ning Wei, Yoichiro Mori, and Elena G Tolkacheva. The role of short term memory and conduction velocity restitution in alternans formation. *Journal of Theoretical Biology*, 367:21–28, 2015.

[235] E. G. Tolkacheva, D. G. Schaeffer, Daniel J. Gauthier, and W. Krassowska. Condition for alternans and stability of the 1:1 response pattern in a "memory" model of paced cardiac dynamics. *Physical Review E*, 67:031904, 2003.

[236] Soma S Kalb, Hana M Dobrovolny, Elena G Tolkacheva, Salim F Idriss, Wanda Krassowska, and Daniel J Gauthier. The restitution portrait. *Journal of Cardiovascular Electrophysiology*, 15(6):698–709, 2004.

[237] Soma S Kalb, Elena G Tolkacheva, David G Schaeffer, Daniel J Gauthier, and Wanda Krassowska. Restitution in mapping models with an arbitrary amount of memory. *Chaos: An Interdisciplinary Journal of Nonlinear Science*, 15(2):023701, 2005.

[238] Giedrius Kanaporis and Lothar A. Blatter. The mechanisms of calcium cycling and action potential dynamics in cardiac alternans. *Circulation Research*, 116(5):846–856, 2015.

[239] E Chudin, J Goldhaber, A Garfinkel, J Weiss, and B Kogan. Intracellular ca 2+ dynamics and the stability of ventricular tachycardia. *Biophysical journal*, 77(6):2930–2941, 1999.

[240] Jörg Hüser, Yong Gao Wang, Katherine A Sheehan, Fredy Cifuentes, Stephen L Lipsius, and

Lothar A Blatter. Functional coupling between glycolysis and excitation—contraction coupling underlies alternans in cat heart cells. *The Journal of Physiology*, 524(3):795–806, 2000.

[241] Marc Courtemanche, Leon Glass, and James P Keener. Instabilities of a propagating pulse in a ring of excitable media. *Physical Review Letters*, 70(14):2182, 1993.

[242] Marc Courtemanche, James P Keener, and Leon Glass. A delay equation representation of pulse circulation on a ring in excitable media. *SIAM Journal on Applied Mathematics*, 56(1):119–142, 1996.

[243] S Bauer, G Röder, and M Bär. Alternans and the influence of ionic channel modifications: Cardiac three–dimensional simulations and one-dimensional numerical bifurcation analysis. *Chaos: An Interdisciplinary Journal of Nonlinear Science*, 17(1):015104, 2007.

[244] Blas Echebarria and Alain Karma. Mechanisms for initiation of cardiac discordant alternans. *The European Physical Journal-Special Topics*, 146(1):217–231, 2007.

[245] Zhilin Qu, Alan Garfinkel, Peng-Sheng Chen, and James N Weiss. Mechanisms of discordant alternans and induction of reentry in simulated cardiac tissue. *Circulation*, 102(14):1664–1670, 2000.

[246] Mari A Watanabe, Flavio H Fenton, Steven J Evans, Harold M Hastings, and Alain Karma. Mechanisms for discordant alternans. *Journal of Cardiovascular Electrophysiology*, 12(2):196–206, 2001.

[247] Blas Echebarria and Alain Karma. Amplitude equation approach to spatiotemporal dynamics of cardiac alternans. *Physical Review E*, 76(5):051911, 2007.

[248] Jeffrey J Fox, Mark L Riccio, Fei Hua, Eberhard Bodenschatz, and Robert F Gilmour. Spatiotemporal transition to conduction block in canine ventricle. *Circulation Research*, 90(3):289–296, 2002.

[249] M Radszuweit, E Alvarez-Lacalle, M Bär, and B Echebarria. Cardiac contraction induces discordant alternans and localized block. *Physical Review E*, 91(2):022703, 2015.

[250] Mark C Cross and Pierre C Hohenberg. Pattern formation outside of equilibrium. *Reviews of Modern Physics*, 65(3):851, 1993.

[251] Blas Echebarria and Alain Karma. Instability and spatiotemporal dynamics of alternans in paced cardiac tissue. *Physical Review Letters*, 88(20):208101, 2002.

[252] Blas Echebarria, Georg Röder, Harald Engel, Jörn Davidsen, and Markus Bär. Supernormal conduction in cardiac tissue promotes concordant alternans and action potential bunching. *Physical Review E*, 83(4):040902, 2011.

[253] Blas Echebarria and Alain Karma. Spatiotemporal control of cardiac alternans. *Chaos: An Interdisciplinary Journal of Nonlinear Science*, 12(3):923–930, 2002.

[254] David J Christini, Mark L Riccio, Calin A Culianu, Jeffrey J Fox, Alain Karma, and Robert F Gilmour Jr. Control of electrical alternans in canine cardiac purkinje fibers. *Physical Review Letters*, 96(10):104101, 2006.

[255] Trine Krogh-Madsen, Alain Karma, Mark L Riccio, Peter N Jordan, David J Christini, and Robert F Gilmour Jr. Off-site control of repolarization alternans in cardiac fibers. *Physical Review E*, 81(1):011915, 2010.

[256] Alejandro Garzon, Roman O Grigoriev, and Flavio H Fenton. Model-based control of cardiac alternans on a ring. *Physical Review E*, 80(2):021932, 2009.

[257] Alejandro Garzon, Roman O Grigoriev, and Flavio H Fenton. Model-based control of cardiac alternans in purkinje fibers. *Physical Review E*, 84(4):041927, 2011.

[258] Y Shiferaw, D Sato, and A Karma. Coupled dynamics of voltage and calcium in paced cardiac cells. *Physical Review E*, 71(2):021903, 2005.

[259] Per Sebastian Skardal, Alain Karma, and Juan G Restrepo. Unidirectional pinning and hysteresis of spatially discordant alternans in cardiac tissue. *Physical Review Letters*, 108(10):108103, 2012.

[260] Juan G Restrepo and Alain Karma. Line-defect patterns of unstable spiral waves in cardiac tissue. *Physical Review E*, 79(3):030906, 2009.

[261] John Guckenheimer and Philip Holmes. *Nonlinear oscillations, dynamical systems, and bifurcations of vector fields*, volume 42. Springer Science & Business Media, 1983.

[262] Alexander V Panfilov and Arun V Holden. *Computational biology of the heart*. Wiley New York, 1997.

[263] Jean-Pierre Drouhard and Fernand A Roberge. Revised formulation of the hodgkin-huxley representation of the sodium current in cardiac cells. *Computers and Biomedical Research*, 20(4):333–350, 1987.

[264] Rüdiger Seydel. *Practical bifurcation and stability analysis*, volume 5. Springer Science & Business Media, 2009.

[265] Doedel E, Paffenroth RC, Champneys AR, FairgrieveTF, Kuznetsov YA, Oldeman BE, Sandstede B, and Wang X. Auto2000: Continuation and bifurcation software for ordinary differential equations (with homcont). *Technical report, Concordia University*, 2002.

[266] Björn Sandstede. Stability of travelling waves. *Handbook of dynamical systems*, 2:983–1055, 2002.

[267] Jens DM Rademacher, Björn Sandstede, and Arnd Scheel. Computing absolute and essential spectra using continuation. *Physica D: Nonlinear Phenomena*, 229(2):166–183, 2007.

[268] Michal Or-Guil, Ioannis G Kevrekidis, and Markus Bär. Stable bound states of pulses in an excitable medium. *Physica D: Nonlinear Phenomena*, 135(1):154–174, 2000.

[269] Norbert Wiener and Arturo Rosenblueth. The mathematical formulation of the problem of conduction of impulses in a network of connected excitable elements, specifically in cardiac muscle. *Archivos del instituto de Cardiología de México*, 16(3):205–265, 1946.

[270] Arthur T Winfree. Spiral waves of chemical activity. *Science*, 175(4022):634–636, 1972.

[271] Sami F Noujaim, Omer Berenfeld, Jérôme Kalifa, Marina Cerrone, Kumaraswamy Nanthakumar, Felipe Atienza, Javier Moreno, Sergey Mironov, and José Jalife. Universal scaling law of electrical turbulence in the mammalian heart. *Proceedings of the National Academy of Sciences*, 104(52):20985–20989, 2007.

[272] Francis X Witkowski, L Joshua Leon, Patricia A Penkoske, Wayne R Giles, Mark L Spano, William L Ditto, and Arthur T Winfree. Spatiotemporal evolution of ventricular fibrillation. *Nature*, 392(6671):78–82, 1998.

[273] Richard A Gray, Arkady M Pertsov, and José Jalife. Spatial and temporal organization during cardiac fibrillation. *Nature*, 392(6671):75–78, 1998.

[274] Arthur T Winfree. Varieties of spiral wave behavior: An experimentalist5̧s approach to the theory of excitable media. *Chaos: An Interdisciplinary Journal of Nonlinear Science*, 1(3):303–334, 1991.

[275] H Zhang and AV Holden. Chaotic meander of spiral waves in the fitzhugh-nagumo system. *Chaos, Solitons & Fractals*, 5(3):661–670, 1995.

[276] VN Biktashev and AV Holden. Deterministic brownian motion in the hypermeander of spiral waves. *Physica D: Nonlinear Phenomena*, 116(3):342–354, 1998.

[277] Dwight Barkley. Spiral meandering. In *Chemical waves and patterns*, pages 163–189. Springer, 1995.

[278] Alexandre Panfilov and Pauline Hogeweg. Spiral breakup in a modified fitzhugh-nagumo model. *Physics Letters A*, 176(5):295–299, 1993.

[279] Alexandre V Panfilov. Spiral breakup as a model of ventricular fibrillation. *Chaos: An Interdisciplinary Journal of Nonlinear Science*, 8(1):57–64, 1998.

[280] AT Winfree. *Advances in Biological and Medical Physics*. New York, Academic Press, 1973.

[281] Erzsébet Lugosi. Analysis of meandering in zykov kinetics. *Physica D: Nonlinear Phenomena*, 40(3):331–337, 1989.

[282] W Jahnke, WE Skaggs, and Arthur T Winfree. Chemical vortex dynamics in the belousov-zhabotinskii reaction and in the two-variable oregonator model. *The Journal of Physical Chemistry*, 93(2):740–749, 1989.

[283] AS Mikhailov, VA Davydov, and VS Zykov. Complex dynamics of spiral waves and motion of

curves. *Physica D: Nonlinear Phenomena*, 70(1):1–39, 1994.

[284] Alain Karma. Meandering transition in two-dimensional excitable media. *Physical Review Letters*, 65(22):2824, 1990.

[285] Dwight Barkley. Linear stability analysis of rotating spiral waves in excitable media. *Physical Review Letters*, 68(13):2090, 1992.

[286] Dwight Barkley. Euclidean symmetry and the dynamics of rotating spiral waves. *Physical Review Letters*, 72(1):164, 1994.

[287] Björn Sandstede and Arnd Scheel. Superspiral structures of meandering and drifting spiral waves. *Physical Review Letters*, 86(1):171, 2001.

[288] Valentin I Krinsky, Igor R Efimov, and Jose Jalife. Vortices with linear cores in excitable media. *Proceedings of the Royal Society of London. Series A: Mathematical and Physical Sciences*, 437(1901):645–655, 1992.

[289] Igor R Efimov, Valentin I Krinsky, and Jose Jalife. Dynamics of rotating vortices in the beeler-reuter model of cardiac tissue. *Chaos, Solitons & Fractals*, 5(3):513–526, 1995.

[290] Qi Ouyang, Harry L Swinney, and Ge Li. Transition from spirals to defect-mediated turbulence driven by a doppler instability. *Physical Review Letters*, 84(5):1047, 2000.

[291] Denis Noble. Modeling the heart–from genes to cells to the whole organ. *Science*, 295(5560):1678–1682, 2002.

[292] Flavio Fenton and Alain Karma. Fiber-rotation-induced vortex turbulence in thick myocardium. *Physical Review Letters*, 81(2):481, 1998.

[293] Alexandre V Panfilov and Paulien Hogeweg. Scroll breakup in a three-dimensional excitable medium. *Physical Review E*, 53(2):1740, 1996.

[294] Zhilin Qu, Fagen Xie, and Alan Garfinkel. Diffusion-induced vortex filament instability in 3-dimensional excitable media. *Physical Review Letters*, 83(13):2668, 1999.

[295] Aric Hagberg and Ehud Meron. From labyrinthine patterns to spiral turbulence. *Physical Review Letters*, 72(15):2494, 1994.

[296] Aric Hagberg and Ehud Meron. Complex patterns in reaction-diffusion systems: A tale of two front instabilities. *Chaos: An Interdisciplinary Journal of Nonlinear Science*, 4(3):477–484, 1994.

[297] Athanasius FM Marée and Alexander V Panfilov. Spiral breakup in excitable tissue due to lateral instability. *Physical Review Letters*, 78(9):1819, 1997.

[298] VS Zykov, AS Mikhailov, and SC Müller. Wave instabilities in excitable media with fast inhibitor diffusion. *Physical Review Letters*, 81(13):2811, 1998.

[299] Marc Courtemanche. Complex spiral wave dynamics in a spatially distributed ionic model of cardiac electrical activity. *Chaos: An Interdisciplinary Journal of Nonlinear Science*, 6(4):579–600, 1996.

[300] A Giaquinta, S Boccaletti, and FT Arecchi. Superexcitability induced spiral breakup in excitable systems. *International Journal of Bifurcation and Chaos*, 6(09):1753–1759, 1996.

[301] Markus Bär and Michal Or-Guil. Alternative scenarios of spiral breakup in a reaction-diffusion model with excitable and oscillatory dynamics. *Physical Review Letters*, 82(6):1160, 1999.

[302] Ehud Meron. Pattern formation in excitable media. *Physics Reports*, 218(1):1–66, 1992.

[303] Lutz Brusch, Alessandro Torcini, and Markus Bär. Doppler effect of nonlinear waves and superspirals in oscillatory media. *Physical Review Letters*, 91(10):108302, 2003.

[304] Markus Bär and Lutz Brusch. Breakup of spiral waves caused by radial dynamics: Eckhaus and finite wavenumber instabilities. *New Journal of Physics*, 6(1):5, 2004.

[305] Q Ouyang and J-M Flesselles. Transition from spirals to defect turbulence driven by a convective instability. *Nature*, 379(6561):143–146, 1996.

[306] Hugues Chaté and Paul Manneville. Phase diagram of the two-dimensional complex ginzburg-landau equation. *Physica A: Statistical Mechanics and its Applications*, 224(1):348–368, 1996.

[307] SM Tobias and E Knobloch. Breakup of spiral waves into chemical turbulence. *Physical Review Letters*, 80(21):4811, 1998.

[308] Björn Sandstede and Arnd Scheel. Absolute versus convective instability of spiral waves. *Physical Review E*, 62(6):7708, 2000.

[309] Lu Qun Zhou and Qi Ouyang. Experimental studies on long-wavelength instability and spiral breakup in a reaction-diffusion system. *Physical Review Letters*, 85(8):1650, 2000.

[310] Lu Qun Zhou and Qi Ouyang. Spiral instabilities in a reaction-diffusion system. *The Journal of Physical Chemistry A*, 105(1):112–118, 2001.

[311] M Falcke, M Bär, JD Lechleiter, and JL Hudson. Spiral breakup and defect dynamics in a model for intracellular ca 2+ dynamics. *Physica D: Nonlinear Phenomena*, 129(3):236–252, 1999.

[312] Arthur T Winfree. Electrical instability in cardiac muscle: phase singularities and rotors. *Journal of Theoretical Biology*, 138(3):353–405, 1989.

[313] Igor Aranson and Igor Mitkov. Helicoidal instability of a scroll vortex in three-dimensional reaction-diffusion systems. *Physical Review E*, 58(4):4556, 1998.

[314] Hervé Henry and Vincent Hakim. Linear stability of scroll waves. *Physical Review Letters*, 85(25):5328, 2000.

[315] Hervé Henry. Spiral wave drift in an electric field and scroll wave instabilities. *Physical Review E*, 70(2):026204, 2004.

[316] A Rusakov, AB Medvinsky, and AV Panfilov. Scroll waves meandering in a model of an excitable medium. *Physical Review E*, 72(2):022902, 2005.

[317] AV Panfilov, AN Rudenko, and AM Pertsov. Twisted scroll waves in three-dimensional active media. In *Self-Organization Autowaves and Structures Far from Equilibrium*, pages 103–105. Springer, 1984.

[318] Ulrich Storb, Camilo Rodrigues Neto, Markus Bär, and Stefan C Müller. A tomographic study of desynchronization and complex dynamics of scroll waves in an excitable chemical reaction with a gradient. *Physical Chemistry Chemical Physics*, 5(11):2344–2353, 2003.

[319] C Henze, E Lugosi, and AT Winfree. Helical organizing centers in excitable media. *Canadian Journal of Physics*, 68(9):683–710, 1990.

[320] AS Mikhailov, AV Panfilov, and AN Rudenko. Twisted scroll waves in active three-dimensional media. *Physics Letters A*, 109(5):246–250, 1985.

[321] S Setayeshgar and Andrew J Bernoff. Scroll waves in the presence of slowly varying anisotropy with application to the heart. *Physical review letters*, 88(2):028101, 2001.

[322] Wouter-Jan Rappel. Filament instability and rotational tissue anisotropy: a numerical study using detailed cardiac models. *Chaos: An Interdisciplinary Journal of Nonlinear Science*, 11(1):71–80, 2001.

[323] LV Yakushevich. Vortex filament elasticity in active medium. *Studia Biophysica*, 100(3):195–200, 1984.

[324] AV Panfilov and AM Pertsov. Vortex ring in a 3-dimensional active medium described by reaction-diffusion equations. *Doklady Akademii Nauk SSSR*, 274(6):1500, 1984.

[325] PK Brazhnik, VA Davydov, VS Zykov, and AS Mikhailov. Vortex rings in excitable media. *Zh. Eksp. Teor. Fiz*, 93:1725–1736, 1987.

[326] Hans Dierckx and Henri Verschelde. Effective dynamics of twisted and curved scroll waves using virtual filaments. *Physical Review E*, 88(6):062907, 2013.

[327] Sergio Alonso and Alexander V Panfilov. Negative filament tension at high excitability in a model of cardiac tissue. *Physical Review Letters*, 100(21):218101, 2008.

[328] Sergio Alonso, Ralf Kähler, Alexander S Mikhailov, and Francisco Sagués. Expanding scroll rings and negative tension turbulence in a model of excitable media. *Physical Review E*, 70(5):056201, 2004.

[329] Chaiya Luengviriya, Ulrich Storb, Gert Lindner, Stefan C Müller, Markus Bär, and Marcus JB Hauser. Scroll wave instabilities in an excitable chemical medium. *Physical Review Letters*, 100(14):148302, 2008.

[330] Tamás Bánsági Jr and Oliver Steinbock. Negative filament tension of scroll rings in an excitable system. *Physical Review E*, 76(4):045202, 2007.

[331] AV Panfilov and AV Holden. Computer simulation of re-entry sources in myocardium in two and three dimensions. *Journal of Theoretical Biology*, 161(3):271–285, 1993.

[332] Hans Dierckx, Henri Verschelde, Özgür Selsil, and Vadim N Biktashev. Buckling of scroll waves. *Physical Review Letters*, 109(17):174102, 2012.

[333] VN Biktashev. A three-dimensional autowave turbulence. *International Journal of Bifurcation and Chaos*, 8(04):677–684, 1998.

[334] Roman M Zaritski, Sergey F Mironov, and Arkady M Pertsov. Intermittent self-organization of scroll wave turbulence in three-dimensional excitable media. *Physical Review Letters*, 92(16):168302, 2004.

[335] Roman M Zaritski and Arkady M Pertsov. Stable spiral structures and their interaction in two-dimensional excitable media. *Physical Review E*, 66(6):066120, 2002.

[336] MC Cross and PC Hohenberg. Spatiotemporal chaos. *Science*, 263(5153):1569–1569, 1994.

[337] Matthew C Strain and Henry S Greenside. Size-dependent transition to high-dimensional chaotic dynamics in a two-dimensional excitable medium. *Physical Review Letters*, 80(11):2306, 1998.

[338] Greg Byrne, Christopher D Marcotte, and Roman O Grigoriev. Exact coherent structures and chaotic dynamics in a model of cardiac tissue. *Chaos: An Interdisciplinary Journal of Nonlinear Science*, 25(3):033108, 2015.

[339] Ghislain St-Yves and Jörn Davidsen. Influence of the medium's dimensionality on defect-mediated turbulence. *Physical Review E*, 91(3):032926, 2015.

[340] P Coullet, L Gil, and J Lega. Defect-mediated turbulence. *Physical Review Letters*, 62(14):1619, 1989.

[341] L Gil, J Lega, and JL Meunier. Statistical properties of defect-mediated turbulence. *Physical Review A*, 41:1138–1141, 1990.

[342] M Bär, M Hildebrand, M Eiswirth, M Falcke, H Engel, and M Neufeld. Chemical turbulence and standing waves in a surface reaction model: The influence of global coupling and wave instabilities. *Chaos: An Interdisciplinary Journal of Nonlinear Science*, 4(3):499–508, 1994.

[343] M Hildebrand, M Bär, and M Eiswirth. Statistics of topological defects and spatiotemporal chaos in a reaction-diffusion system. *Physical Review Letters*, 75(8):1503, 1995.

[344] Kirsten HWJ Ten Tusscher, Azzam Mourad, MP Nash, Richard H Clayton, Chris P Bradley, David J Paterson, Rok Hren, Martin Hayward, Alexander V Panfilov, and Peter Taggart. Organization of ventricular fibrillation in the human heart: experiments and models. *Experimental Physiology*, 94(5):553–562, 2009.

[345] Kirsten HWJ Ten Tusscher, Alexander V Panfilov, et al. Organization of ventricular fibrillation in the human heart. *Circulation Research*, 100(12):e87–e101, 2007.

[346] Jörn Davidsen, Meng Zhan, and Raymond Kapral. Filament-induced surface spiral turbulence in three-dimensional excitable media. *Physical Review Letters*, 101(20):208302, 2008.

[347] Martin J Bishop, Edward J Vigmond, and Gernot Plank. The functional role of electrophysiological heterogeneity in the rabbit ventricle during rapid pacing and arrhythmias. *American Journal of Physiology-Heart and Circulatory Physiology*, 304(9):H1240–H1252, 2013.

[348] Alain Karma. Scaling regime of spiral wave propagation in single-diffusive media. *Physical Review Letters*, 68(3):397, 1992.

[349] Daniel Margerit and Dwight Barkley. Selection of twisted scroll waves in three-dimensional excitable media. *Physical Review Letters*, 86(1):175, 2001.

[350] Daniel Margerit and Dwight Barkley. Large-excitability asymptotics for scroll waves in three-dimensional excitable media. *Physical Review E*, 66(3):036214, 2002.

[351] Vincent Hakim and Alain Karma. Spiral wave meander in excitable media: the large core limit. *Physical Review Letters*, 79(4):665, 1997.

[352] O Steinbock, J Schütze, and SC Müller. Electric-field-induced drift and deformation of spiral waves in an excitable medium. *Physical Review Letters*, 68(2):248, 1992.

[353] AP Muñuzuri, M Gómez-Gesteira, V Pérez-Muñuzuri, VI Krinsky, and V Pérez-Villar. Mechanism of the electric-field-induced vortex drift in excitable media. *Physical Review E*,

48(5):R3232, 1993.

[354] V Krinsky, E Hamm, and V Voignier. Dense and sparse vortices in excitable media drift in opposite directions in electric field. *Physical Review Letters*, 76(20):3854, 1996.

[355] Valerii A Davydov, VS Zykov, and AS Mikhailov. Kinematics of autowave structures in excitable media. *Physics-Uspekhi*, 34(8):665–684, 1991.

[356] VN Biktashev and AV Holden. Design principles of a low voltage cardiac defibrillator based on the effect of feedback resonant drift. *Journal of Theoretical Biology*, 169(2):101–112, 1994.

[357] AS Mikhailov and VS Zykov. Kinematical theory of spiral waves in excitable media: comparison with numerical simulations. *Physica D: Nonlinear Phenomena*, 52(2):379–397, 1991.

[358] Vincent Hakim and Alain Karma. Theory of spiral wave dynamics in weakly excitable media: asymptotic reduction to a kinematic model and applications. *Physical Review E*, 60(5):5073, 1999.

[359] Alexander S Mikhailov. Three-dimensional kinematics. *Chaos, Solitons & Fractals*, 5(3):673–679, 1995.

[360] S Alonso, F Sagues, and AS Mikhailov. Periodic forcing of scroll rings and control of winfree turbulence in excitable media. *Chaos: An Interdisciplinary Journal of Nonlinear Science*, 16(2):023124, 2006.

[361] James P Keener. The dynamics of three-dimensional scroll waves in excitable media. *Physica D: Nonlinear Phenomena*, 31(2):269–276, 1988.

[362] Rolf-Martin Mantel and Dwight Barkley. Periodic forcing of spiral waves in excitable media. *Physical Review E*, 54(5):4791, 1996.

[363] Björn Sandstede and Arnd Scheel. Absolute and convective instabilities of waves on unbounded and large bounded domains. *Physica D: Nonlinear Phenomena*, 145(3):233–277, 2000.

[364] Robert J Deissler. Noise-sustained structure, intermittency, and the ginzburg-landau equation. *Journal of Statistical Physics*, 40(3-4):371–395, 1985.

[365] Mark Kness, Laurette S Tuckerman, and Dwight Barkley. Symmetry-breaking bifurcations in one-dimensional excitable media. *Physical Review A*, 46(8):5054, 1992.

[366] Martín G Zimmermann, Sascha O Firle, Mario A Natiello, Michael Hildebrand, Markus Eiswirth, Markus Bär, Anil K Bangia, and Ioannis G Kevrekidis. Pulse bifurcation and transition to spatiotemporal chaos in an excitable reaction-diffusion model. *Physica D: Nonlinear Phenomena*, 110(1):92–104, 1997.

[367] IS Aranson, L Aranson, L Kramer, and A Weber. Stability limits of spirals and traveling waves in nonequilibrium media. *Physical Review A*, 46(6):R2992, 1992.

[368] John Rinzel and Joseph B Keller. Traveling wave solutions of a nerve conduction equation. *Biophysical Journal*, 13(12):1313, 1973.

[369] EJ Doedel, Xianjun Wang, and Thomas Fairgrieve. Software for continuation and bifurcation problems in ordinary differential equations. In *Technical report*. California Institute of Technology Pasadena, CA, 1994.

[370] Neil W Ashcroft and N David Mermin. Solid state phys. *Saunders, Philadelphia*, page 293, 1976.

[371] Paul Wheeler and Dwight Barkley. Computation of spiral spectra. *SIAM Journal on Applied Dynamical Systems*, 5(1):157–177, 2006.

[372] Kirsten HWJ Ten Tusscher and Alexander V Panfilov. Alternans and spiral breakup in a human ventricular tissue model. *American Journal of Physiology-Heart and Circulatory Physiology*, 291(3):H1088–H1100, 2006.

[373] V Perez-Mufiuzuri, R Aliev, B Vasiev, V Pérez-Villar, and VI Krinsky. Super-spiral structures in an excitable medium. *Nature*, 353, 1991.

[374] Michael Rubart and Douglas P Zipes. Mechanisms of sudden cardiac death. *Journal of Clinical Investigation*, 115(9):2305, 2005.

[375] Vincent Jacquemet and Craig S Henriquez. Genesis of complex fractionated atrial electrograms in zones of slow conduction: a computer model of microfibrosis. *Heart Rhythm*, 6(6):803–810, 2009.

[376] Gordon K Moe, Werner C Rheinboldt, and JA Abildskov. A computer model of atrial fibrillation. *American heart journal*, 67(2):200–220, 1964.

[377] Xiaohui Yuan, Takashi Teramoto, and Yasumasa Nishiura. Heterogeneity-induced defect bifurcation and pulse dynamics for a three-component reaction-diffusion system. *Physical Review E*, 75(3):036220, 2007.

[378] Yasumasa Nishiura, Takashi Teramoto, Xiaohui Yuan, and Kei-Ichi Ueda. Dynamics of traveling pulses in heterogeneous media. *Chaos: An interdisciplinary journal of nonlinear science*, 17(3):037104, 2007.

[379] Yasumasa Nishiura, Yoshihito Oyama, Kei-ichi Ueda, et al. Dynamics of traveling pulses in heterogeneous media of jump type. *Hokkaido mathematical journal*, 36(1):207–242, 2007.

[380] Takashi Teramoto, Xiaohui Yuan, Markus Bär, and Yasumasa Nishiura. Onset of unidirectional pulse propagation in an excitable medium with asymmetric heterogeneity. *Physical Review E*, 79(4):046205, 2009.

[381] Bryan J Caldwell, Mark L Trew, and Arkady M Pertsov. Cardiac response to low energy field pacing challenges the standard theory of defibrillation. *Circulation: Arrhythmia and Electrophysiology*, pages CIRCEP–114, 2015.

[382] Hans Dierckx, Olivier Bernus, and Henri Verschelde. Accurate eikonal-curvature relation for wave fronts in locally anisotropic reaction-diffusion systems. *Physical Review Letters*, 107(10):108101, 2011.

[383] Sergey F Pravdin, Hans Dierckx, Leonid B Katsnelson, Olga Solovyova, Vladimir S Markhasin, and Alexander V Panfilov. Electrical wave propagation in an anisotropic model of the left ventricle based on analytical description of cardiac architecture. *PLoS ONE*, 9(5):e93617, 2014.

[384] H Zhang, X Ruan, B Hu, and Q Ouyang. Spiral breakup due to mechanical deformation in excitable media. *Physical Review E*, 70(1):16212, 2004.

[385] H Zhang, BW Li, ZM Sheng, Z Cao, and G Hu. The effect of mechanical deformation on spiral turbulence. *EPL (Europhysics Letters)*, 76:1109, 2006.

[386] RH Keldermann, MP Nash, and AV Panfilov. Pacemakers in a reaction-diffusion mechanics system. *Journal of Statistical Physics*, 128(1-2):375–392, 2007.

[387] E Alvarez-Lacalle and B Echebarria. Global coupling in excitable media provides a simplified description of mechanoelectrical feedback in cardiac tissue. *Physical Review E*, 79(3):031921, 2009.

[388] Michael R Franz, Robert Cima, Dale Wang, D Profitt, and Robert Kurz. Electrophysiological effects of myocardial stretch and mechanical determinants of stretch-activated arrhythmias. *Circulation*, 86(3):968–978, 1992.

[389] Louis D Weise and Alexander V Panfilov. New mechanism of spiral wave initiation in a reaction-diffusion-mechanics system. *PloS ONE*, 6(11):e27264, 2011.

[390] LD Weise and AV Panfilov. Emergence of spiral wave activity in a mechanically heterogeneous reaction-diffusion-mechanics system. *Physical Review Letters*, 108(22):228104, 2012.

[391] Rikkert H Keldermann, Martyn P Nash, Hanneke Gelderblom, Vicky Y Wang, and Alexander V Panfilov. Electromechanical wavebreak in a model of the human left ventricle. *American Journal of Physiology-Heart and Circulatory Physiology*, 299(1):H134–H143, 2010.

[392] Yuxuan Hu, Viatcheslav Gurev, Jason Constantino, Jason D Bayer, and Natalia A Trayanova. Effects of mechano-electric feedback on scroll wave stability in human ventricular fibrillation. *PloS ONE*, 8(4):e60287, 2013.